QUASI-OPTIMAL STEADY STATE AND TRANSIENT MANEUVERS WITH AND WITHOUT THRUST VECTORING

by

Michael E. Dwyer

Thesis submitted to the Faculty of the

Virginia Polytechnic Institute and State University

in partial fulfillment of the requirements for the degree of

MASTER OF SCIENCE

in

Aerospace Engineering

APPROVED:

Dr. F.H. Lutze, Chairman

Dr. E.M. Cliff

Dr. W.C. Durham

July 19, 1993
Blacksburg, Virginia

QUASI-OPTIMAL STEADY STATE AND TRANSIENT MANEUVERS WITH AND WITHOUT THRUST VECTORING

by

Michael E. Dwyer

Dr. Frederick H. Lutze, Chairman

Aerospace and Ocean Engineering Department

(ABSTRACT)

Steady state and transient maneuver problems for a high performance fighter aircraft with and without thrust vectoring are investigated. The steady state aspect of these studies determines control combinations with and without thrust vectoring which optimize selected level-flight point performance criteria including minimum speed, maximum instantaneous range, and maximum sustained turn rate. The transient maneuvers are initiated from straight and level flight and include a longitudinal pitch-up to a desired fuselage pointing angle and a lateral-directional transition (wind-up) to a desired steady level turn rate. For the transient maneuvers a full six-degree-of-freedom model of the aircraft is used with three conventional aerodynamic controls, throttle control and pitch and yaw thrust vectoring control. Each of the control time histories are parameterized so as to include both the rate and range limits of the controls. A nonlinear programming algorithm is used to determine the control parameter values which yield the minimum time to execute the prescribed maneuvers.

Results indicate that thrust vectoring does not significantly change the steady state behavior in the scenarios investigated. However, flight times for the transient maneuvers are found to be reduced by up to 28%. The greatest effect of thrust vectoring occurs at low Mach number.

Acknowledgements

I would like to thank the following individuals for their contributions to this research effort: Dr. F. H. Lutze for the critical insight and guidance he has provided over the course of this research; Dr. E. M. Cliff and Dr. W. C. Durham for serving on my thesis committee; and Dr. J. A. Schetz for the advise and encouragement he has provided throughout my studies at Virginia Tech.

I am also indebted to ANSER Corporation for providing me with educational assistance funding and a leave of absence to complete this degree.

List of Symbols

Symbols in Alphabetic Order

a	Speed of sound
b	Wing span
B	Hessian matrix
c	Chord
C_l	Roll moment coefficient
C_m	Pitch moment coefficient
C_n	Yaw moment coefficient
C_D	Drag coefficient
C_L	Lift coefficient
C_Y	Side force coefficient
d	Search direction
D	Drag
f	Cost function
F_x, F_y, F_z	Total force components along body axes
F_{xa}, F_{ya}, F_{za}	Aerodynamic force components along body axes
g, G	Constraint function or acceleration of gravity
h	altitude (height above sea level)
Ix, Iy, Iz, Ixz	Moments of inertia
L	Lift
m	Mass
M	Mach number
M_{xa}, M_{ya}, M_{za}	Aerodynamic moment components about body axes
M_{xp}, M_{yp}, M_{zp}	Propulsive moment components about body axes
n_{max}	Maximum allowable load factor

p	Optimization parameter or body roll rate
q	Body pitch rate
r	Body yaw rate
S	Reference area
%T	T/T_{max}, "percent" of maximum thrust
T_{max}	Thrust magnitude at maximum throttle setting
T_{min}	Thrust magnitude at idle power
T_x, T_y, T_z	Thrust vector components along body axes
u	Velocity component along body x-axis
U	Control vector
v	Velocity component along body y-axis
V	Magnitude of the velocity vector
w	Velocity component along body z-axis
W	Weight
X_a, X_b	State vectors
Y	Side force

Greek Symbols

α	Angle-of-attack
β	Sideslip angle
δ_a	Aileron deflection
δ_e	Elevator deflection
δ_r	Rudder deflection
δ_t	Throttle deflection
Δ	Finite difference step
Δ	Runge-Kutta integration time step or control time segment duration
ε	Pitch Thrust Vector (PTV) angle
θ	Elevation angle

λ	Line search step length
υ	Yaw Thrust Vector (YTV) angle
σ_F, σ_G	Cost and constraint function scale factors
ϕ	Bank angle
ψ	Heading angle
Ω	Level turn rate

Subscripts

$( )_0$	Initial value
$( )_d$	Desired value

Superscripts

$\dot{( )}$	Time derivative, d( )/dt
$( )^T$	Vector transpose

List of Abbreviations

BFGS	Broyden-Fletcher-Goldfarb-Shanno
CTH	Control Time History
DN0ONF	Optimization Subroutine Name
HARV	High Angle-of-Attack Research Vehicle
LAM	Linear Aerodynamic Model
LPM	Linear Propulsion Model
NLP	Non-Linear Programming
PTV	Pitch Thrust Vector
P/U	Pitch-up (to specified elevation angle)
SAM	Splined Aerodynamic Model
SPM	Splined Propulsion Model
TAM	Tabular Aerodynamic Model
TOF	Time Of Flight
TPM	Tabular Propulsion Model
T/V	Thrust Vectoring
W/U	Wind-up (to specified sustained turn rate)
YTV	Yaw Thrust Vector

Table of Contents

LIST OF FIGURES

Chapter 1: Introduction

In recent years considerable attention has been given to improving the maneuverability of high performance fighter aircraft. To achieve this improvement, thrust vectoring is being considered for inclusion in new designs and for retrofit to current aircraft [1-3]. Cost and weight constraints require careful evaluation of thrust vectoring against other options for improving overall weapon system performance, such as improved avionics or missile technology. Initial design evaluations can be based on analytic studies similar to the research effort presented in this thesis. Consequently, a primary goal of this research is to quantify the performance improvement gained by adding thrust vectoring capability to modern high performance aircraft.

An equitable comparison of candidate configurations should exclude the effects of pilot technique. One way to remove these undesired effects is to compare only optimal performance. Several authors in the past have applied nonlinear programming and optimal control theory to solving performance problems of this type. Generally, the nonlinear programming approach is used to solve point performance problems while optimal control theory is used to solve integral performance problems. Although few assumptions are necessary to solve the nonlinear programming point performance problem, several strong assumptions are usually made to obtain solutions to the optimal control problem. These assumptions typically include an order reduction scheme to reduce the complexity of the governing equations of motion so that optimal solutions can be obtained [4-8]. In most cases, the results are obtained for either an "energy" model or a "point-mass" model. Furthermore, although control deflection limits are often included, control rate limits are rarely, if ever, included.

In the research effort presented here, the effect of thrust vectoring on steady state and transient performance is investigated. The initial phase of the research employs nonlinear programming to determine optimal performance for aircraft with and without

thrust vectoring at three steady state flight conditions: minimum sustained speed, maximum instantaneous range, and maximum sustained turn rate. All three problems were solved for an altitude of 10 kft, and the latter two were solved for a range of subsonic Mach numbers. The complete aerodynamic and propulsion (thrust magnitude and fuel flow) data base for the NASA High Angle-of-attack Research Vehicle (HARV) was used in the form of splines fit to tabulated HARV data. The splined aerodynamic and propulsion models provide smooth functions with continuous derivatives suitable for the optimization algorithm. A thrust vectoring model simulated the pitch and yaw thrust vectoring capability of axisymmetric thrust vectoring nozzles.

The second phase of the research investigates transient maneuvers by determining the minimum flight time for a transition from a steady, level, symmetric flight condition to a specified final condition. The two transient maneuver problems considered are: (1) a longitudinal pitch-up maneuver to a specified fuselage elevation angle; and, (2) a lateral-directional transition to a steady, level turn at a specified rate. Both were solved for an initial altitude of 10 kft and a range of subsonic Mach numbers. Simplified representations of the aerodynamic and propulsion data were used. Such problems require the determination of the control time histories which perform the maneuver in minimum time, and are classified as optimal control problems. Generally, such solutions are difficult to obtain and require the solution of an associated two point boundary problem. As a result, most authors resort to approximations to solve this type of problem. Here the complete six degree of freedom dynamic model is retained with a parametric characterization of the aerodynamic and propulsion control deflections versus time, including realistic control deflection and rate limits. By parameterizing the control in this manner, the transient maneuver problem is recast as a nonlinear programming problem. Hence, this research constitutes one of the first efforts to determine optimal transient maneuvers using the full six degree of freedom dynamic model with control deflection and rate limits.

The remainder of this thesis describes the data and methods used to obtain results for the steady state and transient maneuver problems, and presents the results and conclusions. Detailed aircraft properties are presented in Chapter 2, including aerodynamic, propulsive, and thrust vectoring models. The equations used to define the aircraft steady state and to integrate the aircraft motion during transient maneuvers are given in Chapter 3. Chapter 4 describes the optimization program and the general methodology used to obtain optimal solutions. Specific methodology is detailed, and results are presented for the steady state and transient maneuver problems in Chapters 5 and 6, respectively. Finally, Chapter 7 gives conclusions and recommendations for future research.

Chapter 2: Aerodynamic and Propulsion Models

Solution of the steady state and transient maneuver problems requires a mathematical model of HARV characteristics including the physical configuration, aerodynamic forces and moments, net propulsive force, and forces and moments resulting from thrust vectoring. In general, the more detailed the model, the more difficult it is to obtain optimal solutions. Consequently, trade-offs must be made between model accuracy and the ease with which solutions are obtained. In this chapter, three aerodynamic and propulsive models are described: the full tabular HARV model, and two progressively simplified derivatives. Basic aircraft characteristics and a thrust vectoring model are also described.

2.1. Basic Aircraft Properties.

The aircraft modeled in this study is an approximation to the NASA High Alpha Research Vehicle (HARV). The basic properties of the HARV for a "combat" configuration with two wingtip air-to-air missiles and 60% internal fuel are:

Weight, W		33,310	lb
Reference Area, S		400	ft^2
Wing Span, b		37.42	ft
Chord, c		11.52	ft
Moments of Inertia,	I_x	23,000	$slug \cdot ft^2$
	I_y	151,293	$slug \cdot ft^2$
	I_z	169,945	$slug \cdot ft^2$
	I_{xz}	-2,971	$slug \cdot ft^2$

These values were used in all problems considered unless explicitly stated otherwise.

2.2. Tabular Models.

The aerodynamic and propulsion data used in this study is based on a HARV model obtained from NASA Langley Research Center in September 1989. The model includes two components which are designated the Tabular Aerodynamic Model (TAM) and Tabular Propulsion Model (TPM) in this paper. Each of these models consists of tabular data which provides aerodynamic force and moment coefficients, net thrust, and fuel flow as a function of the aircraft state variables and control deflections.

2.2.1. Tabular Aerodynamic Model.

Given the aircraft state variables and control deflections, the TAM performs linear interpolation of tabular data to determine the resulting force and moment coefficients. The TAM data is based primarily on wind tunnel measurements with minor corrections made to improve agreement with flight test data.

Each force and moment coefficient output by the TAM is a function of the state variables α, $\dot{\alpha}$, β, M, h, p, q, and r (where p, q, and r are the aircraft angular rates in body axes) and the control variables $(\delta_e)_{R/L}$, $(\delta_a)_{R/L}$, $(\delta_r)_{R/L}$, $(\delta_{LEF})_{R/L}$, $(\delta_{TEF})_{R/L}$, and (δ_{SB}), which represent the elevator, aileron, rudder, leading edge flap, trailing edge flap, and speed brake deflections. The subscript R/L denotes that the right and left control surfaces are capable of independent operation. Each force and moment coefficient is calculated as the sum of a basic airframe term (a function of α, M, and h) plus increments due to $\dot{\alpha}$, β, the body angular rates, and the control deflections.

The range limits on the TAM input variables are shown in Table (2.1). The aerodynamic control deflections are defined such that for both right and left surfaces δ_e, δ_a, and δ_{TEF} are positive trailing edge down, δ_{LEF} and δ_{SB} are positive leading edge down, and δ_r is positive trailing edge left. There are no limits on the body angular rates that may be input to the TAM.

2.2.2. Tabular Propulsion Model. The TPM also performs linear interpolation of tabular data to provide the net installed thrust and fuel flow rate for a modern low-bypass ratio turbofan engine. Two such engines power the HARV. The thrust is a function of the state variables M and h, and the throttle position, δ_t.

The range limits on the TPM input variables are also shown in Table (2.1). The throttle is defined such that 30.0 degrees is idle, 106.5 degrees is military power, and 131.0 degrees is maximum afterburner.

TABLE 2.1. TAM/TPM Input Variable Limits

Variable	Lower Limit	Upper Limit
α (deg)	-10.0	90.0
β (deg)	-20.0	20.0
M	0.2	2.0
h (ft)	0.0	60000.0
δ_e (deg)	-24.0	10.5
δ_a (deg)	-25.0	45.0
δ_r (deg)	-30.0	30.0
δ_{LEF} (def)	-3.0	34.0
δ_{TEF} (deg)	-8.0	45.0
δ_{SB} (deg)	0.0	60.0
δ_t (deg)	30.0	131.0

The tabular data contained in the TAM and TPM was not used directly in this study, but served as a basis for the development of other models that were more compatible with the optimization algorithm. These derivative models are explained in the remainder of this chapter.

2.3. Splined Models.

Splined representations of the TAM and TPM were developed to obtain smooth data required by the optimization program. These representations are designated the Splined Aerodynamic Model (SAM) and the Splined Propulsion Model (SPM). The following sections describe simplifications made to the tabular models, and the resulting splined models.

2.3.1. Simplifications.

Simplifications were made to the TAM to reach a form suitable for generating splines of the tabular data, and to reduce the complexity of the optimization problem by limiting the number of variables to be optimized.

Altitude Dependence. Airframe flexibility, which is a function of dynamic pressure, and hence, air density, causes the aerodynamic coefficients output by the TAM to vary with altitude. However, since the maneuvers in this study are performed within a small neighborhood of the initial altitude, the effects of altitude change are negligible. The splines were calculated with the altitude constant at 10 kft.

Differential Control Deflection. As stated previously, the TAM allows the right and left aerodynamic controls to be operated independently. This capability was not exploited in order to reduce the complexity of this study. In the problems examined in this study, the left and right elevator and rudder deflections are of equal magnitude and in the same direction. The left and right aileron deflections are of equal magnitude and in opposite directions, with a positive δ_a generating negative roll moment (right wing trailing edge down, left wing trailing edge up).

Miscellaneous Variables. Several available TAM inputs were also not used in order to reduce the complexity of the model including the flap deflections, speed brake deflection, and α rate. Since the objective of this study is to compare an aircraft with only basic aerodynamic controls (δ_e, δ_a, δ_r), to one enhanced with pitch and yaw thrust vectoring controls (ε,υ), the flaps and speed brake were not used. The effect of α rate was calculated and observed to be negligible.

2.3.2. Splined Aerodynamic Model. After the simplifications described above have been made, the force and moment coefficients are functions of only nine variables. The coefficients are shown in functional form in Equation (2.1).

$$\begin{aligned} C_D &= C_D(\alpha, M, \delta_e) \\ C_Y &= C_Y(\alpha, M, \beta, \delta_a, \delta_r, p, r) \\ C_L &= C_L(\alpha, M, \delta_e, \delta_a, q) \\ C_l &= C_l(\alpha, M, \beta, \delta_a, \delta_r, p, r) \\ C_m &= C_m(\alpha, M, \delta_e, \delta_a, \delta_r, q) \\ C_n &= C_n(\alpha, M, \beta, \delta_a, \delta_r, p, r) \end{aligned} \tag{2.1}$$

The TAM structure is such that with the simplifications from the previous section, the total aerodynamic force and moment coefficients become linear combinations of terms that depend on only two or three variables. This structure suggests that the TAM can be accurately represented using two- and three-dimensional splines. In parallel with the structure of the TAM, separate splines are generated for a basic airframe term and increments due to β, the body angular rates, and control deflections.

To illustrate, consider the calculation of the lift coefficient. First, C_L is splined with respect to α and M to form the basic airframe spline:

$$S_{L_0}(\alpha, M)$$

The data for this spline is generated by varying α and M while holding the other variables (β, p, q, r, δ_e, δ_a, and δ_r) at zero and making repeated calls to the TAM. Next, C_L is splined with respect to α, M, and, in turn, δ_e, δ_a, and q to form three additional splines:

$$S_{L_{\delta_e}}(\alpha, M, \delta_e) \qquad S_{L_{\delta_a}}(\alpha, M, \delta_a) \qquad S_{L_q}(\alpha, M, q)$$

The data for these splines is generated by varying α, M, and either δ_e, δ_a, or q while holding the other variables at zero and making repeated calls to the TAM. To get the value of the increment to C_L due to a given variable, the value of the basic airframe spline is subtracted from the spline of that variable. The total lift coefficient is then calculated as follows:

$$\begin{aligned} C_L = {} & S_{L_0}(\alpha,M) + (S_{L_{\delta_e}}(\alpha,M,\delta_e) - S_{L_0}(\alpha,M)) \\ & + (S_{L_{\delta_a}}(\alpha,M,\delta_a) - S_{L_0}(\alpha,M)) \\ & + (S_{L_q}(\alpha,M,q) - S_{L_0}(\alpha,M)) \end{aligned}$$

2.3.3. Splined Propulsion Model. The Splined Propulsion Model (SPM) uses a three-dimensional spline to represent the variations of thrust and fuel flow as functions of δ_t, M, and h without simplification.

2.4. Linear Models.

Simplified analytic models were developed to reduce the cost and time required to obtain solutions to the relatively complex transient maneuver problems. These are designated the Linear Aerodynamic Model (LAM) and the Linear Propulsion Model (LPM). The following subsections describe the linear models and discuss their accuracy.

2.4.1. Linear Aerodynamic Model. The LAM represents the six aerodynamic coefficients as analytic functions of α, β, p, q, r, δ_e, δ_a, and δ_r. The functions were generated by visually fitting straight lines and curves to graphs of TAM data generated for M = 0.60 and h = 10 kft. Using a single altitude is acceptable since the aircraft altitude remains near 10 kft throughout each transient maneuver. Neglecting the Mach dependence yields a reasonable approximation to the TAM data up to M = 0.8. As with the SAM, the effect of α rate is neglected. Also neglected are the effects of: δ_e on C_D; p and r on C_Y; δ_a and q on C_L; δ_a and δ_r on C_m; and p on C_n.

The resulting functional forms of the aerodynamic coefficients are shown below in Equation (2.2). Nearly all of the functional dependencies are linear. The only exceptions are $C_L(\alpha)$ and $C_D(\alpha)$ which are parabolic functions.

$$\begin{aligned} C_D &= C_D(\alpha) \\ C_Y &= C_Y(\alpha,\beta,\delta_a,\delta_r) \\ C_L &= C_L(\alpha,\delta_e) \\ C_l &= C_l(\alpha,\beta,\delta_a,\delta_r,p,r) \\ C_m &= C_m(\alpha,\delta_e,q) \\ C_n &= C_n(\alpha,\beta,\delta_a,\delta_r,r) \end{aligned} \tag{2.2}$$

Complete details of the LAM functions are given in Appendix A.

2.4.2. Linear Propulsion Model. In the transient optimization problems, a variable called "percent thrust" (%T) is used instead of the throttle position to control the thrust level. Using %T rather than the actual throttle setting avoids discontinuities (caused by afterburner staging) found in the thrust versus δ_t curves for certain parts of the flight envelope. %T is defined as:

$$\%T = \frac{T - T_{min}}{T_{max} - T_{min}}$$

The thrust is then calculated as:

$$T = T_{min} + \%T \cdot (T_{max} - T_{min})$$

Using %T as a control effectively linearizes the thrust versus δ_t dependency. The altitude dependence is again neglected. For subsonic Mach numbers the thrust is reasonably linear with Mach number, allowing the entire TPM to be condensed into a single function. For a maximum afterburner throttle setting and 10 kft altitude, T_{max} = 10100.0 + 5500M pounds (for one engine). T_{min} = 0 was used for this study.

2.4.3. Accuracy of Linear Models. Appendix B contains graphs of aerodynamic coefficient data from the TAM, SAM, and LAM for the ranges of α and Mach values of interest in this study. The SAM data matches the TAM data well, however, at some flight conditions the LAM data deviates from the TAM data. Such deviations are not significant, provided that key results have similar trends for calculations made with the LAM and the highly accurate SAM. Here "key results" are defined to be the flight time for a given maneuver, and the difference in flight times for aircraft with and without thrust vectoring. To verify the fidelity of the LAM, flight times and flight time differences from selected LAM and SAM transient maneuver runs were compared. The LAM results were within 10% of the SAM results.

2.5. Thrust Vectoring Model.

This section describes the axisymmetric thrust vectoring nozzle model developed for this study. The thrust vectoring model calculates propulsive forces and moments and is independent of the propulsion model used. The propulsion models provide the net thrust which is typically assumed to be along either the body x-axis or the line of flight. For this study, the undeflected thrust vector points along the positive body x-axis. Using thrust vectoring, the thrust line of action may be deflected away from the body x-axis in the x-z plane and the x-y plane independently. Deflections into the x-z and x-y planes are called pitch and yaw thrust vectoring, respectively. As shown in Figure (1), the Pitch Thrust Vector (PTV) angle, ε, is defined such that a positive deflection produces a thrust component in the negative z-direction and a negative pitch moment. The Yaw Thrust Vector (YTV) angle, υ, is defined such that a positive deflection produces a thrust component in the positive y-direction and a negative yaw moment. Equation (2.3) below shows the thrust vector components.

$$
\begin{aligned}
T_x &= T\cos\varepsilon\cos\upsilon \\
T_y &= T\cos\varepsilon\sin\upsilon \\
T_z &= T\sin\varepsilon
\end{aligned}
\tag{2.3}
$$

Deflecting the thrust line of action is assumed to cause negligible thrust loss. The thrust line of action for each engine is assumed to pass through the center of the nozzle exit, regardless of thrust vector angle. The moments generated by thrust vectoring are calculated as $M_{prop} = r_N \times T$, where r_N is the vector from the CG to the center of the nozzle exit. The only significant component of r_N is r_x with a value of -19.08 feet. The resulting propulsive moment equations are given in Equation (2.4), with T_y and T_z representing the sum of the thrust components of both engines in the y and z directions respectively.

$$
\begin{aligned}
M_x &= 0.0 \\
M_y &= -T_z r_x \\
M_z &= T_y r_x
\end{aligned}
\tag{2.4}
$$

Chapter 3: Equations of Motion

This chapter describes the state variables and equations of motion used in this study. The steady state problems used the equations of motion to specify zero state acceleration. In the transient maneuver problems, aircraft motion and orientation were represented using 12 state variables which were integrated during the solution process using the equations in this chapter. To maintain generality and facilitate future studies, all 12 state variables were included even though some were not explicitly required in this study. In particular, the ground track variables x and y are not needed for the purpose of this study and could have been excluded.

3.1. State Variable Vector.

Equation (3.1) shows X_b, the state variable vector. An alternate form, X_a, will be defined in a later section. X_b uses the Earth-surface-fixed axes variables x, y, and z to represent aircraft position, the Euler angles ϕ, θ, and ψ to represent aircraft orientation, and the body axes variables u, v, w, p, q, and r to represent aircraft translational and angular velocities.

$$X_b = \{x\ y\ z\ \phi\ \theta\ \psi\ u\ v\ w\ p\ q\ r\}^T \tag{3.1}$$

3.2. Force and Moment Equations.

The thrust force components and both the aerodynamic and propulsive moment contributions are provided in body axes by the aerodynamic, propulsion, and thrust vectoring models described previously. The aerodynamic force components (D, Y, and L) are transformed to body axes using Equation (3.2).

$$
\begin{aligned}
F_{x_a} &= -L\sin\alpha - Y\cos\alpha\sin\beta - D\cos\alpha\cos\beta \\
F_{y_a} &= -Y\cos\beta - D\sin\beta \\
F_{z_a} &= -L\cos\alpha - Y\sin\alpha\sin\beta - D\sin\alpha\cos\beta
\end{aligned}
\tag{3.2}
$$

As shown in Equation (3.3), the total force (F_x, F_y, and F_z) and moment (M_x, M_y, M_z) body axis components include both aerodynamic and propulsive contributions.

$$
\begin{aligned}
F_x &= F_{x_a} + T_x \\
F_y &= F_{y_a} + T_y \\
F_z &= F_{z_a} + T_z \\
M_x &= M_{x_a} + M_{x_p} \\
M_y &= M_{y_a} + M_{y_p} \\
M_z &= M_{z_a} + M_{z_p}
\end{aligned}
\tag{3.3}
$$

The force and moment equations used in this study are those given in Etkin [9] for a rigid vehicle having a plane of symmetry in flight over a flat Earth. These equations, shown here as Equation (3.4) and Equation (3.5), provide the instantaneous translational and angular accelerations in body axes given the aircraft state and control deflections. Use of body axes facilitated the integration of the thrust vectoring model and the definition of optimization problem constraints.

$$
\begin{aligned}
F_x - mg\sin\theta &= m(\dot{u} + qw - rv) \\
F_y + mg\cos\theta\sin\phi &= m(\dot{v} + ru - pw) \\
F_z + mg\cos\theta\cos\phi &= m(\dot{w} + pv - qu)
\end{aligned}
\tag{3.4}
$$

$$
\begin{aligned}
M_x &= I_x\dot{p} - I_{xz}(\dot{r}+pq) - (I_y-I_z)qr \\
M_y &= I_y\dot{q} - I_{xz}(r^2-p^2) - (I_z-I_x)rp \\
M_z &= I_z\dot{r} - I_{xz}(\dot{p}-qr) - (I_x-I_y)pq
\end{aligned}
\tag{3.5}
$$

3.3. Kinematic Relations.

The rates of change of the aircraft position variables x, y, and z are calculated by transforming the body velocity components u, v, and w into Earth-fixed reference axes using Equation (3.6). The rates of change of the aircraft orientation variables ϕ, θ, and ψ are calculated using Equation (3.7). These equations are also found in Etkin. [9]

$$
\begin{Bmatrix} \dot{x} \\ \dot{y} \\ \dot{z} \end{Bmatrix} =
\begin{bmatrix}
\cos\psi\cos\theta & \sin\psi\cos\phi + \cos\psi\sin\theta\sin\phi & \sin\psi\sin\phi + \cos\psi\sin\theta\cos\phi \\
\sin\psi\cos\theta & \cos\psi\cos\phi + \sin\psi\sin\theta\sin\phi & \cos\psi\sin\phi + \sin\psi\sin\theta\cos\phi \\
-\sin\theta & \sin\phi\cos\theta & \cos\phi\cos\theta
\end{bmatrix}
\begin{Bmatrix} u \\ v \\ w \end{Bmatrix}
\tag{3.6}
$$

$$
\begin{aligned}
\dot{\phi} &= p + q\sin\phi\tan\theta + r\cos\phi\tan\theta \\
\dot{\theta} &= q\cos\phi - r\sin\phi \\
\dot{\psi} &= (q\sin\phi + r\cos\phi)\sec\theta
\end{aligned}
\tag{3.7}
$$

3.4. Alternate State Variable Vector.

Equation (3.8) shows an alternate state variable vector, X_a, which represents the aircraft velocity using the aerodynamic angles α and β, and M instead of u, v, and w. This form improves convergence of the optimization algorithm because the magnitude of the variables α, β, and M more nearly matches the magnitude of the aircraft orientation and angular rate state variables.

$$X_a = \{x \;\; y \;\; z \;\; \phi \;\; \theta \;\; \psi \;\; \alpha \;\; \beta \;\; M \;\; p \;\; q \;\; r\}^T \tag{3.8}$$

The transient maneuver problems include state variable vector integration. Integration of X_a requires conversion of the translational acceleration from u, v, and w variables into α, β, and M variables using Equation (3.9) given below. Thus, the full set of 12 integrated equations are Equations (3.5), (3.6), (3.7), and (3.9).

$$\dot{\alpha} = \frac{u\dot{w} - w\dot{u}}{u^2 + w^2}$$

$$\dot{\beta} = \frac{\frac{\dot{v}}{V} - \frac{V(u\dot{u} + v\dot{v} + w\dot{w})}{V^3}}{\sqrt{1 - \left(\frac{v}{V}\right)^2}} \tag{3.9}$$

$$\dot{M} = \frac{(u\dot{u} + v\dot{v} + w\dot{w})}{Ma^2}$$

Chapter 4. General Solution Procedure

This chapter presents the nonlinear programming problem solved in this study, and describes the general methodology used to find optimal aircraft performance for several steady state flight conditions and transient maneuvers. Here "methodology" includes the problem elements (variables and functional relationships) selected to define each problem, and the algorithms used to process the chosen elements and arrive at a solution. The specific elements and algorithms differ between the steady state and transient maneuvers, and are discussed in detail in subsequent chapters.

4.1. General Nonlinear Programming Problem. The general Nonlinear Programming (NLP) problem solved in this research may be stated as follows:

$$\begin{aligned} &\min f(p),\ p \in \Re^n \\ \textit{subject to: } &g_j(p) = 0,\ j = 1,\ldots,m_e \\ &g_j(p) \geq 0,\ j = m_e+1,\ldots,m \\ &p_{LB} \leq p \leq p_{UB} \end{aligned} \tag{4.1}$$

Here p is the parameter vector, f is the cost function, and g_j are the constraint functions. Definition of specific steady state or transient maneuver problems is accomplished by making appropriate choices for the elements of p, and the functions f and g_j. The following paragraphs briefly describe how p, f, and g_j are selected to define steady state and transient maneuver problems. The specific parameter vectors and functions selected are detailed in subsequent chapters.

For the steady state problems, the parameter vector contains both state and control variables. The cost function is defined as the negative of the desired performance criteria, thus maximizing the criteria. The constraints specify the desired steady state flight condition. The solution algorithm manipulates the parameter vector to maximize the

desired performance criteria while satisfying the constraints. The maximum instantaneous range problem, for example, finds the combination of the variables α, δe, δt, and ε that satisfies x-force, z-force, and y-moment equilibrium while maximizing aircraft range for a given Mach number.

For the transient maneuver problems, the parameter vector contains variables which model the time histories of the aerodynamic and propulsive controls. The cost function for all of the transient maneuvers is the time of flight. The constraints limit the control deflection rates and specify the desired final aircraft state. The solution algorithm manipulates the parameter vector to find the control time histories that will transition the aircraft from a given initial state to the specified final state in minimum time.

4.2. Optimization Program. The optimization program employed in this research is the double precision subroutine DN0ONF, available in the IMSL Math Library [10]. DN0ONF, a version of the subroutine DNCONF, requires the user to calculate and supply cost and constraint function values and gradient information. These calculations required additional effort, however, direct access to the gradient information provided valuable insight and positive control over this aspect of the optimization process.

DN0ONF uses a sequential quadratic programming method to solve the NLP problem. The method iteratively formulates and solves quadratic programming subproblems obtained using a quadratic approximation of the Lagrange function and linearized constraints as shown in Equation (4.2).

$$\begin{aligned} &\min \frac{1}{2} d^T B_k d + \nabla f(p_k)^T d,\ p_k \in \Re^n \\ &\textit{subject to: } \nabla g_j(p_k)^T d + g_j(p_k) = 0,\ j = 1,\ldots,m_e \\ &\nabla g_j(p_k)^T d + g_j(p_k) \geq 0,\ j = m_e+1,\ldots,m \\ &p_l - p_k \leq d \leq p_u - p_k \end{aligned} \tag{4.2}$$

Here p_k is the value of the parameter vector at the k^{th} iteration, and d_k is the solution to the subproblem. B_k is a positive definite approximation of the Hessian of the Lagrangian function. B_k is updated at each iteration using a quasi-Newton BFGS formula. [11,12] A line search of the form shown in Equation (4.3) is conducted along d_k to find an updated parameter vector that reduces the value of a merit function.

$$p_{k+1} = p_k + \lambda d_k, \text{ where } 0 < \lambda \leq 1 \tag{4.3}$$

The merit function used by DN0ONF is the augmented Lagrangian function shown in Equation (4.4), where u_k is the estimate for the vector of Lagrange multipliers at the k^{th} iteration, and s_k is a penalty parameter [13,14,15]. The value of the penalty parameter is initially set equal to zero, and may be increased by DN0ONF as required to ensure descent of the merit function. The value of penalty parameter was observed to remain at zero during the solution of most of the problems in the study. The penalty term acts to make the solution vector p^* an unconstrained minimum of the merit function rather than a stationary point by making the Hessian of the Lagrangian positive semi-definite.

$$F(p_k,u_k,s_k) = f(p_k) - u_k^T g(p_k) + \frac{s_k}{2} g(p_k)^T g(p_k) \tag{4.4}$$

DN0ONF is incorporated as a subroutine which interactively requests cost and constraint function values and derivatives by altering the value of a reverse communication parameter. Before starting the first iteration, the user supplies DN0ONF with cost and constraint function values and derivatives for use in calculating a search direction. On subsequent iterations, DN0ONF first requests function values to support the line search, and then function derivatives to calculate a new search direction. An optimal solution is reached when the Kuhn-Tucker conditions are satisfied within a specified convergence accuracy. This study achieved convergence accuracies of 1.00E-08 for the steady state problems, and 1.00E-06 for the transient maneuver problems.

4.3. General Solution Procedure. The steady state and transient maneuver problems start with an initial guess, P_0, for the parameter vector, which is used to calculate initial values of the cost and constraint functions and the partial derivatives of the cost and constraint functions with respect to the parameter vector elements. The steady state problem constraints are analytic functions of the parameter vector, however, in the transient maneuver problems calculation of the constraint values requires state integration. Partial derivatives are calculated using finite difference equations, which will be described in detail in the next section. This information is passed to DN0ONF, which calculates a search direction and conducts a line search to find and updated parameter vector. If the Kuhn-Tucker optimality criteria for a converged solution are satisfied, the program writes the solution to a file and terminates. Otherwise, function values and derivatives are again calculated for another iteration.

4.4. Finite Differencing. During the optimization process, calculation of the gradient of the cost function and the Jacobian of the constraint vector is required. Partial derivatives of the cost and constraint functions with respect to the parameter vector elements were obtained using second order central, forward, and backward finite difference equations. Central differences were the default type used, however, forward and backward differences were used as required when the parameter value was against the lower or upper bound. The specific equations employed are shown in Equation (4.5) [16]. A finite difference step of Δ = 1.00E-06 was used in all cases.

$$\begin{aligned}
\textit{Central} \quad & \frac{\partial G}{\partial p} = \frac{G(p+\Delta) - G(p-\Delta)}{2\Delta} \\
\textit{Forward} \quad & \frac{\partial G}{\partial p} = \frac{-3G(p) + 4G(p+\Delta) - G(p+2\Delta)}{2\Delta} \\
\textit{Backward} \quad & \frac{\partial G}{\partial p} = \frac{3G(p) - 4G(p+\Delta) + G(p+2\Delta)}{2\Delta}
\end{aligned} \tag{4.5}$$

4.5. Summary of Subroutines Used. This study employed a combination of original and externally acquired subroutines. The external subroutines include HARV tabular models obtained from NASA, and optimization and spline generation routines available in the IMSL Math Library. The original subroutines developed specifically for this study include: (1) the SAM and SPM, which include spline management subroutines that convert tabular data into two- and three-dimensional splines and manipulate the splines to generate the aerodynamic coefficients, thrust, and fuel consumption as a function of nine variables; (2) the LAM and LPM, simplified aerodynamic and propulsion models; (3) a fourth order Runge-Kutta state integrator; (4) second order finite difference evaluators; and (5) a control parameterization model. The subroutines for the aerodynamic and propulsive models were discussed in Chapter 2. The optimization and finite differencing subroutines were discussed in this chapter. The Runge-Kutta integrator, which was used only in the transient maneuver problems, will be discussed in Chapter 6.

The following chapters describe the specific parameter vectors, cost functions, and constraint functions used to define the steady state and transient maneuver problems, and present the results obtained.

Chapter 5: Steady State Problems

Optimal aircraft performance with and without thrust vectoring was determined using the splined models for three steady state conditions: (1) minimum speed level flight; (2) maximum instantaneous range level flight; and (3) maximum rate sustained level turn. Problems (1) and (2) use only longitudinal states and controls. Problem (3) uses both longitudinal and lateral-directional states and controls. Optimal aircraft performance was found to be nearly independent of thrust vectoring for these steady state conditions. The following sections describe the setup of these problems and give the results obtained.

5.1. Minimum Speed Steady Level Symmetric Flight. This problem determines the minimum Mach number at which steady, level, symmetric flight can be sustained. The altitude is specified to be 10 kft, and throttle deflections of 106.5 deg (military power) and 131.0 deg (maximum afterburner) are used. The parameter vector is:

$$P = \{\alpha \quad M \quad \delta_e \quad \varepsilon\}^T$$

For this problem only, a weight of 45,000 lb is used rather than the 33,310 lb weight used in the remainder of this research. This weight corresponds to an aircraft configured with full internal fuel, three external fuel tanks, two 2000 lb bombs, and two wingtip air-to-air missiles. The higher weight is used to increase the margin between the minimum sustainable Mach and the lower bound of the aerodynamic data range. Convergence is difficult for the lighter configuration because the aircraft can sustain steady, level, symmetric flight at M = 0.2, the lower bound of the Mach parameter.

Kinematic relations within the constraint calculations ensure that the aircraft remains in a level, symmetric flight condition. Symmetric flight is enforced by setting $\phi = \beta = p = r = 0$. The condition for level flight is obtained by first substituting the symmetric flight equalities into the z-component of Equation (3.6) to yield Equation (5.1):

$$\dot{z} = -u\sin\theta + w\cos\theta = 0 \tag{5.1}$$

The definitions $u = V\cos\alpha$ and $w = V\sin\alpha$ may be substituted into Equation (5.1) to yield, after suitable algebraic manipulation, the condition that $\theta = \alpha$ for level flight.

As shown in Equation (5.2), the cost is the Mach number. Steady flight is enforced by three equality constraints which specify body x-force, z-force, and y-moment equilibrium. These constraints consist of the longitudinal components of Equations (3.4) and (3.5), used in the form of Equations (5.2). The variables σ_F and σ_G shown in Equation (5.2) scale the cost and constraint functions, with the values $\sigma_F = 1.0$ and $\sigma_G = 100.0$ used for this problem.

$$\begin{aligned} \min f &= \sigma_F M \\ g_1 &= \frac{\sigma_G}{m}(F_x + T_x - W\sin\theta) = 0 \\ g_2 &= \frac{\sigma_G}{m}(F_z + T_z + W\cos\theta) = 0 \\ g_3 &= \frac{\sigma_G}{I_y}(M_{y_a} + M_{y_p}) = 0 \end{aligned} \tag{5.2}$$

The constraints given in Equation (5.2) are actually scaled twice. Division by mass or I_y in the three constraint expressions appears unnecessary since the converged values of the three constraints are zero. However, during the iterative optimization process the constraint values and their derivatives are non-zero. Scaling the individual constraints by mass or I_y tends to make the constraint values and derivatives the same magnitude. The scale factor σ_G then changes the constraint magnitudes as a group to match the magnitudes of the problem parameters and cost.

Table (5.1) shows results for the two throttle settings with and without thrust vectoring. Thrust vectoring has virtually no effect on the minimum sustainable Mach number. With thrust vectoring, moment balance is achieved differently for the two throttle cases. At maximum afterburner, the elevator and PTV controls both generate

positive pitch moment. At military power, the elevator generates positive moment, and the PTV control generates negative moment. These results were reproduced using various initial guesses, and thus may be considered valid and unique global minimum solutions, and not local minima caused by the flatness of the minimum and the "randomness" of the initial guess. However, the differences are not significant given their relatively small magnitude and the negligible change in minimum sustainable Mach.

Table 5.1. Results for Minimum Speed Flight.

δ_t	T/V	α (deg)	Mach	δ_e (deg)	ε (deg)
MAX	YES	30.99	0.2257	-4.839	-0.524
MAX	NO	31.10	0.2257	-5.959	0.000
MIL	YES	20.04	0.2765	-4.293	0.642
MIL	NO	20.00	0.2766	-3.726	0.000

5.2. Maximum Instantaneous Range. This problem determined the maximum instantaneous range possible under steady, level, symmetric flight conditions. Solutions are for an altitude of 10 kft, and a range of Mach numbers. The parameter vector is:

$$P = \{\alpha \quad \delta_e \quad \delta_t \quad \varepsilon\}^T$$

The instantaneous range, calculated as the aircraft velocity divided by the fuel flow rate, is measured in feet traveled per pound of fuel burned. The fuel flow rate is obtained from the SPM. As in the previous problem, kinematic relations ensure that the aircraft remains in a level, symmetric flight condition. As shown in Equation (5.3), the instantaneous range is maximized by minimizing the negative of the instantaneous range. Steady flight is again enforced using three equality constraints which specify body x-force, z-force, and y-moment equilibrium. Scale factors were not used for this problem.

Results for cases with and without thrust vectoring vary by 0.1% maximum for Mach numbers ranging from 0.4 to 1.0. Figure (2) shows both cases as a single curve.

$$\begin{aligned} \min f &= -\frac{V}{\dot{W}_f} \\ g_1 &= \frac{1}{m}(F_x + T_x - W\sin\theta) = 0 \\ g_2 &= \frac{1}{m}(F_z + T_z + W\cos\theta) = 0 \\ g_3 &= \frac{1}{I_y}(M_{y_a} + M_{y_p}) = 0 \end{aligned} \tag{5.3}$$

5.3. Maximum Sustained Turn Rate. This problem determines the maximum steady, level, coordinated turn rate. Solutions are obtained for an altitude of 10 kft, and a range of Mach numbers. The parameter vector for this problem is:

$$P = \{\alpha \ \beta \ \phi \ \theta \ \Omega \ \delta_e \ \delta_a \ \delta_r \ \delta_t \ \varepsilon \ \upsilon\}^T$$

As shown below in Equation (5.4), the turn rate is maximized by minimizing the negative of the turn rate. The equality constraints shown in Equation (5.4) specify conditions for a steady, level, coordinated turn. An inequality constraint limits the load factor to 6.5 maximum. For this problem, $\sigma_F = 1.0$ is used for the cost function, and only two constraints were scaled using $\sigma_G = 0.01$. Figure (3) shows the resulting maximum sustained turn rate for a range of Mach numbers from 0.2 to 1.0. Once again, thrust vectoring provides minimal benefit. In all cases, maximum throttle was used except when the aircraft was at the load factor limit.

$$
\begin{aligned}
&\min f = -\sigma_F \Omega \\
&g_1 = \frac{1}{m}(F_x + T_x - W\sin\theta - m(qw - rv)) = 0 \\
&g_2 = \frac{1}{m}(F_y + T_y + W\cos\theta\sin\phi - m(ru - pw)) = 0 \\
&g_3 = \frac{1}{m}(F_z + T_z + W\cos\theta\cos\phi - m(pv - qu)) = 0 \\
&g_4 = \frac{1}{I_x}(M_{x_a} + M_{x_p} + I_{xz}pq + (I_y - I_z)qr) = 0 \\
&g_5 = \frac{1}{I_y}(M_{y_a} + M_{y_p} + I_{xz}(r^2 - p^2) + (I_z - I_x)rp) = 0 \\
&g_6 = \frac{1}{I_z}(M_{z_a} + M_{z_p} + I_{xz}qr + (I_x - I_y)pq) = 0 \\
&g_7 = -\sigma_G(u\sin\theta + v\cos\theta\sin\phi + w\cos\theta\cos\phi) = 0 \\
&g_8 = \sigma_G(F_y + T_y) = 0 \\
&g_9 = n_{\max} - \frac{1}{W}(L + T_x\sin\alpha + T_z\cos\alpha) \geq 0
\end{aligned}
\tag{5.4}
$$

5.4. Remarks. For steady state problems solved using a rigid body model, any additional force available from thrust vectoring must be negated by aerodynamic forces to maintain moment balance. In a maximum rate sustained turn, for example, one might expect the thrust to be vectored in the negative z-direction to allow additional centripetal force to be balanced. However, the positive pitch moment generated by the thrust component in the z-direction, T_z (which is negative in this case), would need to be balanced by increasing

the elevator deflection. Since the moment arms on T_z and the force generated by the elevator are nearly equal, the additional force generated by the elevator would cancel T_z, being approximately equal in magnitude and opposite in sign. Thrust vectoring thus provides negligible steady state performance improvement to aircraft such as the HARV with conventional aft-mounted control surfaces. Based on these observations, it appears that an aircraft with forward-mounted aerodynamic controls (canards) may gain steady state performance from thrust vectoring.

However, moment balance is not required during transition from one steady state to another. The following chapter will show that thrust vectoring significantly improves aircraft performance in transient maneuvers. Two elements of the steady state results are used in solving the transient maneuver problems. First, the initial state for the transient maneuver problems is calculated using a version of the maximum range optimization program. Second, the maximum sustained turn rate results provide upper bounds for the wind-up maneuver final conditions.

Chapter 6: Transient Maneuver Problems

Unlike the case for steady state maneuvers, this research found thrust vectoring to be of significant benefit in transient maneuvers. Minimum time transient maneuvers were studied using an idealized control deflection model and parameter optimization. The controls were assumed to deflect at constant rate, thus leading to control deflection versus time profiles consisting of linear segments. These profiles, called the control time histories, were parameterized using the overall Time Of Flight (TOF), the individual segment durations, and the deflections at the segment endpoints. Constraints were included in the optimization problem to limit the control deflection rates and to ensure that the desired final state variable conditions were met. The control parameters were then manipulated by the optimizer such that when the aircraft state was integrated over the TOF from some initial condition to a calculated final condition, the specified final condition constraints were met in minimum time.

The LAM and LPM provided the needed aerodynamic and propulsion data. The first part of this chapter details the various elements of the transient maneuver optimization problems including aircraft initial conditions, cost functions, control parameterization, constraints, and the state integration procedure. Results are presented at the end of the chapter.

6.1. Aircraft Initial State and Control.

The transient maneuvers are initiated from steady, level, symmetric, minimum throttle flight at 10 kft altitude with zero thrust vector deflection. For a given Mach number, the algorithm previously used to solve the steady state problems determines the initial aircraft state variables, X_0, and control deflections, U_0, which meet the above initial conditions. X_0 and U_0 are then constant for the given Mach number. The non-zero elements of X_0 and U_0 for a range of Mach numbers are given below in Table (6.1).

Table 6.1. Initial Aircraft State and Control.

Mach	$\alpha = \theta$ (deg)	δ_e (deg)	%T
0.35	8.483	-1.150	0.180
0.45	5.325	0.242	0.125
0.55	3.692	0.961	0.119
0.65	2.747	1.377	0.136
0.75	2.152	1.639	0.166

6.2. Control Parameterization.

The optimizer varies the control time histories of the six aerodynamic and propulsive controls (elevator, aileron, rudder, PTV angle, YTV angle, and throttle) to minimize the time required to satisfy given final condition constraints. To accomplish this, the general control time history shape was assumed and suitable parameters were selected to model the assumed shape. For this study, the control was modeled as a series of control deflection angle changes at constant rate over discrete time intervals, resulting in a control time history composed of a continuous series of linear segments.

Figure (4) shows a sample control time history for a single control. Six such time histories form the parameterized control model used in this study. The elements of the parameter vector, P, for a single control are defined as follows:

-- P(1), TOF (common to all control time histories)

-- P(2..5), "Token" time segment durations

-- P(6..9), Deflections at time segment end points

The TOF must be common to all six time histories because the controls must be integrated over the same time interval. The use of "token" time segment durations allows individual time segment durations to be adjusted without altering the common TOF. To calculate the actual time segment durations, each token time segment is first divided by

the sum of the tokens. This normalized token time segment is then multiplied by the TOF to calculate the actual time segment durations. For example, the steps for calculating the i^{th} time segment of an n-segment control are shown below.

$$T_i, \textit{ token duration (no units)}$$

$$\hat{T}_i = \frac{T_i}{\sum_{j=1}^{n} T_j}, \textit{ normalized token duration}$$

$$\Delta t_i = TOF \cdot \hat{T}_i, \textit{ actual duration in seconds}$$

If all of the token time segment parameters in a given optimal solution are multiplied by a scalar, evaluation of the cost and constraint functions would yield the same values. Thus, the optimal solutions obtained using this method for parameterizing the control are not unique, and the Hessian at the solution is not positive definite. In spite of these potential difficulties, solutions were readily obtained.

The model allows the number of time segments for each control to be varied independently to suit the problem being studied. More time segments are needed as the TOF increases because the controls reach their deflection limits and require an extra segment to remain on the limit (at zero deflection rate) before reversing direction. As shall be shown in detail later, the final condition constraints for both the pitch-up and wind-up transient maneuvers require zero angular acceleration about any aircraft axis. To reach this final condition in minimum time, each control must have at least three rate segments. For example, the pitch-up maneuver first requires substantial negative ε to generate positive pitch rate, then positive ε is used to slow the pitch rate, and finally ε is returned to a relatively small value to obtain pitch equilibrium. Additional segments are added if deflection limits are reached, as shown by the second segment in Figure (4).

To reduce run time and cost, each control was modeled using the minimum number of segments needed to execute the maneuver at the given flight condition, plus one extra segment to ensure that the model was not artificially constrained by having too

few degrees of freedom. Exceptions to this "minimum + 1" rule were inactive controls, such as the lateral-directional controls in the solution of the pitch-up problem, and the thrust vectoring controls in the solution of "without thrust vectoring" cases. Inactive controls were not modeled (zero segments). Overall, the number of time segments employed for each control varied from 0 to 6, with a unique combination for the six controls chosen to suit the given maneuver and flight condition. As an example, the model used for the low Mach number wind-up maneuver problem with thrust vectoring employed 6, 6, 5, 6, 5, and 3 control time segments for the elevator, aileron, rudder, PTV, YTV, and throttle controls, respectively.

Bounds are set on each parameter. The TOF and token segment duration bounds were chosen so as not to impact the results. Table (6.2) shows the deflection parameter bounds, which are representative of HARV capabilities. The deflection rate limits, which were specified in the HARV model obtained from NASA, are also shown. The rate limits will be discussed later.

TABLE 6.2. Control Deflection and Rate Limits

Variable	Deflection Lower Limit (deg)	Deflection Upper Limit (deg)	Rate Limit (deg/sec)
δe	-24.0	10.5	40.00
δa	-25.0	25.0	100.00
δr	-30.0	30.0	56.00
ε	-20.0	20.0	40.00
υ	-20.0	20.0	40.00
%T	0.0	1.0	0.55

6.3. Cost Function.

The cost function shown below was used for both transient maneuver problems.

$$f = \sigma_{F1} TOF + \frac{\sigma_{F2}}{(\%T)_{ave}} \tag{6.1}$$

The primary term is σ_{F1}·TOF which minimizes the time required to execute the transition. A penalty term $\sigma_{F2}/(\%T)_{ave}$ effectively forces the throttle to be operated at maximum rate by maximizing the average thrust level. A scale factor value of $\sigma_{F1} = 0.1$ was generally used to facilitate convergence by matching the cost function magnitude to the constraint magnitudes. A value of $\sigma_{F2} = 0.001$ was used make the penalty term significant without artificially increasing the TOF.

The penalty factor was required for the cases without thrust vectoring because the results were insensitive to throttle position. Without thrust vectoring, the primary effect of the throttle is through dynamic pressure, which is virtually unaffected by the throttle over the 1-2 second flight times considered. Thus, the penalty factor forced the aircraft without thrust vectoring to increase thrust. The penalty factor was approximately two orders of magnitude less than the TOF term.

6.4. Constraints.

The optimization problem included inequality constraints on the control deflection rates and equality constraints on the final aircraft state, as well as limits on the parameters associated with the control deflections. The final aircraft state constraints are implemented using a specialized inequality constraint to reduce programming effort and to allow the use of tolerances on the constraint values. The control deflection rate and final state constraints are discussed separately below.

This section also presents a specialized inequality constraint used in the transient maneuver problems. For reasons given in detail later, this constraint converts equality

constraints to an inequality form. In this section, equality constraints that describe required final conditions will be represented by a lowercase "g". Inequality constraints used in the optimization problem, some of which are converted from equality constraints, will be represented by an uppercase "G".

6.4.1. Control Deflection Rate Constraints. Table (6.2) above gave the limits on the control deflection rates. The control deflection rates were calculated from U_0 and P. In general, the deflection rates are calculated as:

$$\dot{\delta} = \frac{\delta_{i+1} - \delta_i}{\Delta t} \tag{6.2}$$

In this equation, Δt is the duration of a given time segment, and δ_i and δ_{i+1} are the control deflections at the beginning and end of the given segment, respectively. The rate limits given in Table (6.2) are absolute values. Both possible cases of a maximum positive rate and a maximum absolute negative rate were limited using a smoothed absolute value function as shown in Equation (6.3), with a value of 1.0E-12 used for κ. There is a constraint of this type for each control segment.

$$G_j = \sqrt{(\dot{\delta}_{max} - \dot{\delta})^2 + \kappa} \geq 0 \tag{6.3}$$

6.4.2. Final Aircraft State Constraints. During the maneuvers examined in this chapter, the aircraft transitions from the steady level flight conditions given in Section 6.1 to some desired final condition. Constraints within the optimization program ensure that the aircraft reaches the desired final condition. This section defines a specialized inequality constraint and the values used with the constraint to represent desired final aircraft conditions for the pitch-up and wind-up maneuvers.

Specialized Inequality Constraint. This constraint form improves convergence by reducing the magnitude of constraint values and derivatives. Use of this constraint will be explained using a final condition constraint for the pitch-up maneuver an example. Consider the primary pitch-up maneuver constraint, which requires that the calculated final elevation angle, θ, be equal to the desired value, θ_d. The equality form of this constraint is shown in Equation (6.4).

$$g_f - \theta - \theta_d = 0 \tag{6.4}$$

The constraint can also be written in the inequality form shown in Equation (6.5), where the previous definition of g_f still holds.

$$G_f - \left[\frac{g_{max}^2 + 1}{g_f^2 + 1}\right] - 1 \geq 0 \tag{6.5}$$

The term g_{max} represents a tolerance on the maximum absolute value of g_f. Using $g_{max} = 0.0$, this constraint is equivalent to an equality constraint. Alternatively, a non-zero tolerance provides flexibility and improves robustness. For example, a converged solution obtained using a loose tolerance can be used as an initial guess to obtain a more accurate solution at a tighter tolerance.

As shown in Figure (5), this "bell-shaped" form produces well-behaved derivative values even when the constraint is severely violated. Some care must be still be taken to avoid severe constraint violations, because under such conditions the derivative becomes zero. However, these conditions can be avoided by scaling the constraints.

Each transient maneuver problem uses a different set of final condition constraints. The following paragraphs detail the g_f values used with Equation (6.5) to define the final condition constraints for both maneuvers.

Pitch-Up to Specified Elevation Angle. During this maneuver, the aircraft executes a longitudinal pitch-up to capture a specified elevation angle. The final condition constraints for this maneuver are given in equality constraint form in Equation (6.6). For generality, this problem was solved using the full six degree of freedom equations of motion. The apparently duplicative constraints g_{f2} and g_{f3} are used to force the motion to remain in the vertical plane. The constraints specify moment equilibrium only, thus the aircraft velocity and altitude may be changing at the final time.

$$\begin{aligned} g_{f1} &= \theta - \theta_d = 0 \\ g_{f2} &= q = 0 \\ g_{f3} &= \dot{\theta} = 0 \\ g_{f4} &= \dot{q} = 0 \end{aligned} \tag{6.6}$$

Wind-Up to Specified Sustained Turn Rate. During this maneuver, the aircraft transitions from a steady, level, symmetric flight condition to a sustained turn at specified rate. Using Ω_d to represent the desired sustained turn rate, the constraints on the final aircraft state for this maneuver are given in equality constraint form in Equation (6.7).

$$\begin{aligned} \textit{specified rate...}\ & g_{f1} = \dot{\psi} - \Omega_d = 0 \\ \textit{coordinated...}\ & g_{f2} = F_y + T_y = 0 \\ \textit{level...}\ & g_{f3} = \dot{\phi} = 0, \quad g_{f4} = \dot{\theta} = 0, \quad g_{f5} = \dot{z} = 0 \\ \textit{sustained...}\ & g_{f6} = \dot{\alpha} = 0, \quad g_{f7} = \dot{\beta} = 0, \quad g_{f8} = \dot{M} = 0, \\ & g_{f9} = \dot{p} = 0, \quad g_{f10} = \dot{q} = 0, \quad g_{f11} = \dot{r} = 0 \end{aligned} \tag{6.7}$$

6.5. State Integration. An additional step, not detailed in the general solution procedure described in Chapter 4, is required to solve the transient maneuver problems. State integration must be performed to calculate the constraint values passed to DN0ONF. Multiple state integrations must be performed during the calculation of constraint derivatives by finite differencing. This section describes the state integration method.

The equations of motion from Chapter 3 can be written in simplified form as:

$$\dot{x} = f(x,u)$$

The fourth order Runge-Kutta integration method [17] shown below was used to integrate the states:

$$x_{t+\Delta t} = x_t + \frac{1}{6}(k_1 + 2k_2 + 2k_3 + k_4)$$

$$k_1 = f(x_t,u_t)\cdot\Delta t$$

$$k_2 = f(x_t + \frac{k_1}{2},u_{t+\Delta t/2})\cdot\Delta t$$

$$k_3 = f(x_t + \frac{k_2}{2},u_{t+\Delta t/2})\cdot\Delta t$$

$$k_4 = f(x_t + k_3,u_{t+\Delta t})\cdot\Delta t$$

Integration is performed in a piecewise manner. Endpoints of the control time segments are used as "events" which subdivide the TOF into discrete intervals. Each interval is integrated sequentially using equal length time steps, with the size of the last time step in each interval shortened as required.

A time step length of 0.025 sec was used throughout most of this study. For certain computationally intensive runs, a time step length of 0.100 sec was used to reduce

run time and cost while yielding acceptable accuracy. The integration routines were tested by verifying that the aircraft would not diverge from the steady state cruising and turning flight conditions found previously.

6.6. Results. The following sections give the results of the pitch-up and wind-up maneuver problems for cases with and without thrust vectoring.

6.6.1. Pitch-Up Maneuver Results. The pitch-up problems were solved with and without thrust vectoring over a range of Mach numbers from 0.35M to 0.75M. Starting from the steady, level flight conditions given in Table (6.1), the minimum time required to pitch-up and capture an elevation angle of 30 degrees was calculated. Figure (6) shows the resulting minimum flight times. Thrust vectoring capability reduced the TOF for this maneuver by 13.5% at 0.35M and by 3.6% at 0.75M.

Detailed control deflection, state, and moment time histories for this maneuver are shown in Figures (7) to (18). As shown in Figures (7), (8), (13), and (14), in all cases the elevator, PTV, and throttle controls are operated at maximum rate. In spite of being operated at maximum rate, the elevator and PTV controls do not reach their respective deflection limits.

Figures (7) and (8) show that the elevator and PTV controls operate in concert throughout most of the maneuver, however, some control opposition does occur. For example, Figure (8) shows that the elevator and PTV control deflections have opposite signs for a brief interval starting at $t \approx 0.70$ seconds, and for a longer interval starting at $t \approx 0.90$ seconds. Such control opposition might not be expected to occur during an optimal maneuver. This observation will be discussed in greater detail in a subsequent section. (The pitch moment opposition observed in Figures (11) and (12) is not necessarily indicative of control opposition since the aerodynamic moment includes wing, body, and control contributions.)

As shown in Figures (11) and (12), at lower Mach numbers the available

aerodynamic pitch moment is substantially decreased, whereas the available propulsive pitch moment is only slightly decreased. The propulsive moment thus constitutes a higher percentage of the total moment, and a higher TOF reduction is observed.

Apart from the TOF reduction, little difference is observed between the pitch-up maneuver cases with and without thrust vectoring. The elevator deflection, state, and moment time histories have similar shapes. This similarity between cases with and without thrust vectoring is also observed in the following section, which presents the results for the wind-up maneuver. However, the control deflection, state, and moment time histories for the wind-up maneuvers include both longitudinal and lateral-directional components and yield significant insight into the maneuver dynamics.

6.6.2. Wind-Up Maneuver Results. Solutions for wind-up maneuvers to 10.0 deg/sec steady, level turns were obtained over a range of Mach numbers from 0.35M to 0.75M. Figure (19) shows the variation of TOF with Mach number for aircraft with and without thrust vectoring. The percent reduction in TOF is also shown, with a maximum TOF reduction of about 28% observed at 0.35M.

The general shapes of the control deflection, state, and moment time histories shown in Figures (20) to (45) are observed to be similar for aircraft with and without thrust vectoring. The following discussion focuses on the results for aircraft with thrust vectoring. Contrasting results for aircraft without thrust vectoring are discussed briefly at the end of this section.

"Maneuver A" and "Maneuver B" are wind-up maneuvers executed by aircraft with thrust vectoring at 0.35M and 0.75M, respectively. Figures (20) to (33) show the time histories for the control deflections, aircraft state, and moment equation components. The figures indicate that the maneuvers occur as phased rolling and pitching motions involving substantial inertial coupling.

The longitudinal and lateral-directional control time histories are shown in Figures (20) to (23). The elevator and pitch thrust vectoring are rate saturated (operated at

maximum rate) during the latter two-thirds of both maneuvers. The aileron was rate saturated throughout Maneuver B and deflection saturated (held at the deflection limit) in the first part of Maneuver B. The rudder and yaw thrust vectoring were rate saturated through all of Maneuver A, deflection saturated in the first part of Maneuver A, and rate saturated over the first three-quarters of Maneuver B. Thus, the aircraft is yaw control rate and deflection limited in Maneuver A, roll control rate and deflection limited in Maneuver B, and pitch control rate limited in part of both maneuvers.

If we assume that the original aircraft was designed with balanced controls such that each control would reach its limit at the same time, then we might expect the addition of yaw thrust vectoring to cause roll control power to be limiting, as is observed in Maneuver B. At high α the rudder may lose effectiveness due to aerodynamic considerations, thus making the yaw control power limiting, as observed in Maneuver A.

The longitudinal and lateral-directional state time histories are shown in Figures (24) to (27). The state time histories have essentially the same shape for both maneuvers. However, the roll rate attained in Maneuver B is over twice that attained in Maneuver A. Also, in both cases the aircraft initially pitches down slightly before pitching up rapidly to reach the α necessary to sustain the turn. The required α's are approximately 18 and 8 degrees for Maneuvers A and B, respectively.

Figures (28) to (33) show the moment equation component time histories. The moment equations of motion, Equation (3.5) may be rewritten as follows:

$$\begin{aligned} M_{x_{aero}} + M_{x_{prop}} + I_{xz}\dot{r} + I_{xz}pq + (I_y - I_z)qr &= I_x\dot{p} \\ M_{y_{aero}} + M_{y_{prop}} + I_{xz}r^2 - I_{xz}p^2 + (I_z - I_x)rp &= I_y\dot{q} \\ M_{z_{aero}} + M_{z_{prop}} + I_{xz}\dot{p} - I_{xz}qr + (I_x - I_y)pq &= I_z\dot{r} \end{aligned} \tag{6.8}$$

The first two terms in these equations are the applied aerodynamic and propulsive moments. (Note that the aerodynamic moments include the wing, body, and control contributions to the moment. Therefore, the total aerodynamic moment may have a sign opposite the component provided by aerodynamic control.) The next three terms are

apparent moments due to inertial coupling, many of which are negligible and not shown in the figures. The last term is the moment of inertia multiplied by the angular acceleration for each axis, which equals the sum of the applied and apparent moments.

As shown in Figures (28) and (29), the aerodynamic moment is the only significant roll moment component. The aerodynamic roll moment generated in Maneuver B is approximately four times that generated in Maneuver A.

The pitch and yaw moment components are more difficult to analyze. A few basic observations can be immediately made. First, the propulsive moments are a significantly higher proportion of the total applied moment in the low Mach number case. Second, the aerodynamic and propulsive controls generate opposing moments over some portions of the time history. This condition can be observed in the control time histories where δe and ε or δr and υ have opposite signs. However, opposing aerodynamic and propulsive moments observed in the moment time histories do not necessarily indicate control opposition because the aerodynamic moments include body and wing effects. Finally, the apparent moments due to inertial coupling are significant at both Mach numbers.

Closer observation reveals that the rolling, pitching, and yawing motions are phased to take advantage of inertial coupling. Consider the state and moment component time histories for Maneuver B. In the first part of the maneuver, the ailerons, rudders, and YTV are operated at maximum rate to initiate roll and yaw and build up p and r. Maximum aileron deflection and maximum roll acceleration are attained at $t \approx 0.25$ seconds when the ailerons reach the negative deflection limit of -25 degrees. Thereafter, even with the ailerons held at their limit, the roll acceleration decreases due to roll damping. The elevator and PTV are initially operated such that a slight negative pitch rate is attained, increasing the roll and yaw accelerations. For example, observe in Figure (33) that the initial positive surge in the $(I_x-I_y)\cdot p\cdot q$ curve contributes about 7% of the total yaw moment at $t \approx 0.3$ seconds.

At $t \approx 0.3$ seconds, maximum yaw acceleration is attained, and p and r have

rate is attained, increasing the roll and yaw accelerations. For example, observe in Figure (33) that the initial positive surge in the $(I_x-I_y)\cdot p\cdot q$ curve contributes about 7% of the total yaw moment at $t \approx 0.3$ seconds.

At $t \approx 0.3$ seconds, maximum yaw acceleration is attained, and p and r have increased to about 125 and 10 degrees per second, respectively. At this point, the elevator and PTV are operated at maximum rate to initiate positive pitch rate. The pitch acceleration is augmented by the $-I_{xy}\cdot p\cdot p$ and $(I_z-I_x)\cdot r\cdot p$ terms which contribute about 7% and 25%, respectively, of the total pitch moment at $t \approx 0.5$ seconds. The magnitude of these terms was increased by initially delaying positive pitch motion to enable the roll and yaw rates to build up more rapidly. The maximum roll and yaw rates, attained at $t \approx 0.5$ seconds, and the maximum pitch rate, attained slightly later at $t \approx 0.65$ seconds, must be decelerated to meet the specified final conditions. The roll and pitch moments are decelerated by applied aerodynamic and propulsive moments. The yaw moment is decelerated by the $(I_x-I_y)\cdot p\cdot q$ term.

Control Rate Limits. We can gain insight into the effect of control rate limits by assuming that the "Ix$\cdot\dot{p}$", "Iy$\cdot\dot{q}$", and "Iz$\cdot\dot{r}$" lines in Figures (28) to (33) represent the total moments required to perform the given maneuver in minimum time. We might consider these required moments as being met by a combination of applied moments, which are controlled directly, and apparent moments, which are managed by phasing the roll and pitch motions. For example, +165 klb-ft of yaw moment are required at $t \approx 0.3$ seconds, and -120 klb-ft are required at $t \approx 0.65$ seconds. The applied aerodynamic and propulsive yaw moments essentially meet the requirement at $t \approx 0.3$ seconds, but the controls cannot be deflected rapidly enough to enable them to meet the requirement at $t \approx 0.65$ seconds. Instead, phasing of the pitch motion allows this requirement to be met by the apparent moment term $(I_x-I_y)\cdot p\cdot q$. Similar behavior is observed for the pitch moment.

Control Opposition. The benefit of pitch/yaw control opposition is difficult to visualize. For an optimal maneuver, one might expect the controls to act in concert with

each other, as is observed in this study when control power is limited. Control opposition may be caused by synergies across the controls. For example, positive rudder generates positive roll moment. The large final rudder deflections observed in Figures (21) and (22) may result from using extra rudder to assist in reaching zero final roll moment. Alternatively, control opposition may result from tradeoffs associated with control rate limits. In any event, the phenomena of control opposition has little effect on TOF. Preventing final control opposition by constraining the final PTV and YTV deflections to be zero was observed to increase the TOF by less than one one-hundredth of a second.

Results for aircraft without thrust vectoring executing wind-up maneuvers at 0.35M and at 0.75M are shown in Figures (34) to (45). The control deflection, state, and moment time histories shown in these figures have similar shapes to those presented previously for and aircraft with thrust vectoring. The maneuvers again occur as phased rolling and pitching motions. As observed in the pitch-up maneuver results, thrust vectoring has greater benefit at low Mach number because less aerodynamic control power is available.

The rudder, now the only yaw control, is rate saturated throughout both maneuvers, and deflection saturated in the 0.35M maneuver. The aileron, though still rate saturated in part of both maneuvers, is no longer the limiting control at 0.75M. The elevator is again rate saturated in the latter two-thirds of both maneuvers.

Chapter 7: Conclusions and Recommendations

7.1. Conclusions.

Optimal solutions to steady state and transient maneuver problems for cases with and without thrust vectoring have been obtained using a full rigid body model with control deflection and rate limiting. Parameterization of the control time histories allowed these solutions to be obtained. Thrust vectoring is observed to provide minimal performance benefit for the steady state conditions investigated. Thrust vectoring is observed to reduce transient flight times for pitch-up and wind-up maneuvers by 3-6% at high subsonic Mach numbers and 13-28% at low Mach numbers.

7.2. Recommendations for Future Study.

This section briefly discusses various potential topics for further study that have arisen during the course of this research.

Investigate steady state performance with canards. This study concluded that thrust vectoring has minimal steady state performance benefit for an aircraft with a conventional aft-mounted horizontal tail. However, steady state performance benefit may result for aircraft with canards, because the longitudinal forces and moments generated by canards complement those generated by PTV control. Canards and PTV control can be deflected in a manner that generates forces in the same body z-direction and pitch moments in opposite directions, thus tending to maintain moment balance. An add-on canard model could be developed for the HARV, or a new model of an aircraft with canards could be developed to investigate this concept.

Track and limit pilot-sensed acceleration. This study did not consider pilot-sensed acceleration. Improved performance is not desirable if such improvements cause harm to the pilot (or acceleration sensitive aircraft subsystems). This study placed constraints on the aircraft final state, which was the result of state integration. Difficulties arise, however, when trying to constrain variables inside the state integration cycle. Suitable methodology needs to be developed to limit given parameters such as pilot-sensed

acceleration, structural load factor, or aircraft state variables throughout the TOF.

Study increased complexity maneuvers. Execution of complex maneuvers (such as the Herbst maneuver) would require many refinements to the existing model. Appropriate kinematic relations must be included to enable vertical flight. Soft bounds must be included for α and β to allow excursions outside the standard range of aerodynamic model input parameters. Model efficiency must be increased to reduce the time and cost required to study longer duration maneuvers. As described in the previous paragraph, some variables would need to be constrained throughout state integration.

Conduct agility research. This method could be used to study the "agility vector" developed by Dr. E. M. Cliff and others at Virginia Tech [18]. For example, the model used in this research could be used to find the minimum time to reach a specified agility vector value, or maximum "agility" attainable over a specified time. Such studies could be conducted for a single basic aircraft with and without thrust vectoring, or for two different aircraft.

References

1. Kandebo, Stanley W.; "Pratt, G.E. Pursuing Vectored Thrust Nozzles for Current Fighter Fleet,"Aviation Week and Space Technology, 13 August, 1990, pp. 31-34.

2. Anon.; "Lockheed ATF Team Fires First Missile; Demonstrates Pitch Axis Thrust Vectoring," Aviation Week and Space Technology, 3 December, 1990, p. 29.

3. Anon.; "Israel Reviewing Plan to Install GE Vectoring Nozzle in F-16," Aviation Week and Space Technology, 9 March, 1992 p 65.

4. Kelley, H. J.; "Aircraft Maneuver Optimization by Reduced Order Approximation," in Control and Dynamic Systems, C. T. Leondes, Editor, Academic Press, New York, NY, 1973.

5. Cliff, E. M. and Kelley, H. J.; "Thrust Vectored Energy Turns", Automatica, Vol. 18, 1982, pp. 559-564.

6. Lee, Pai-Hung and Lan, C. E.; "Effect of Thrust Vectoring on Level Turn Performance," Journal of Aircraft, Vol 29, No. 3, 1992, pp. 509-511.

7. Schneider, G. L. and Watt, G. W.; "Minimum Time Turns Using Vectored Thrust," Journal of Guidance, Control, and Dynamics, Vol. 12, No. 12, 1989, pp. 777-782.

8. Menon, P. K. A. and Duke, E. L.; "Time Optimal Aircraft Pursuit Evasion with a Weapon Envelope Constraint," Journal of Guidance, Control, and Dynamics, Vol. 15, No. 2, 1992, pp. 448-456.

9. Etkin, B.; Dynamics of Atmospheric Flight, John Wiley & Sons, Inc., New York, NY, 1972.

10. IMSL Math Library User's Manual, Version 1.1, January 1989, pp. 895-902.

11. Powell, M.J.D.; "A Fast Algorithm for Nonlinearly Constrained Optimization Calculations," Numerical Analysis Proceedings, Dundee 1977, Lecture Notes in Mathematics, 630, Springer-Verlag, Berlin, Germany, 1978.

12. Gill, P. E., Murray, W., Saunders, M. A., and Wright, M. H.; "Model Building and Practical Aspects of Non-linear Programming," Computational Mathematical Programming, NATO ASI Series, 15, Springer-Verlag, Berlin, Germany, 1985.

13. Schittkowski, K.; "NLPQL: A FORTRAN Subroutine Solving Constrained Nonlinear Programming Problems," in Annals of Operations Research, C.L. Monma, Editor, 1986, pp. 485-500.

14. Schittkowski, K.; "Non-Linear Programming Codes," Lecture Notes in Economics and Mathematical Systems, 183, Springer-Verlag, Berlin, Germany, 1980.

15. Gill, P. E., Murray, W., and Wright, M. H.; Practical Optimization, Academic Press, Inc., New York, 1981.

16. Anderson, D. A., Tannehill, J. C., and Pletcher, R. H.; Computational Fluid Mechanics and Heat Transfer, McGraw-Hill Book Co., New York, 1984.

17. Gerald, C. F. and Wheatley, P. O.; Applied Numerical Analysis, Third Edition, Addison-Wesley Publishing Co., Reading, Massachusetts, 1985.

18. Cliff, E. M. and Thompson, B. G.; "Aircraft Agility Maneuvers," AIAA Paper 92-4489, presented at the 1992 AIAA Atmospheric Flight Mechanics Conference, Hilton Head, S.C., August 1992.

APPENDIX A: DETAILS OF LAM

This section provides the particular equations used in the Linear Aerodynamic Model (LAM) to calculate C_D, C_Y, C_L, C_l, C_m, and C_n given α, β, δ_e, δ_a, and δ_r measured in degrees, and p, q, r measured in degrees per second. For simplicity, constant values have been rounded to two decimal places. In the FORTRAN subroutine that implements these equations, double precision variables are used for the constant values to ensure continuity of the segmented functions.

DRAG COEFFICIENT

For $-10 < \alpha < 20$:

$C_D = 0.02 + (1.53E\text{-}3)*(\alpha-2)^2$

For $20 < \alpha \leq 90$:

$C_D = 2.17 - (4.59E\text{-}4)*(\alpha-80)^2$

SIDE FORCE COEFFICIENT

$$C_Y = -(1.40E\text{-}2)*\beta + (\delta_r/30)*(-(7.90E\text{-}4)*\alpha + (8.31E\text{-}2)) + (\delta_a/25)*(-(1.20E\text{-}4)*\alpha + (1.58E\text{-}2))$$

LIFT COEFFICIENT

For $-10 < \alpha < 10$:

$C_L = (8.60E\text{-}2)*\alpha + (1.20E\text{-}2)*\delta_e - (6.00E\text{-}2)$

For $10 < \alpha < 87.2$:

$C_L = -(1.79E\text{-}3)*(\alpha - (3.40E+1))^2 + (1.20E\text{-}2)*\delta_e + (1.83E+0)$

For $87.2 < \alpha < 90$:

$C_L = -(1.91E\text{-}1)*\alpha + (1.20E\text{-}2)*\delta_e + (1.72E+1)$

ROLL MOMENT COEFFICIENT

C_l = - (5.00E-5)*α*β

+ (δ_a/25)*((5.00E-4)*α - (4.50E-2))

- (δ_r/30)*((5.00E-5)*α - (6.50E-3))

- (1.00E-2)*p + (4.00E-3)*r

PITCH MOMENT COEFFICIENT

C_m = - (6.30E-3)*α - (1.43E-2)*δ_e - (5.00E-2)*q + (3.70E-2)

YAW MOMENT COEFFICIENT

Computed as sum of four parts: $C_n = C_{no} + C_{nr} + C_{na} + C_{ny}$

(1) Basic Coefficient, C_{no}

For -10 < α < 10: C_{no} = (1.60E-3)*β

For 10 < α < 20: C_{no} = ((5.20E-3) - (3.60E-4)*α)*β

For 20 < α < 90: C_{no} = - (2.00E-3)*β

(2) Increment Due to Rudder, C_{nr}

C_{nr} = (δ_r/30)*((3.50E-4)*α - (3.15E-2))

(3) Increment Due to Aileron, C_{na}

For -10 < α 60: C_{na} = (δ_a/25)*((1.30E-4)*α + (1.30E-3))

For 60 < α 90: C_{na} = - (δ_a/25)*((6.30E-4)*α - (4.70E-3))

(4) Increment Due to Yaw Rate, C_{ny}

C_{ny} = - (6.00E-3)*r

APPENDIX B: DATA FROM TAM, SAM, AND LAM

This section briefly describes Figures (46) to (67) which show sample data from the Tabular Aerodynamic Model (TAM), Splined Aerodynamic Model (SAM), and Linear Aerodynamic Model (LAM). This study used SAM data for steady state problem calculations, and LAM data for transient maneuver problem calculations. The SAM and LAM data must adequately match the original TAM data if the results of this study are to be considered valid. The following paragraphs compare data provided by the models.

SAM versus TAM. The version of the SAM implemented in this study was observed to match the TAM very well. Different "versions" of the SAM are obtained depending on how many data points are used for each variable. More data points provide higher accuracy, but require addition calculation time and cost. For this study, the SAM used a data point interval of approximately three degrees for α, β, δ_e, δ_a, and δ_r. For the Mach number, a data point interval of 0.2M was used. With these data point intervals, the SAM may be characterized as "medium" accuracy.

Since the SAM matches the TAM so well, only Figures (46) and (47) are presented for comparison. Figure (46) shows that the SAM matches the TAM well despite substantial curvature in the C_m versus α plot. Figure (47) shows the largest difference in SAM and TAM data observed during comparative analysis. This difference occurs primarily because the data is given for 0.75M, and the data points used to generate the spline were 0.6M and 0.8M.

LAM versus TAM. For LAM versus TAM comparison, Figures (48) to (67) show the aerodynamic coefficient variations with α. For low and high Mach number cases, separate curves are given for two control deflections and for two body angular rates. For each coefficient, figures are given only for significant control and body angular rate variables. These figures show that the LAM captures the essential features of the TAM.

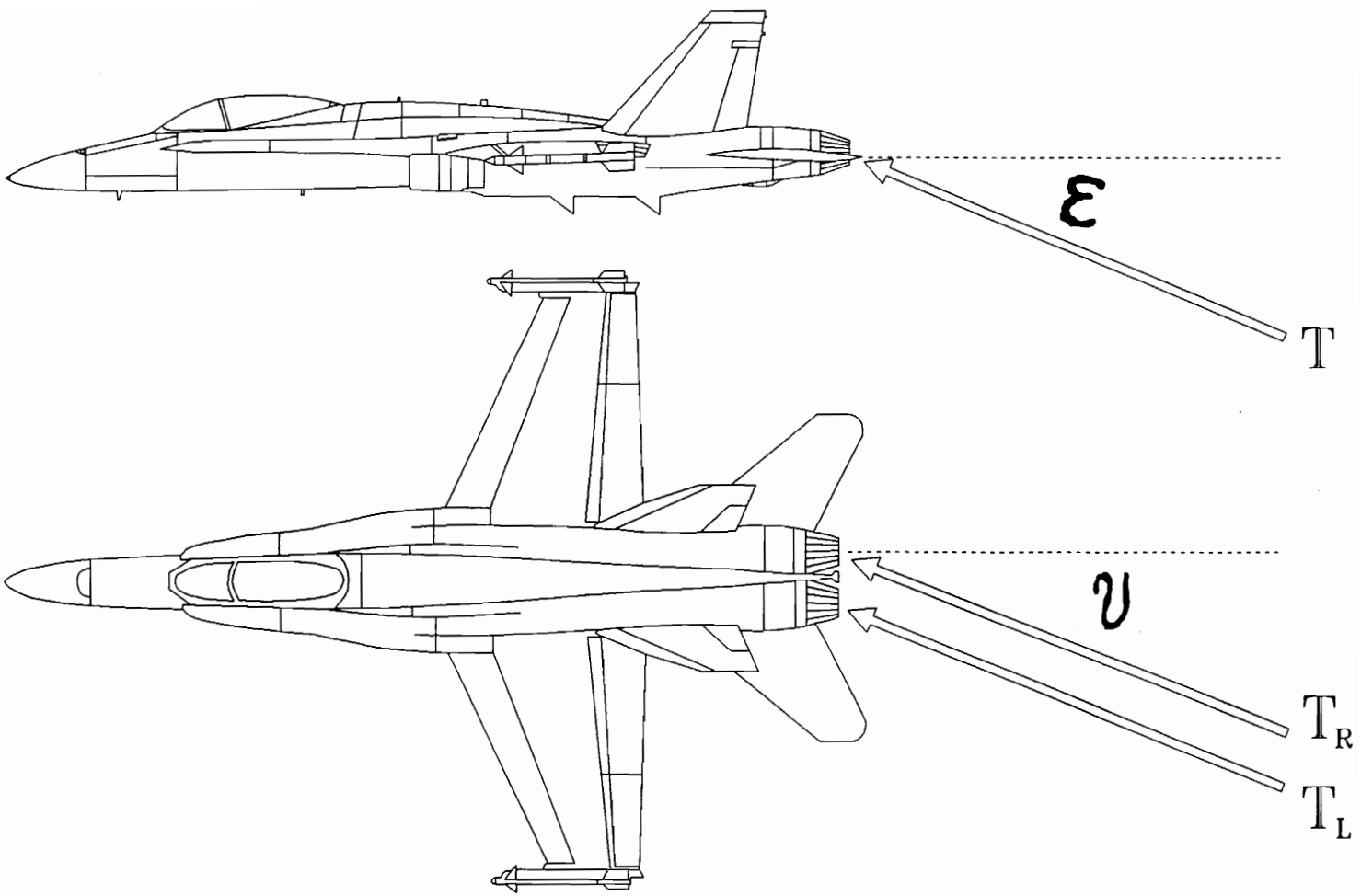

Figure 1. Definition of Positive PTV and YTV Angles

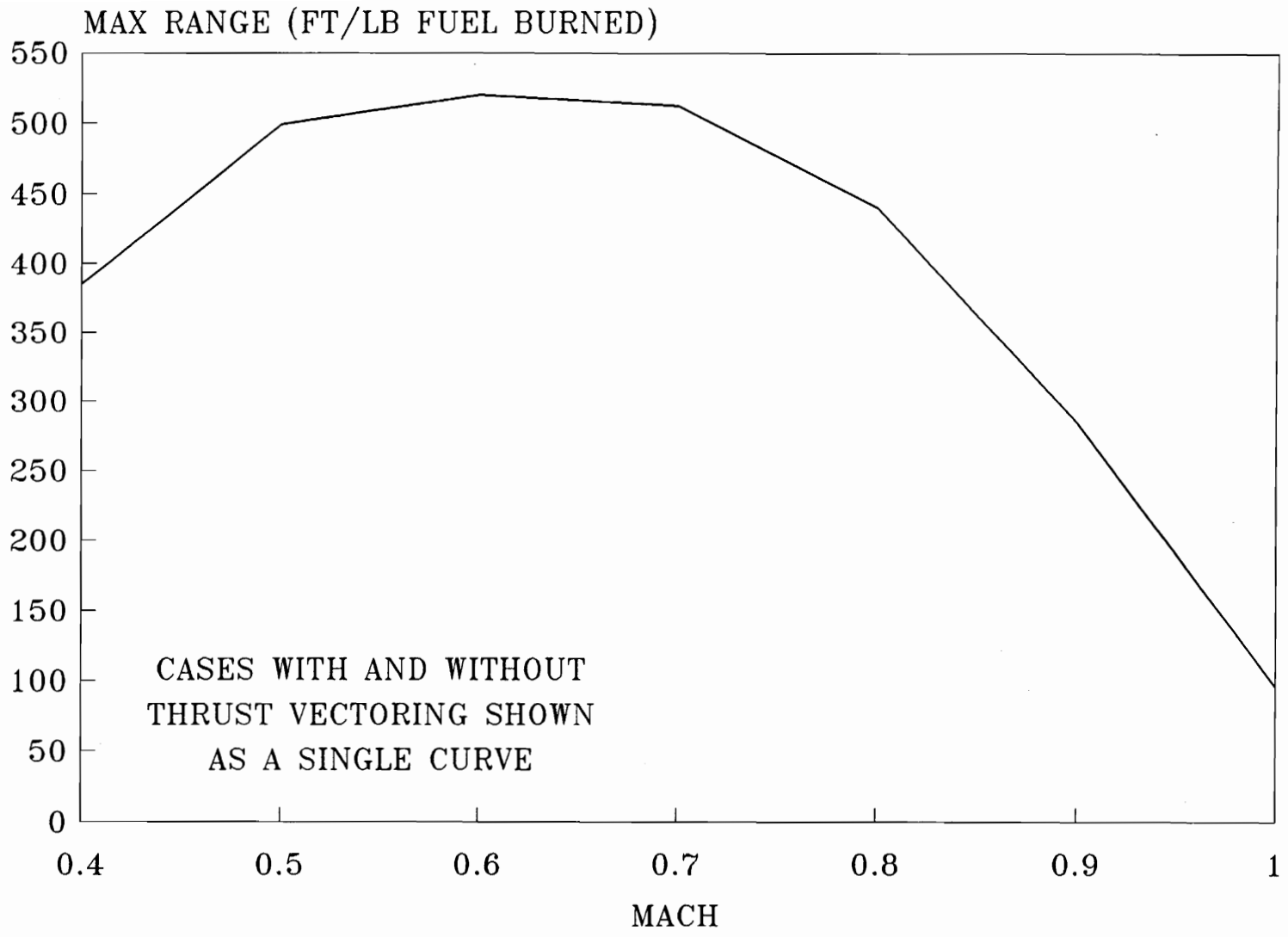

Figure 2. Maximum Instantaneous Range vs M

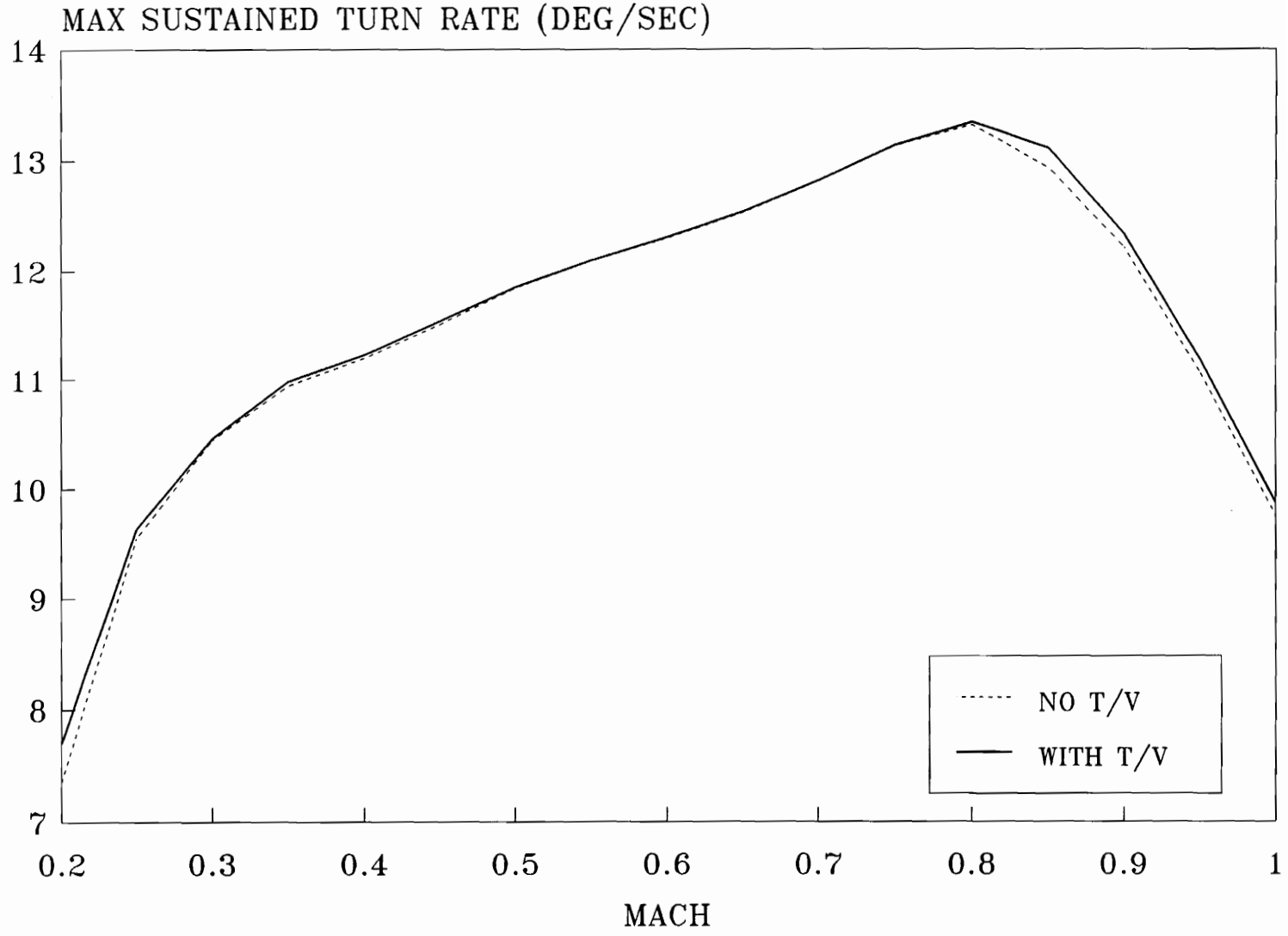

Figure 3. Maximum Sustained Turn Rate vs M

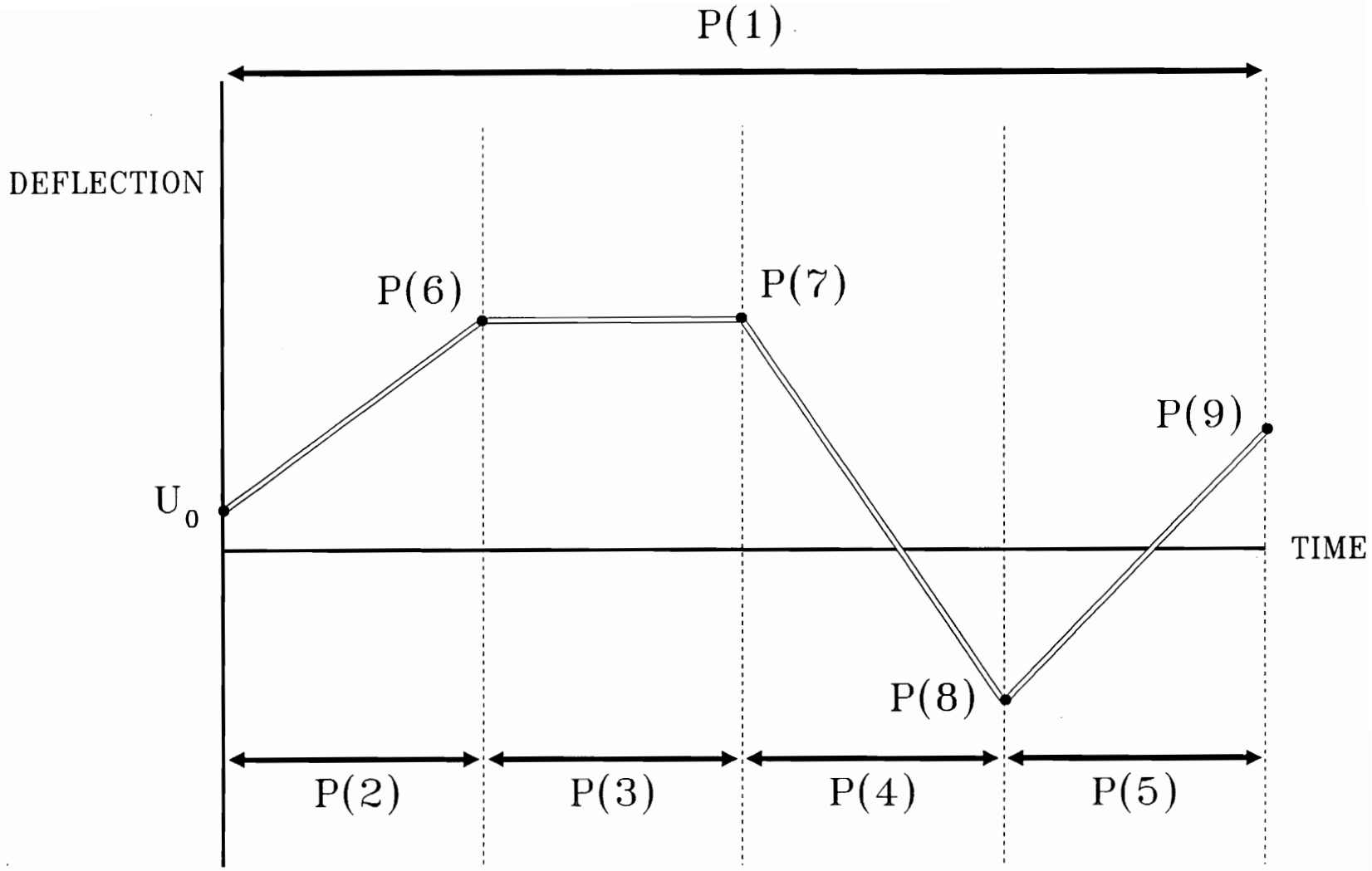

Figure 4. Example of CTH Parameterization

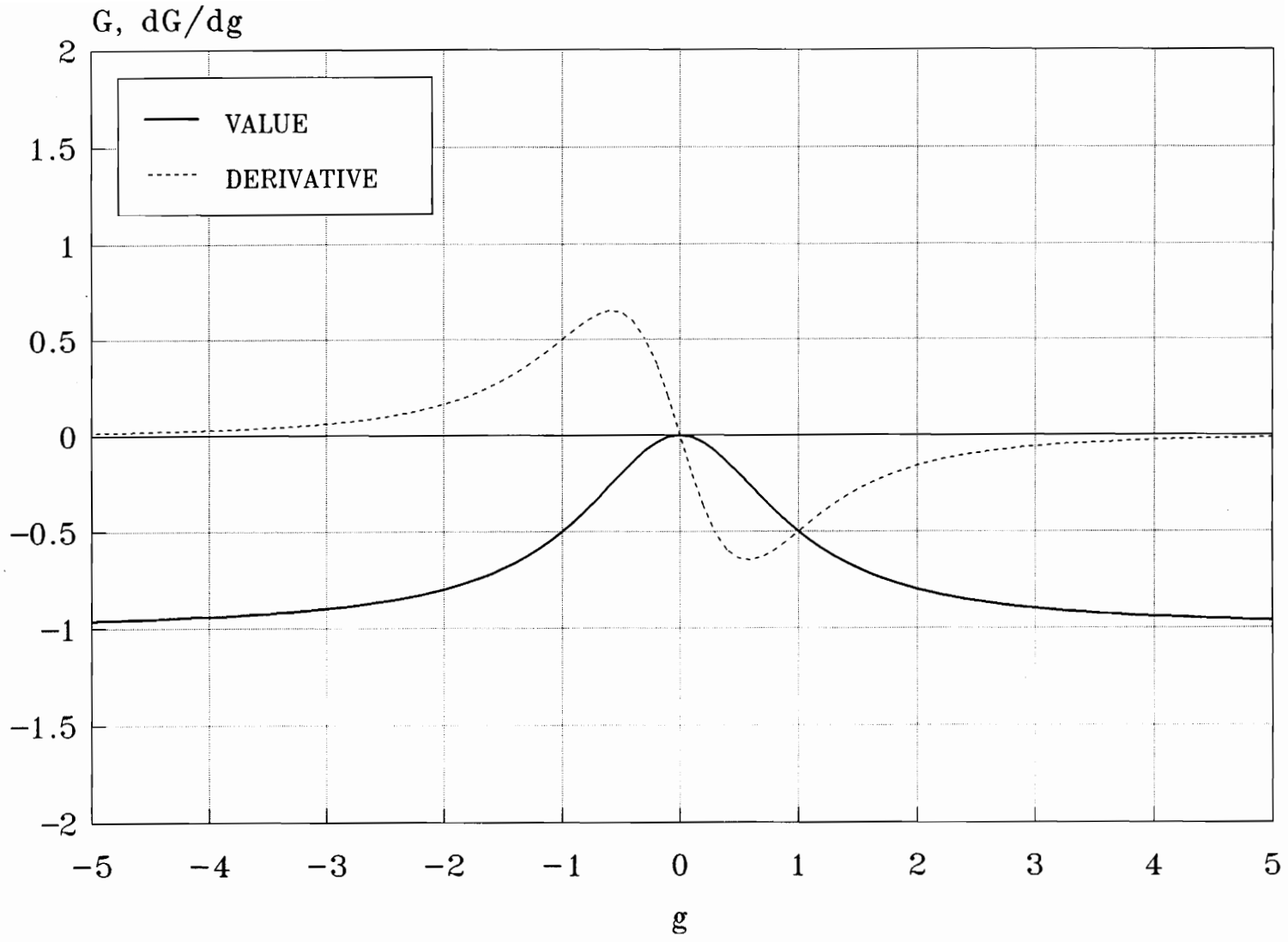

Figure 5. Value and Derivative of Specialized Inequality Constraint

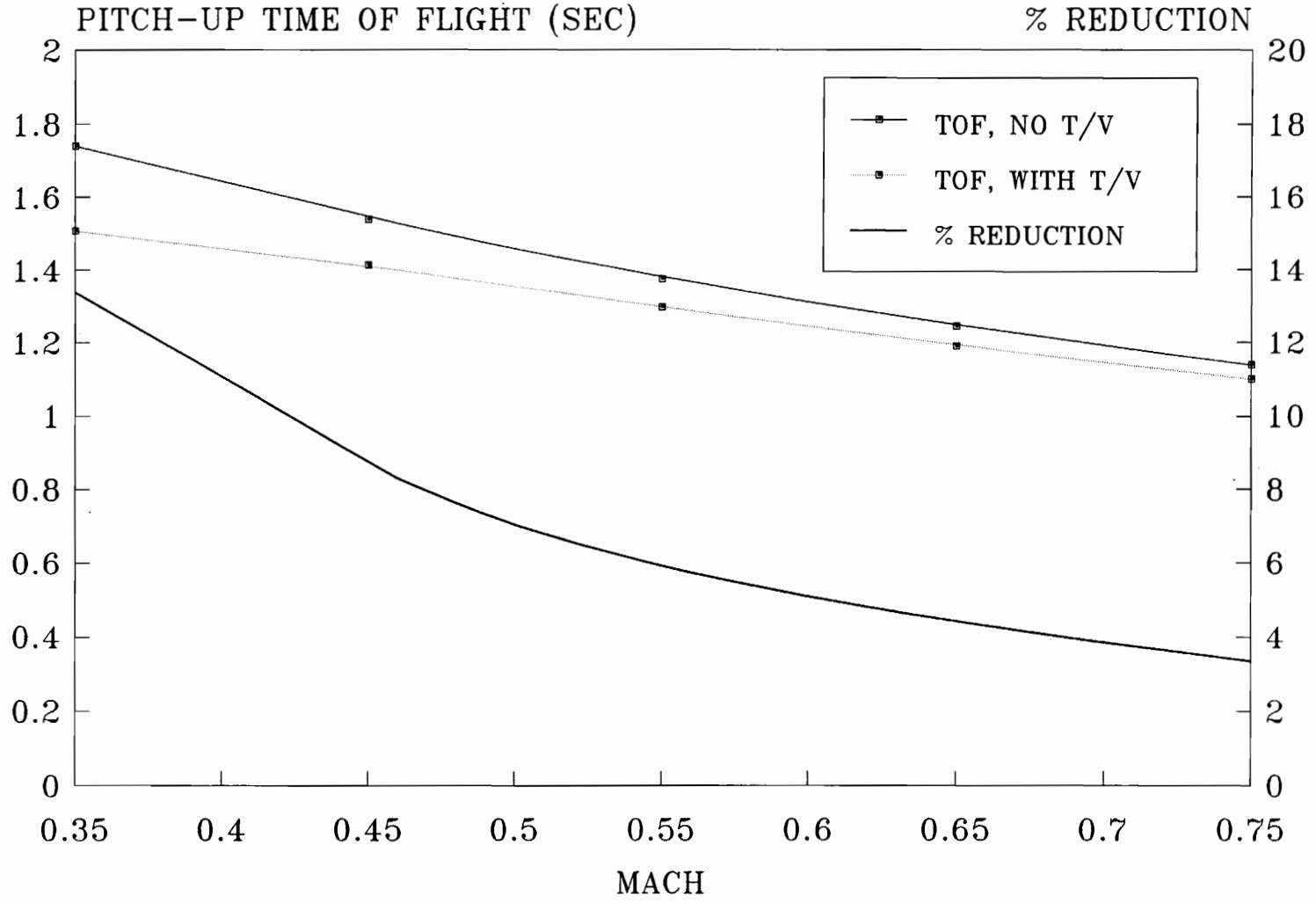

Figure 6. TOF vs M; Pitch-up Maneuver

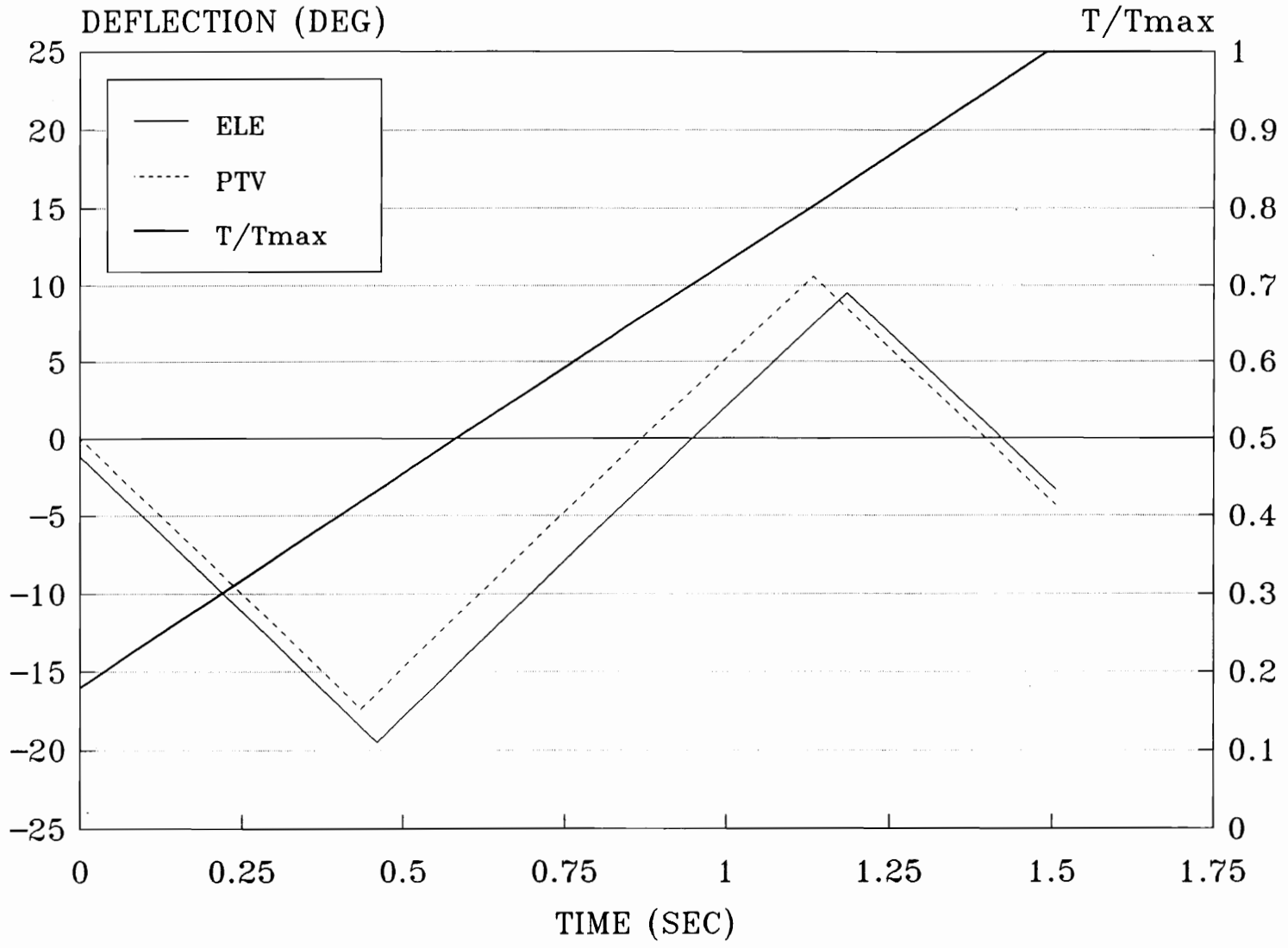

Figure 7. Longitudinal Control vs Time; Pitch-up at 0.35M; with T/V

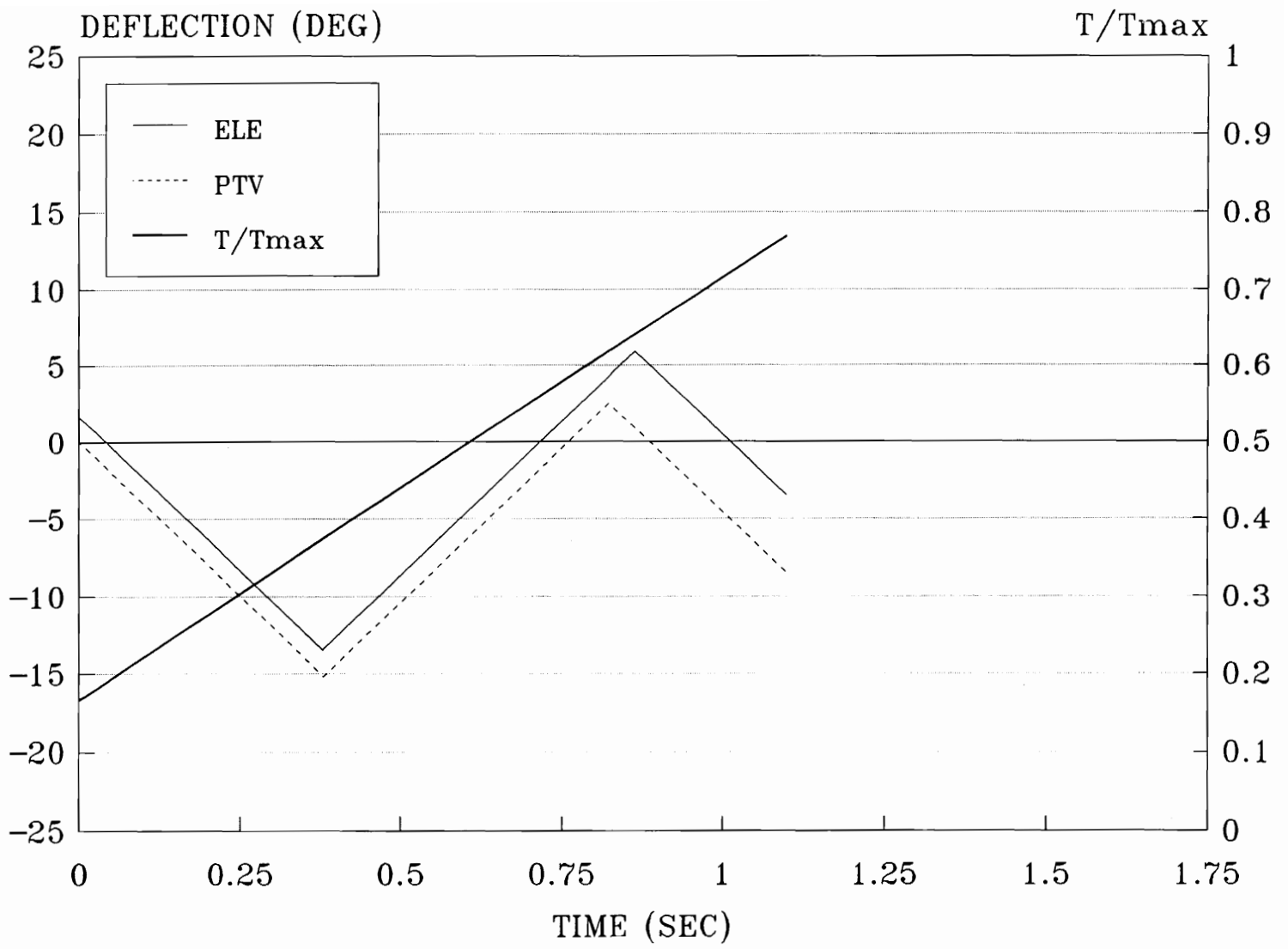

Figure 8. Longitudinal Control vs Time; Pitch-up at 0.75M; with T/V

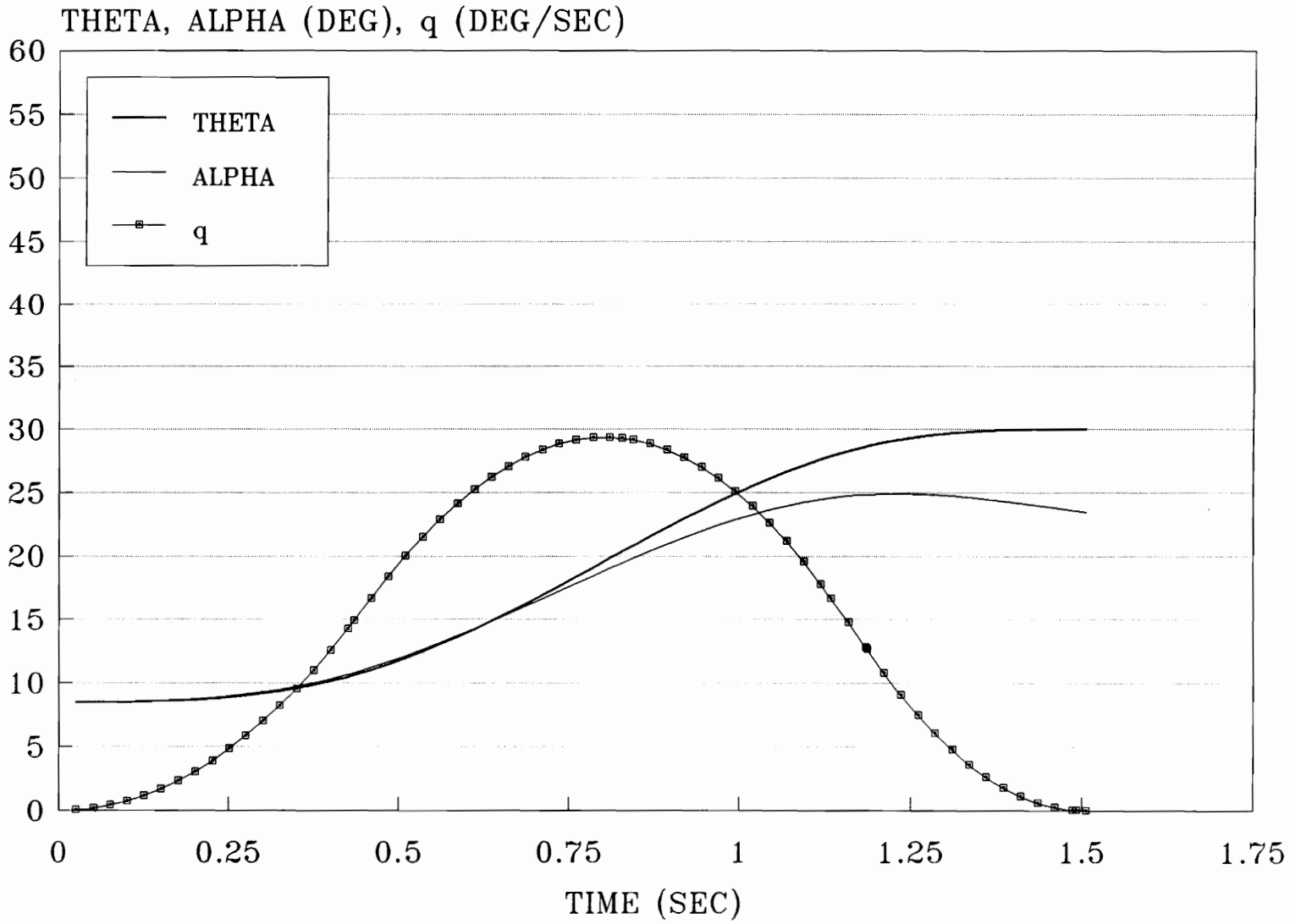

Figure 9. Longitudinal State vs Time; Pitch-up at 0.35M; with T/V

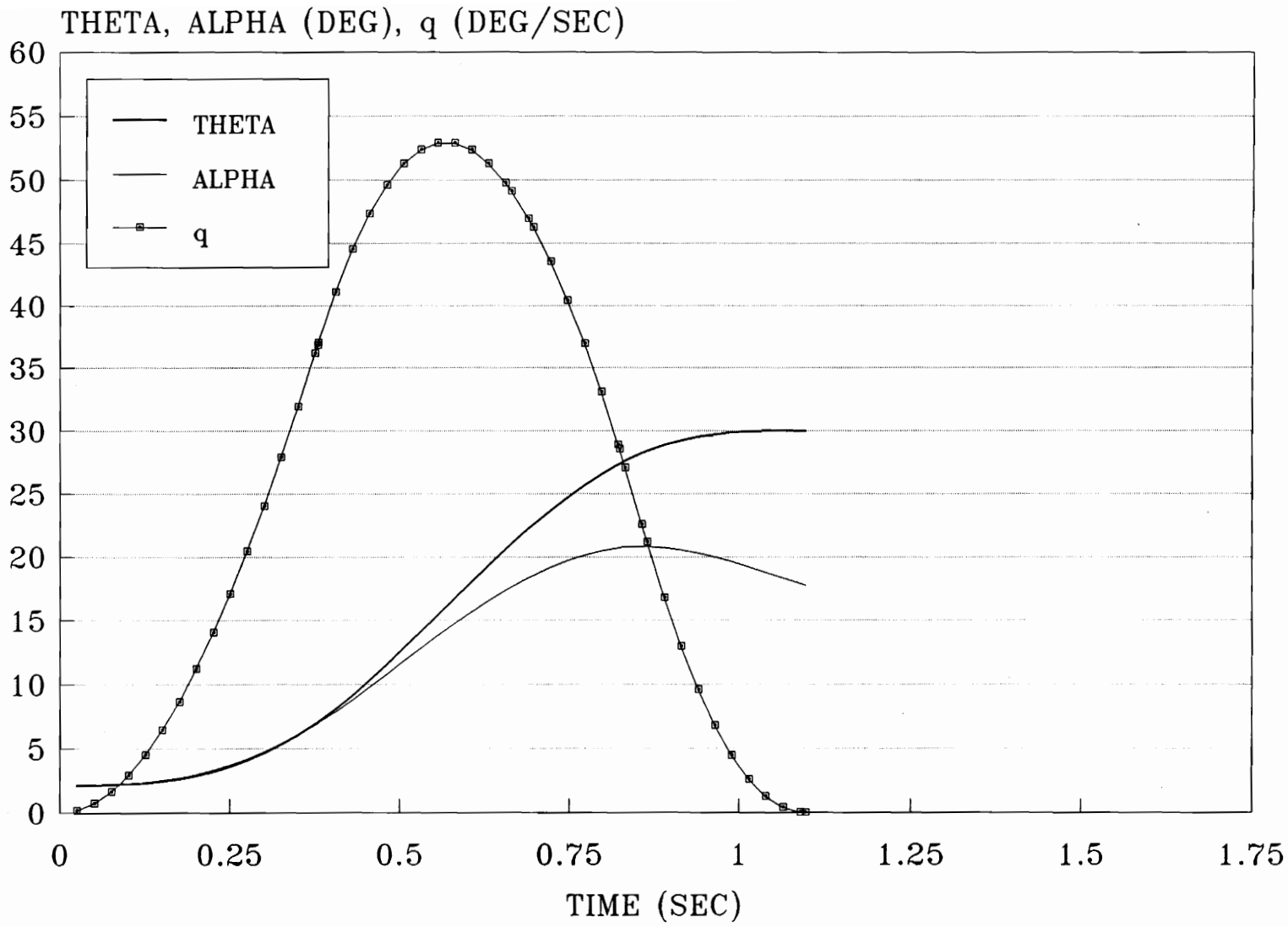

Figure 10. Longitudinal State vs Time; Pitch-up at 0.75M; with T/V

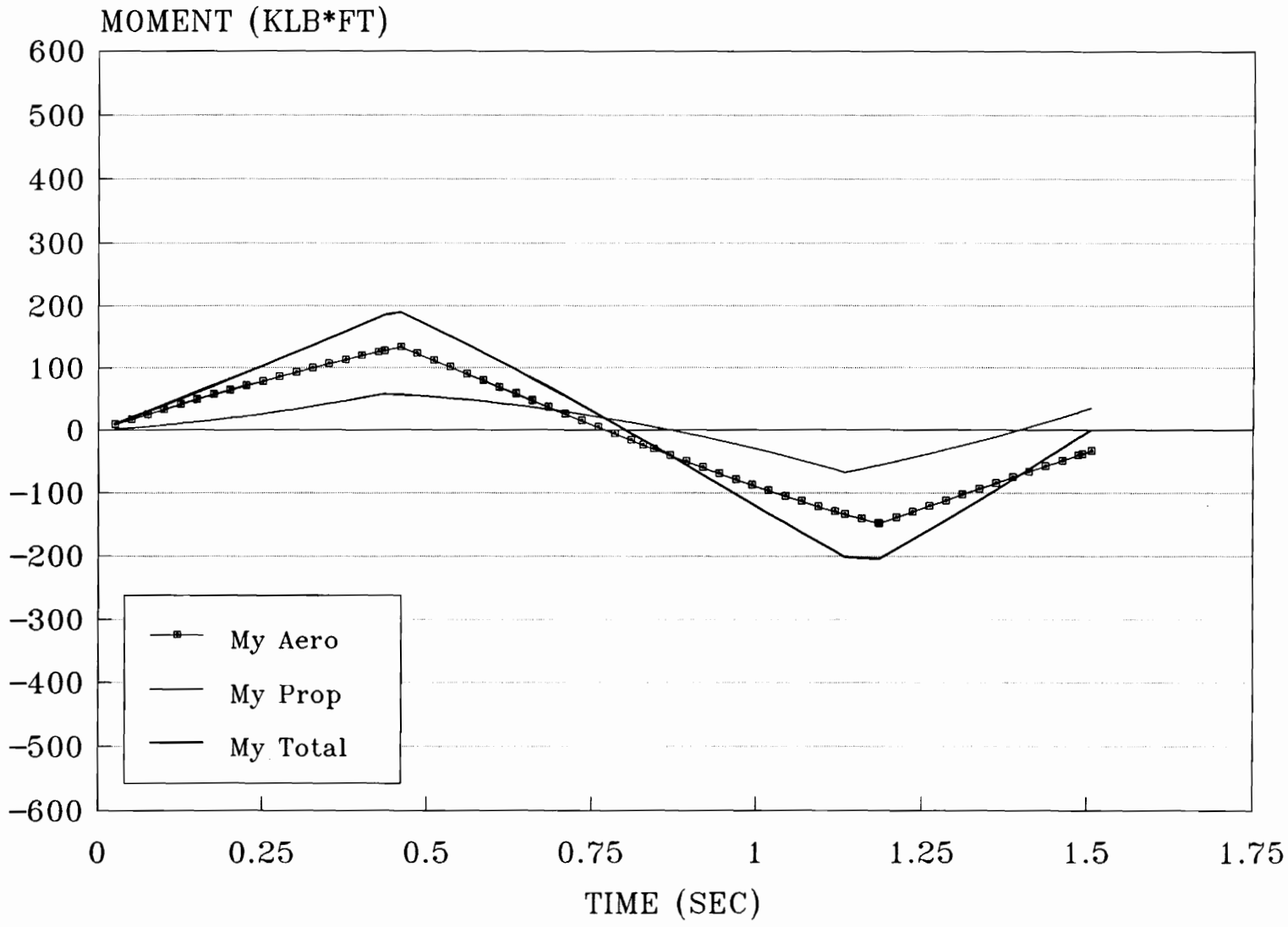

Figure 11. Pitch Moment vs Time; Pitch-up at 0.35M; with T/V

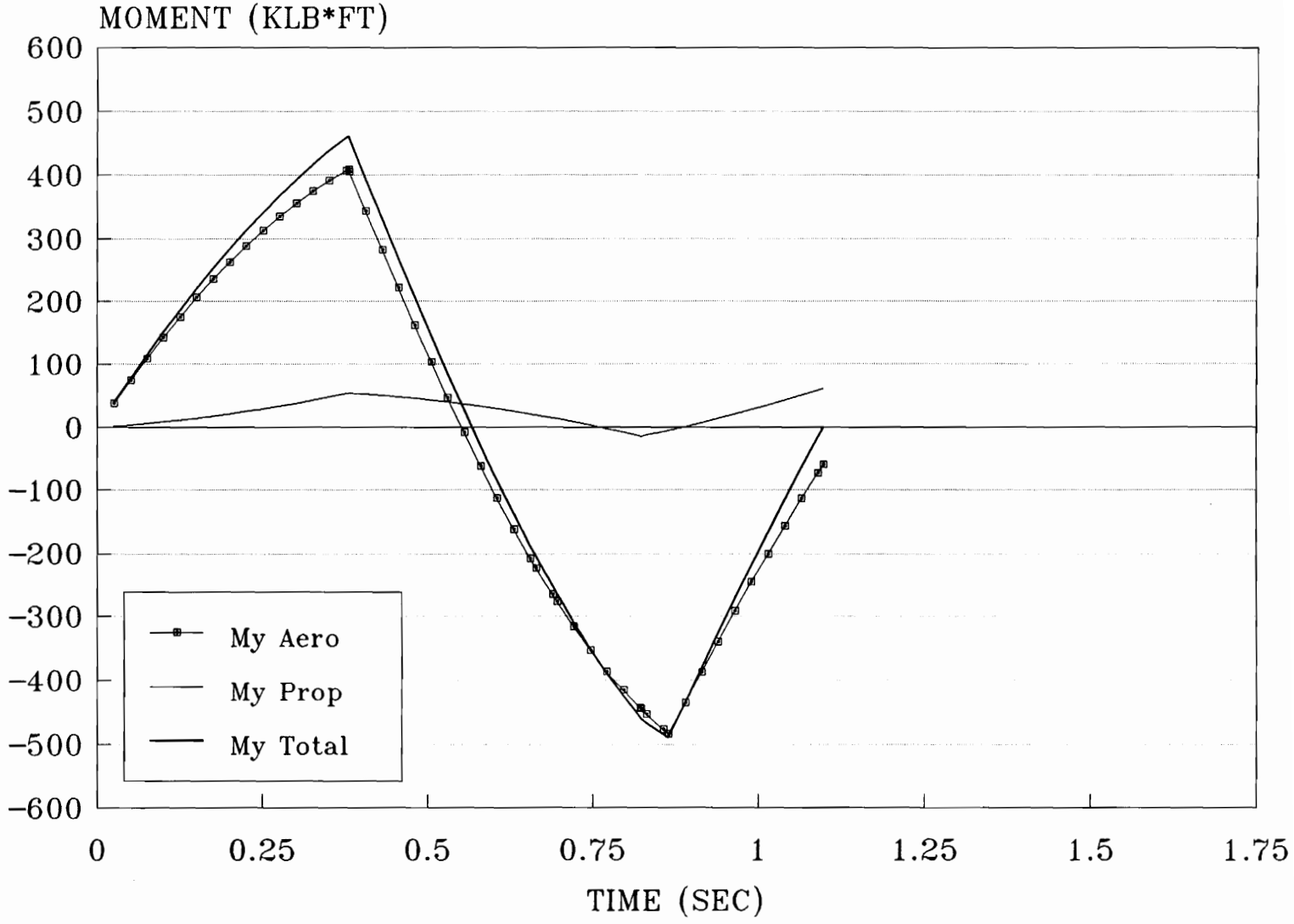

Figure 12. Pitch Moment vs Time; Pitch-up at 0.75M; with T/V

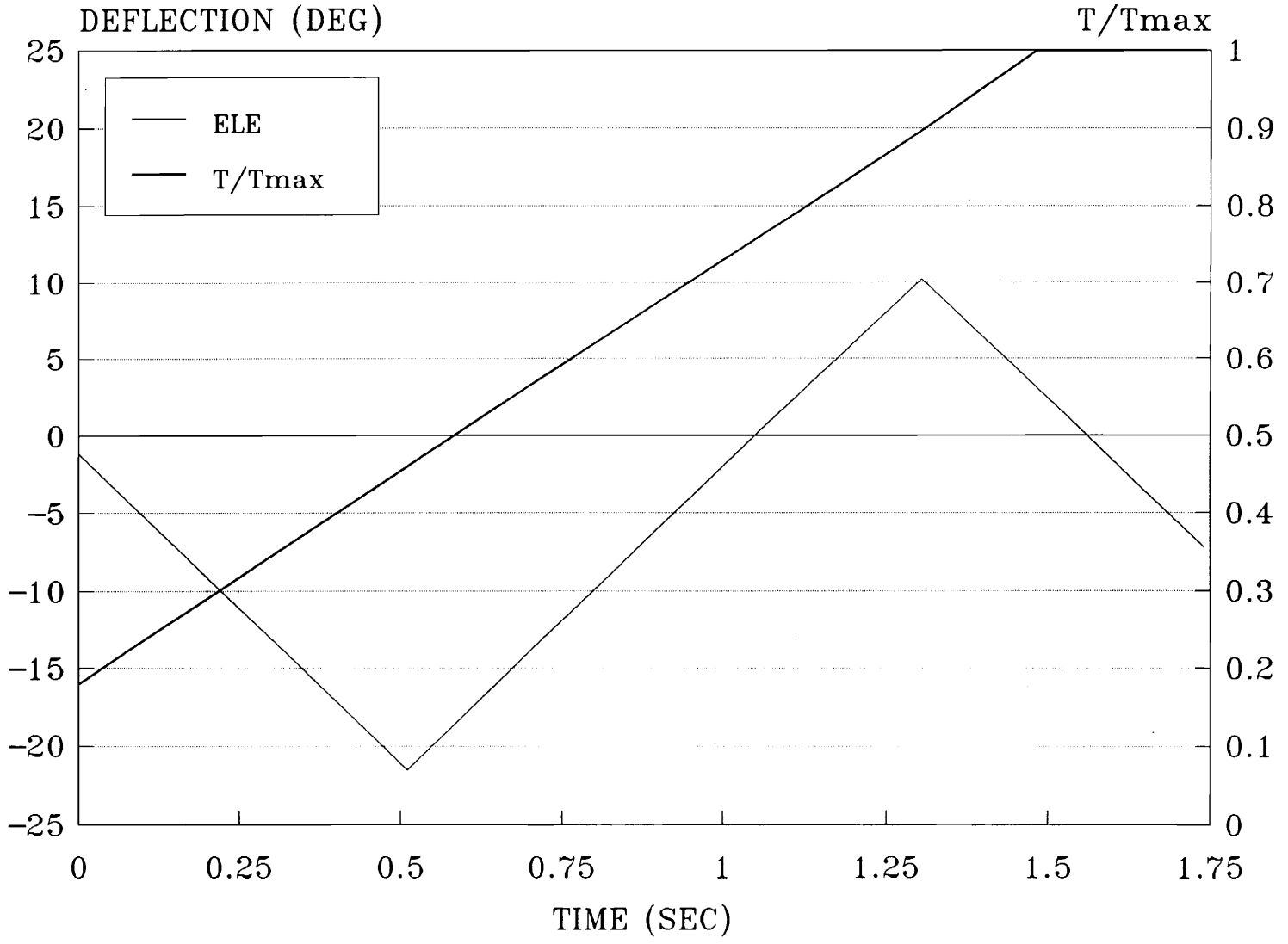

Figure 13. Longitudinal Control vs Time; Pitch-up at 0.35M; no T/V

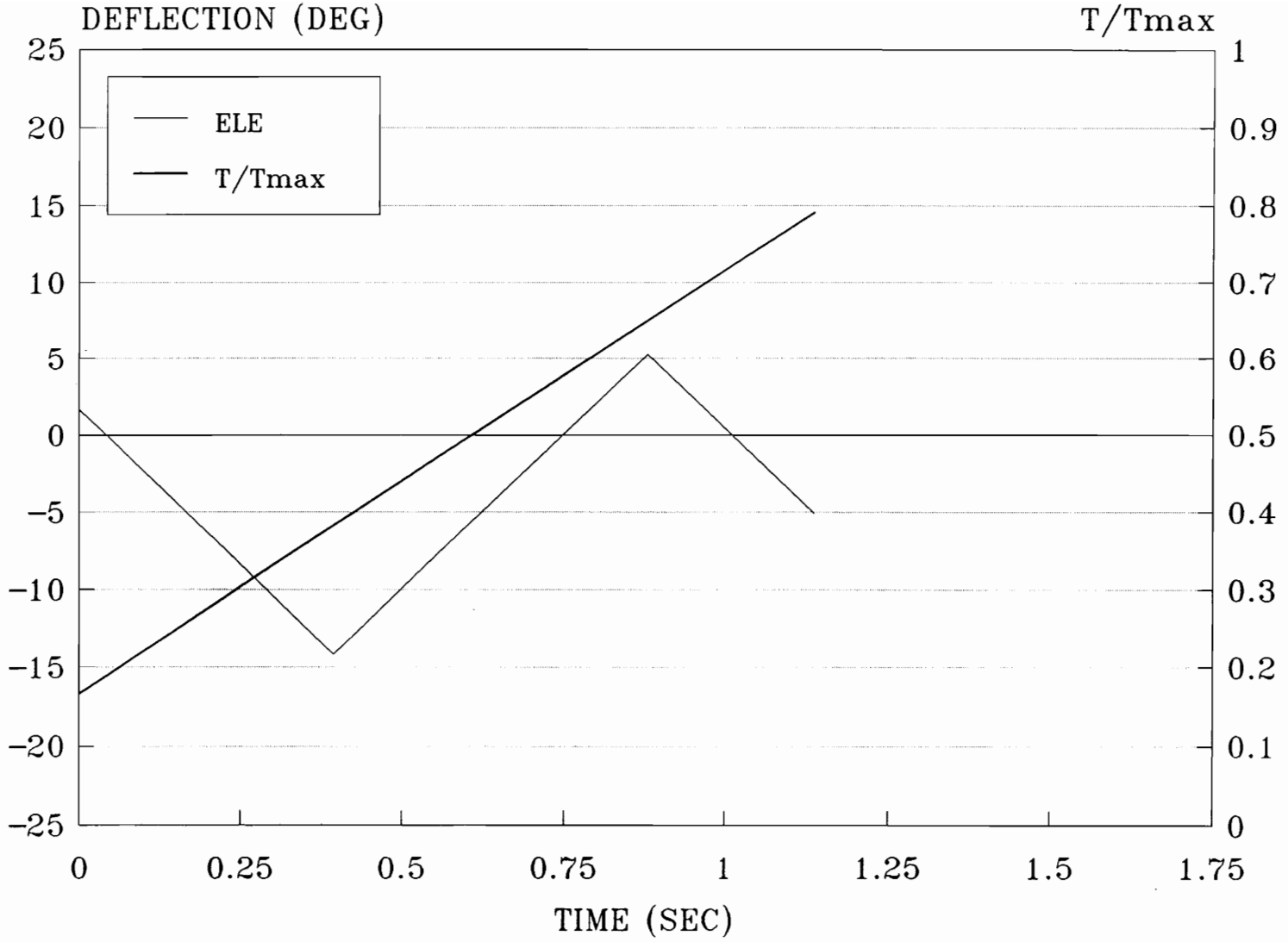

Figure 14. Longitudinal Control vs Time; Pitch-up at 0.75M; no T/V

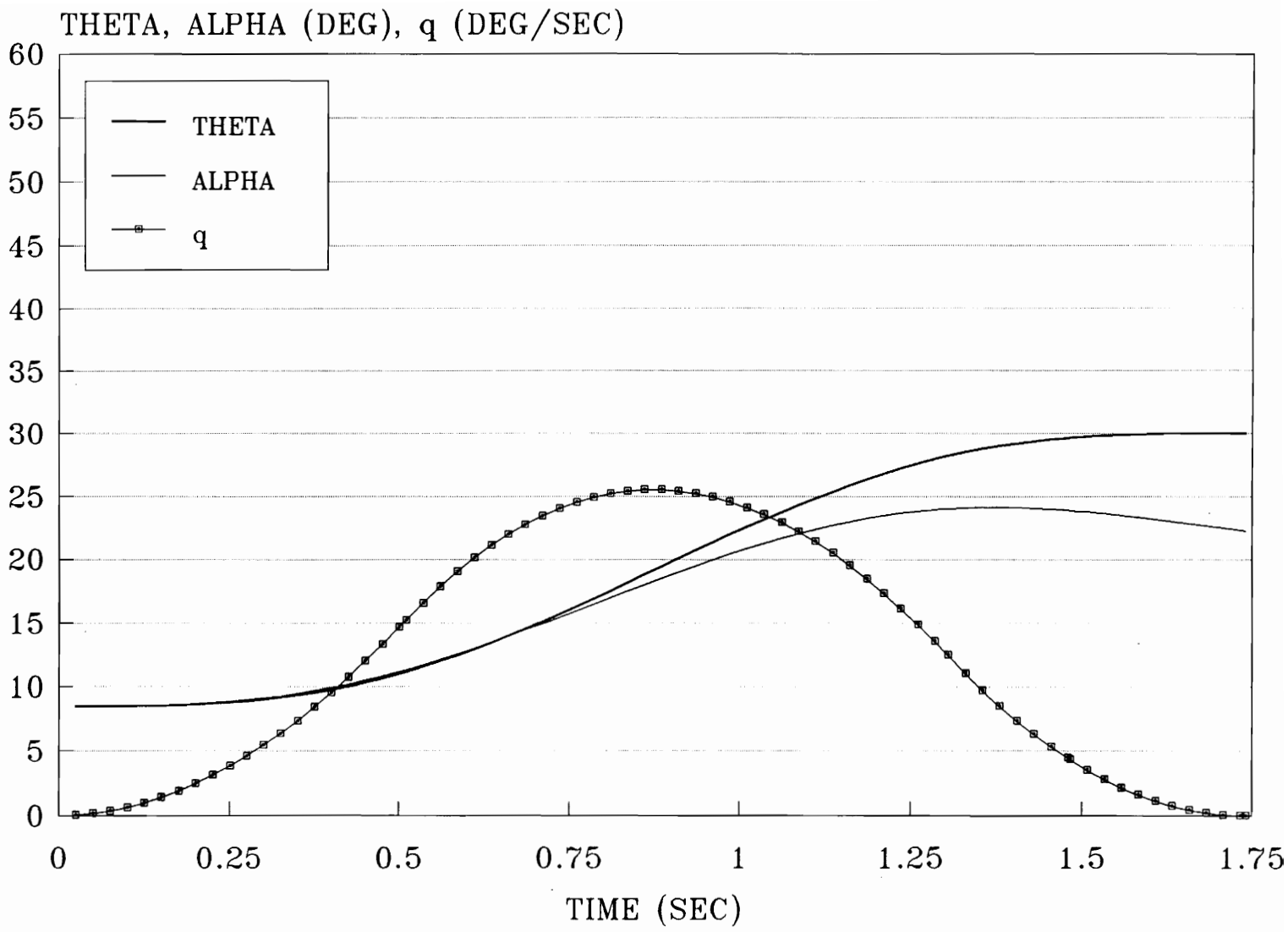

Figure 15. Longitudinal State vs Time; Pitch-up at 0.35M; no T/V

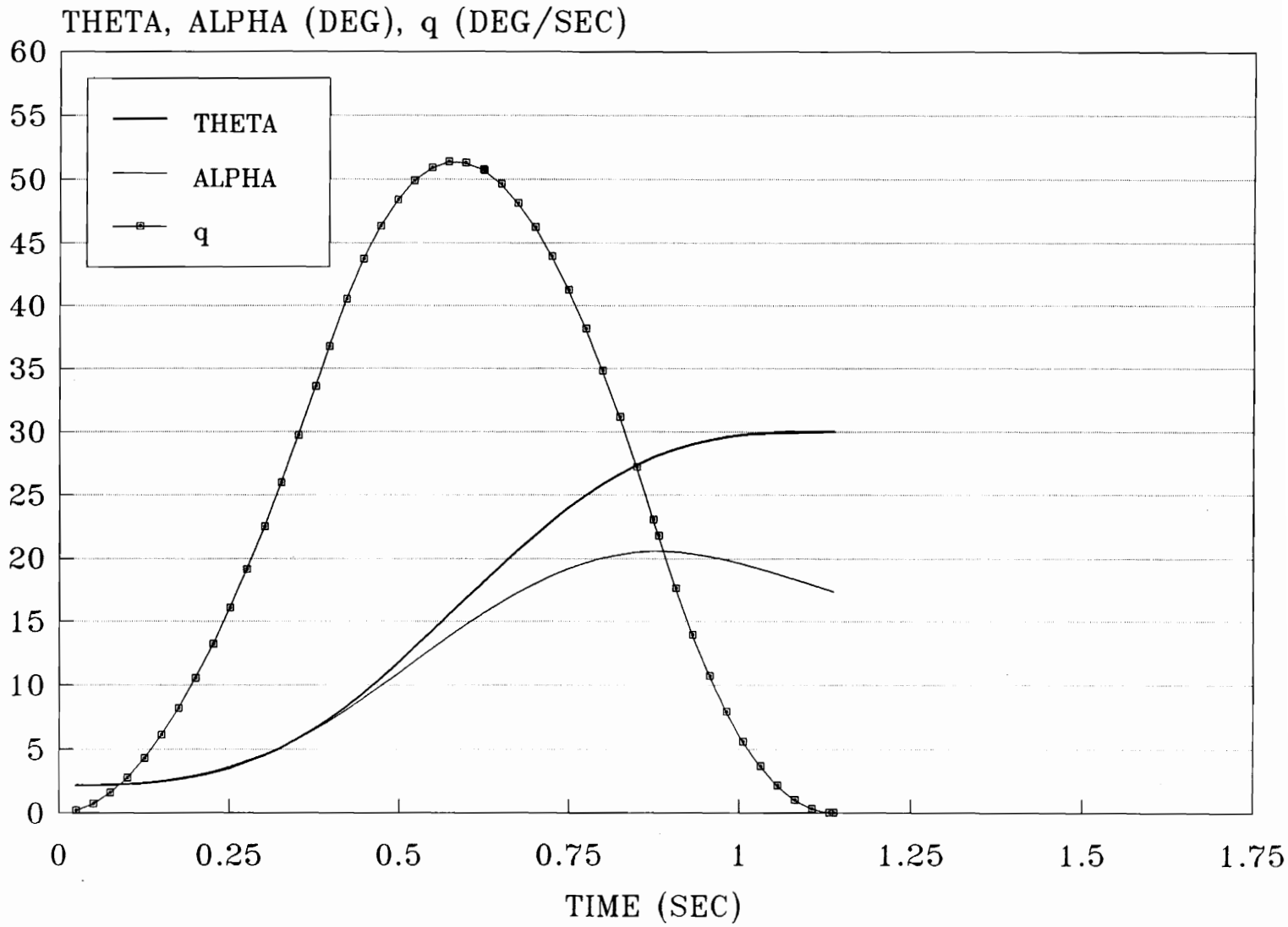

Figure 16. Longitudinal State vs Time; Pitch-up at 0.75M; no T/V

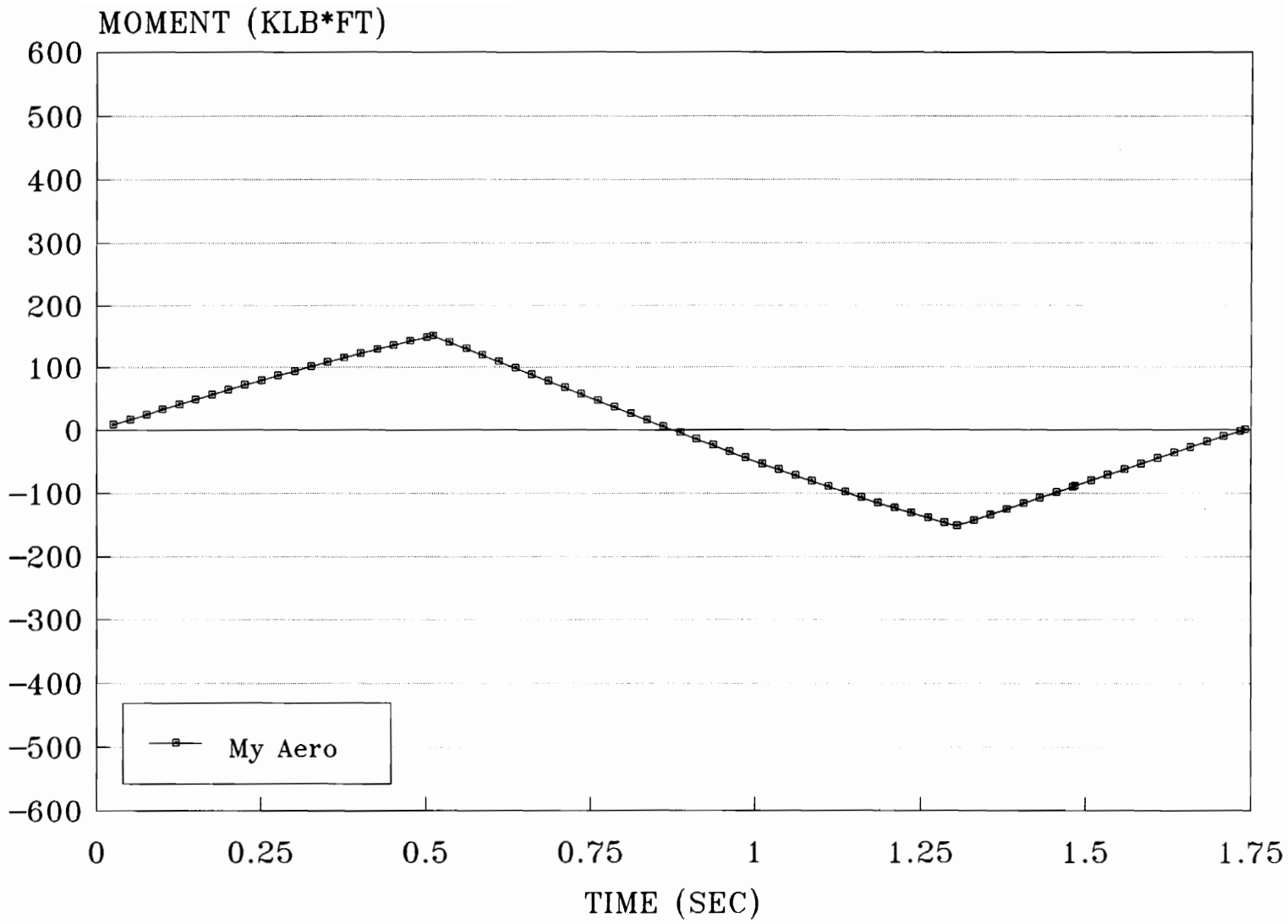

Figure 17. Pitch Moment Components vs Time; Pitch-up at 0.35M; no T/V

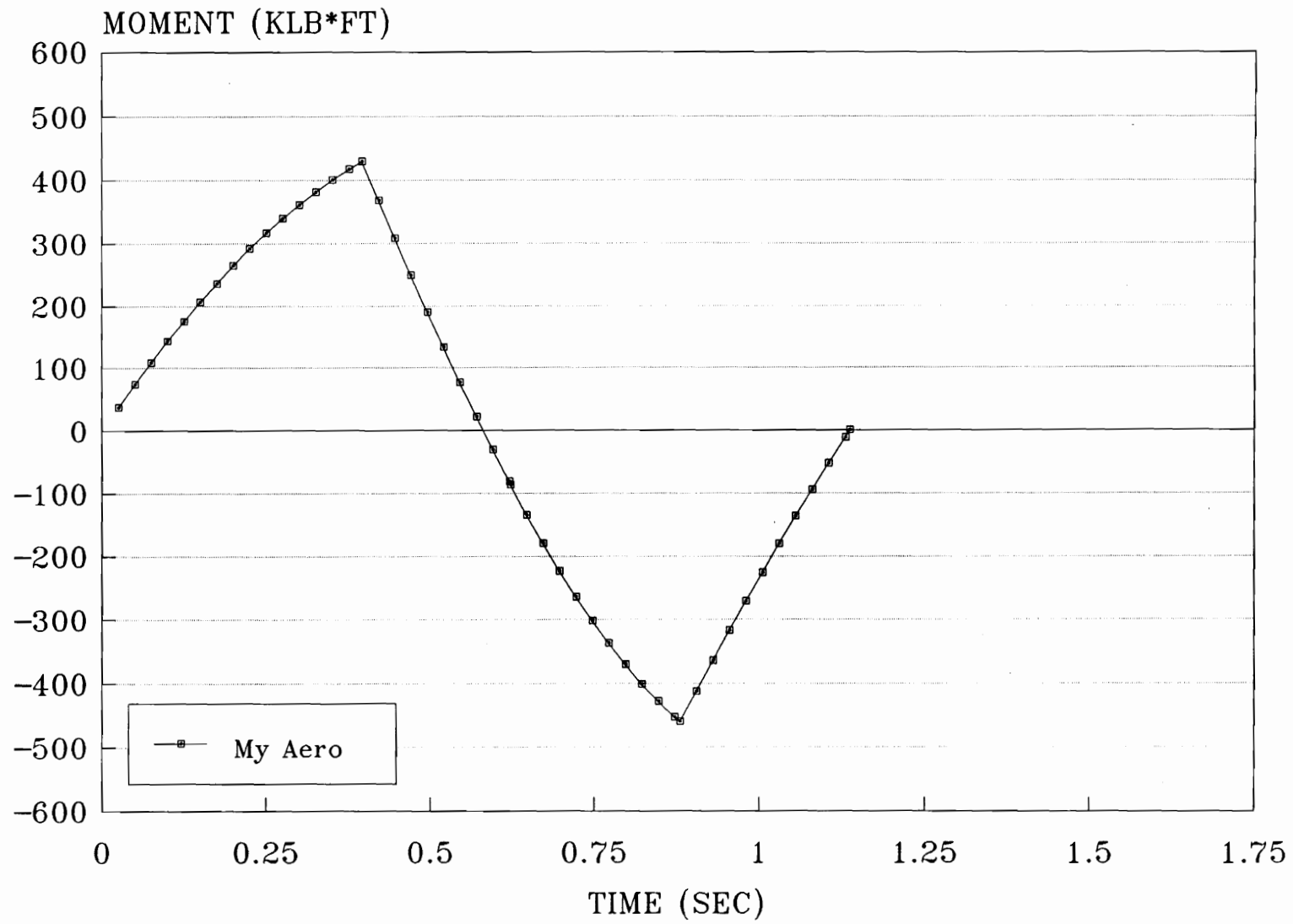

Figure 18. Pitch Moment Components vs Time; Pitch-up at 0.75M; no T/V

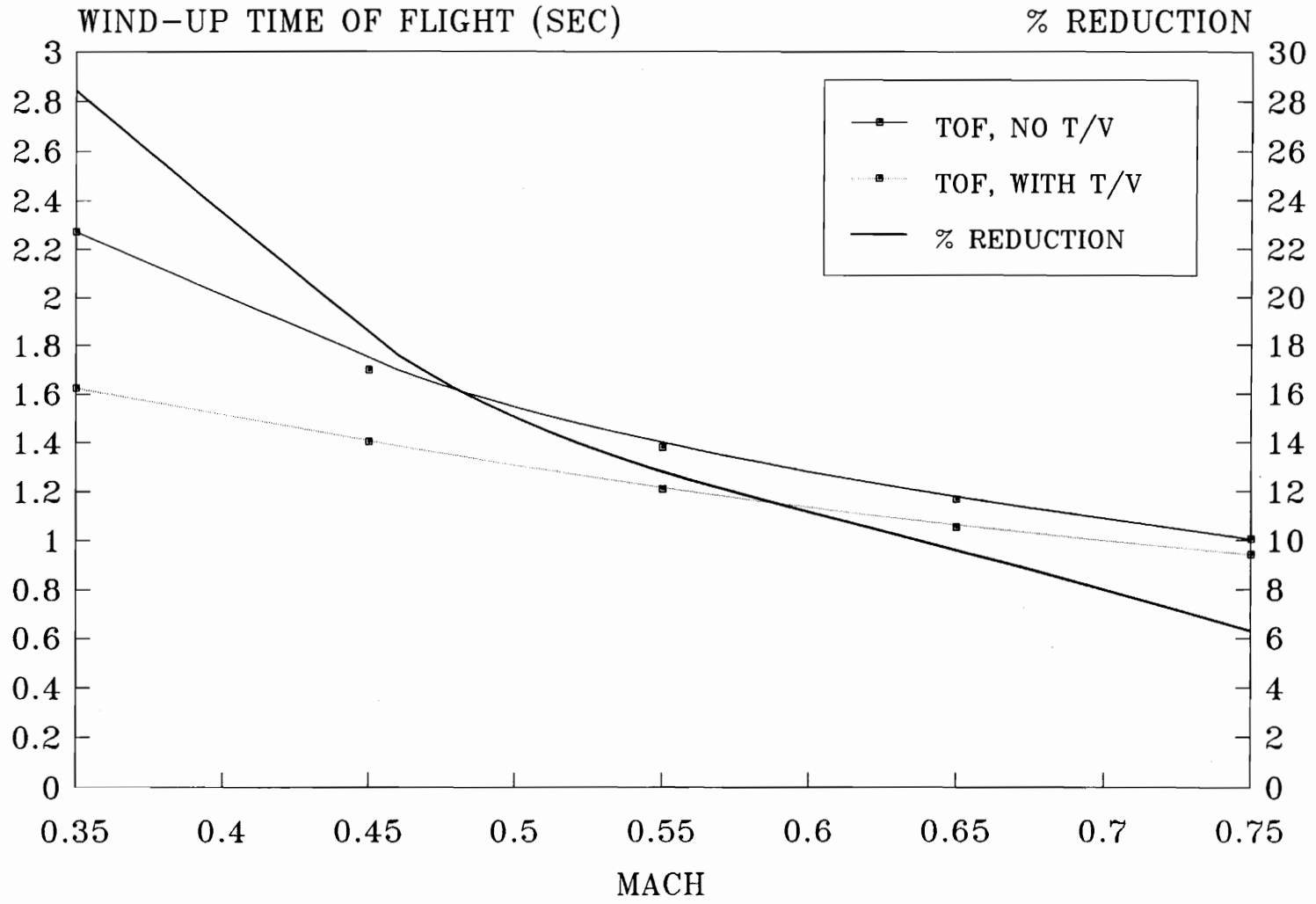

Figure 19. TOF vs M; Wind-up Maneuver

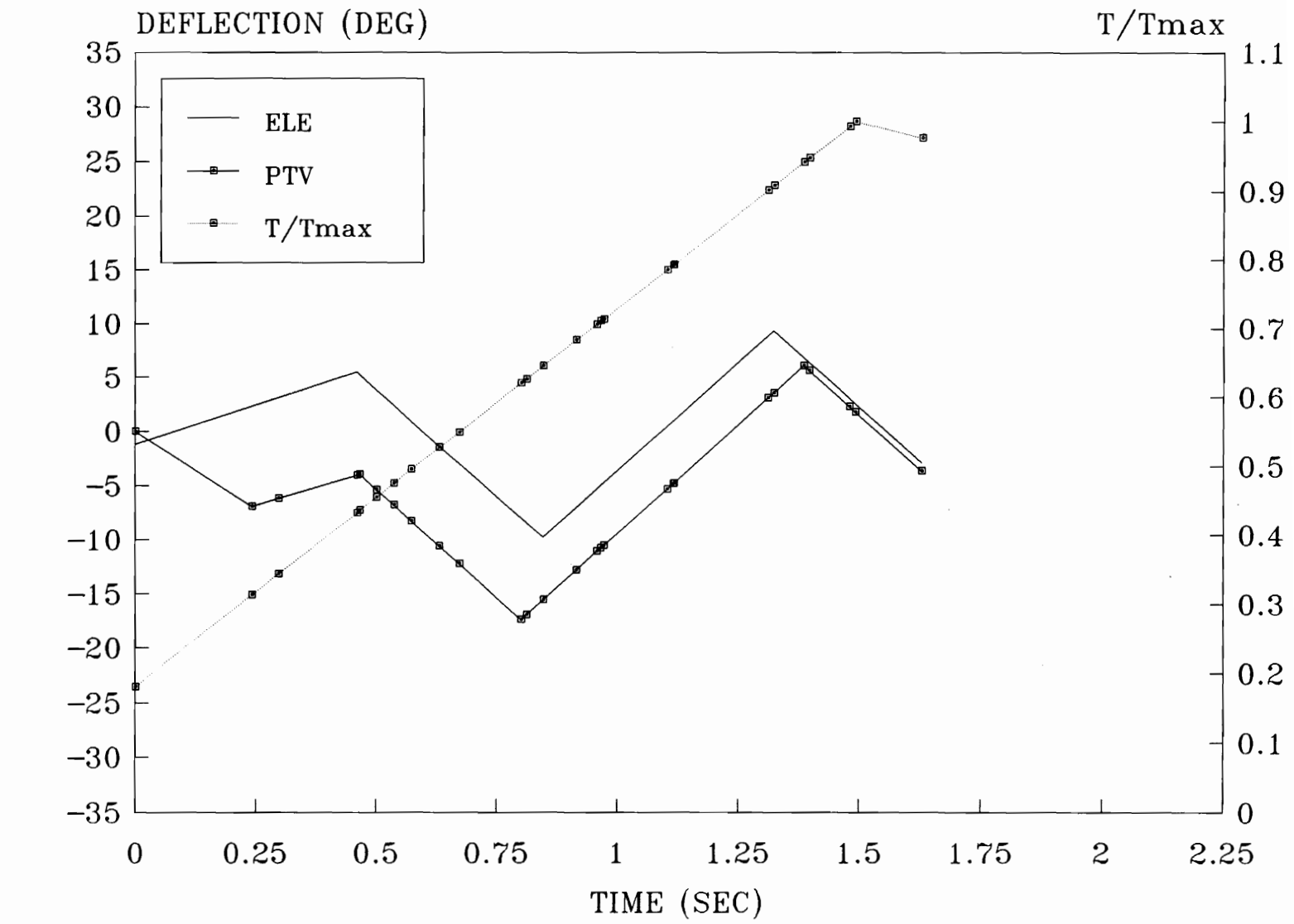

Figure 20. Longitudinal Control vs Time; Wind-up at 0.35M; with T/V

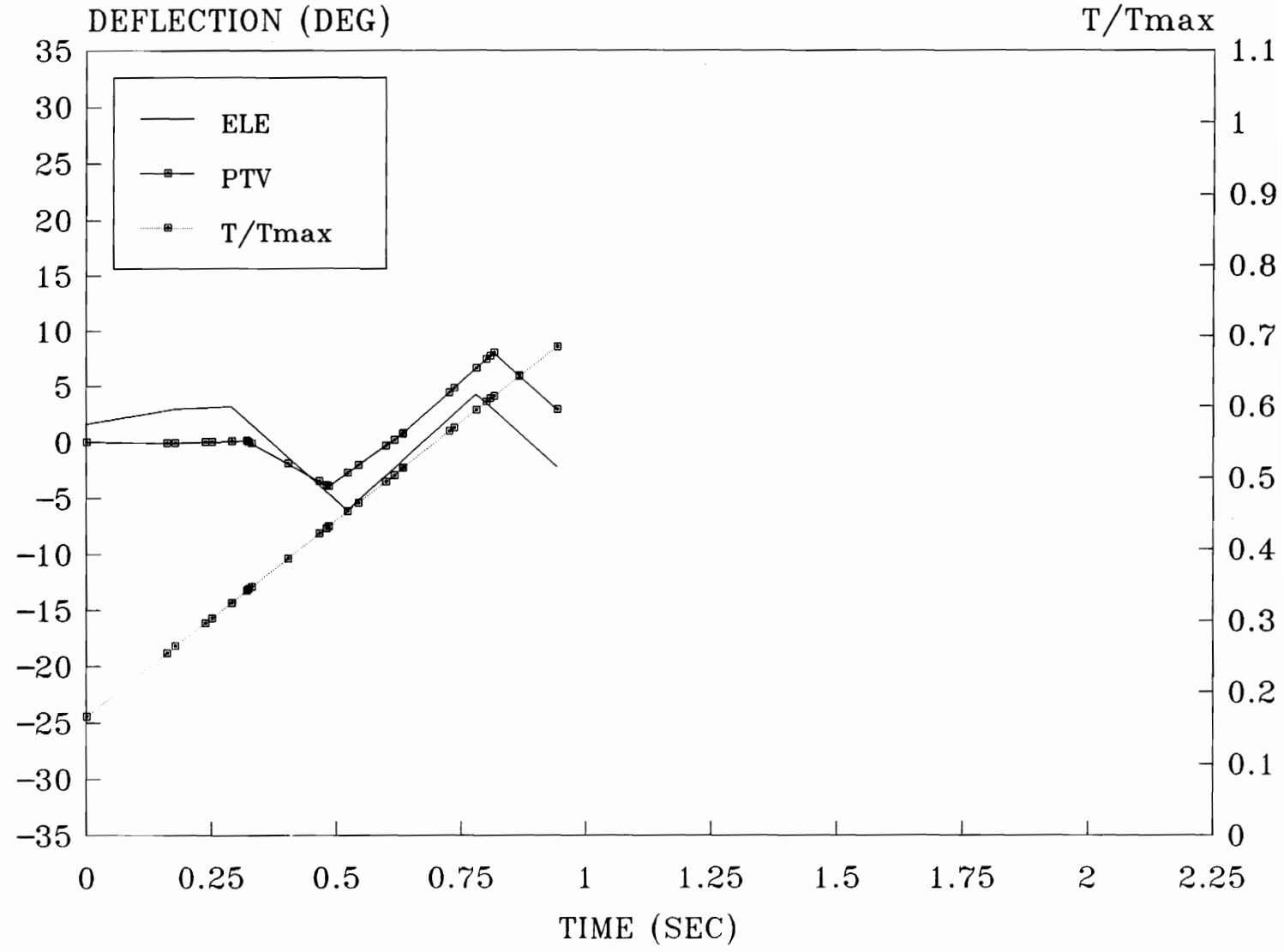

Figure 21. Longitudinal Control vs Time; Wind-up at 0.75M; with T/V

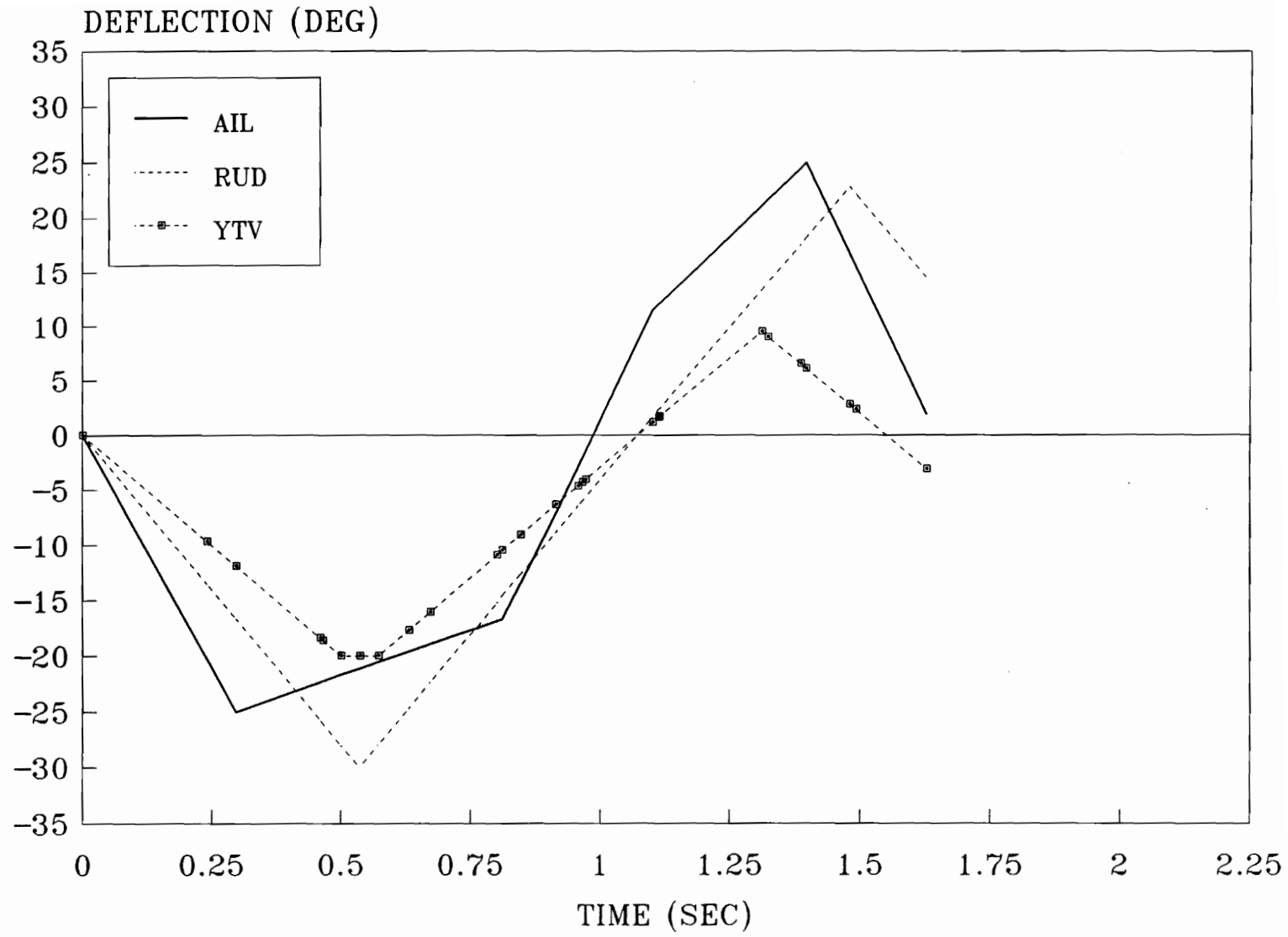

Figure 22. Lat-Dir Control vs Time; Wind-up at 0.35M; with T/V

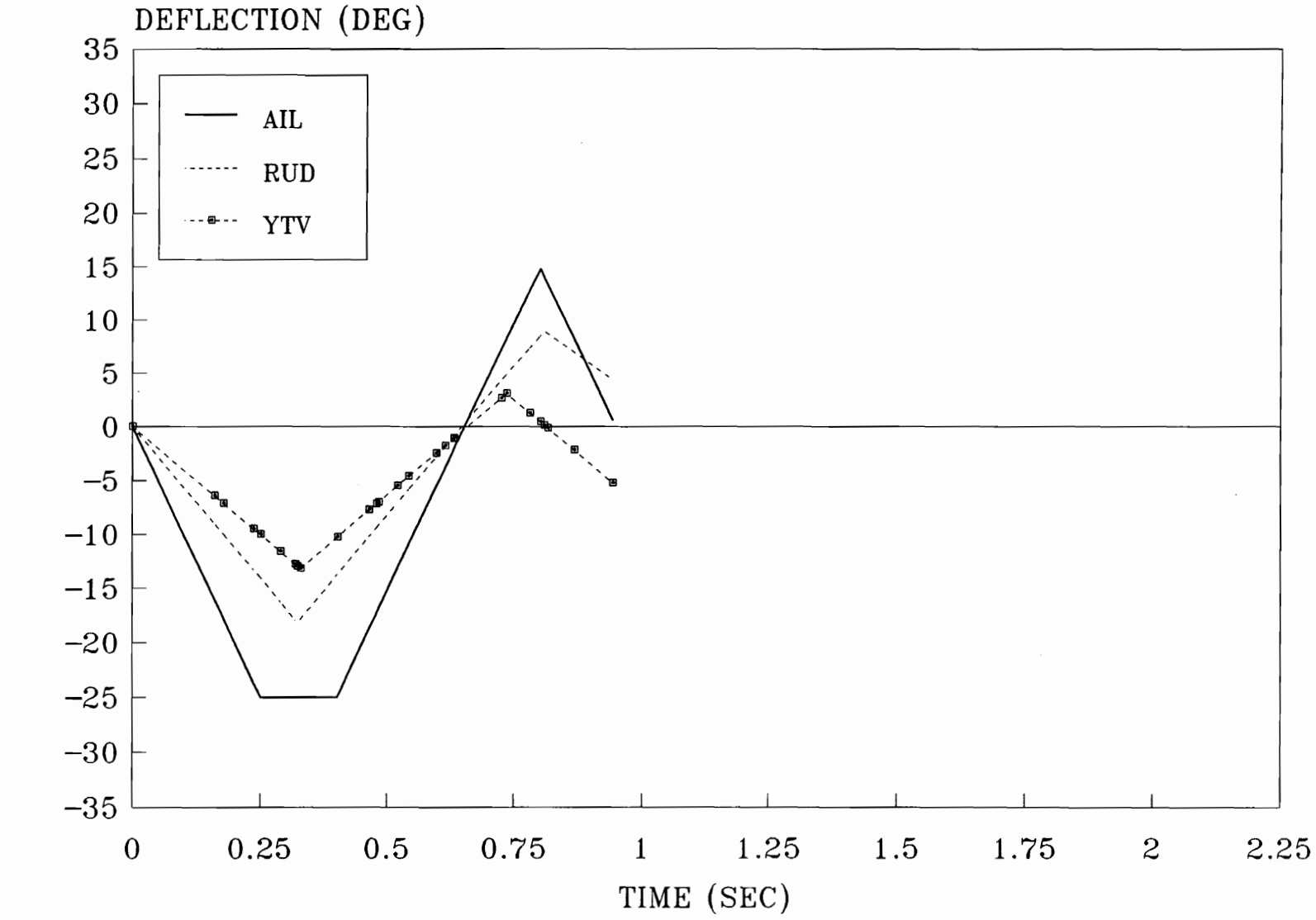

Figure 23. Lat-Dir Control vs Time; Wind-up at 0.75M; with T/V

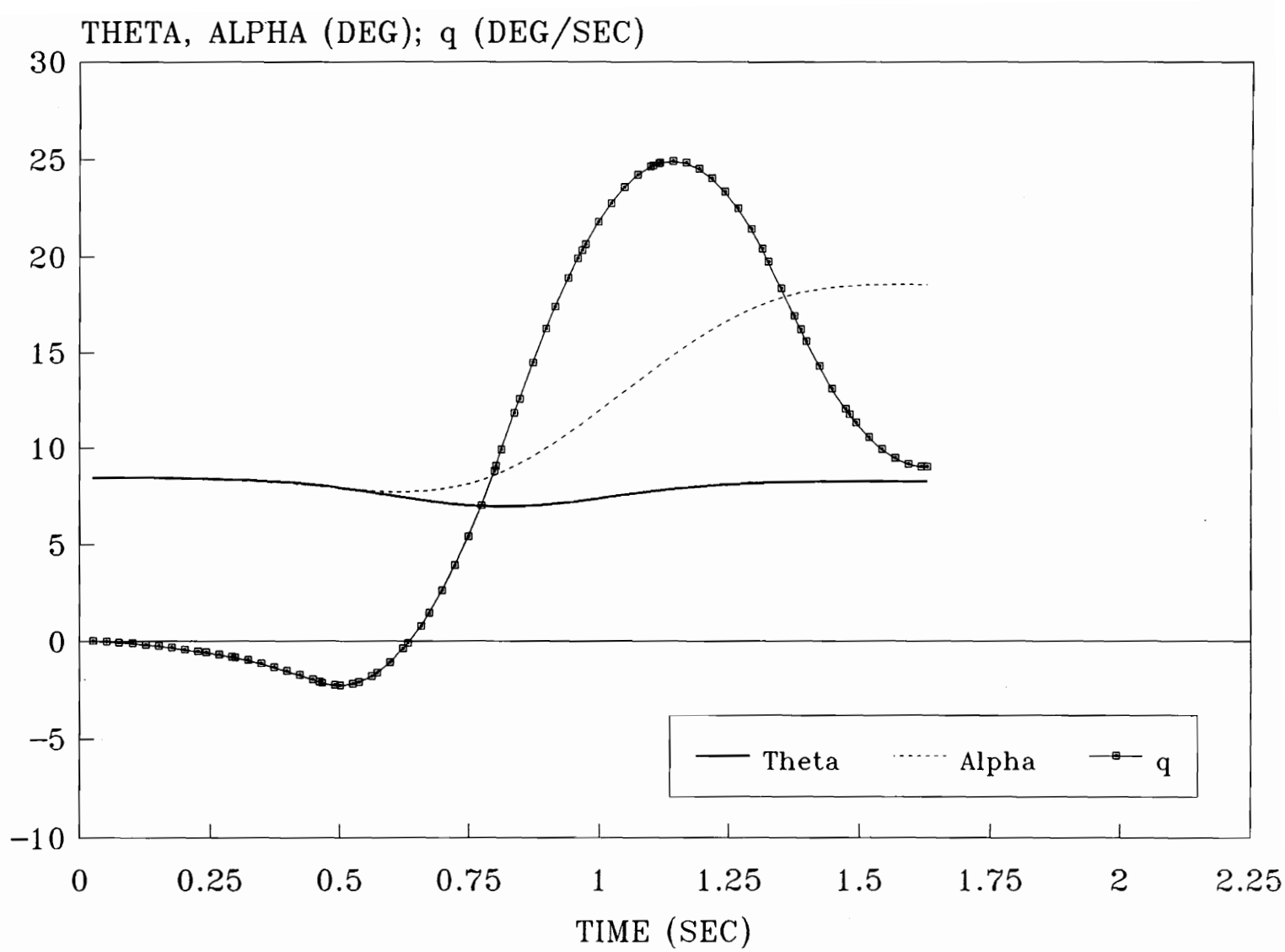

Figure 24. Longitudinal State vs Time; Wind-up at 0.35M; with T/V

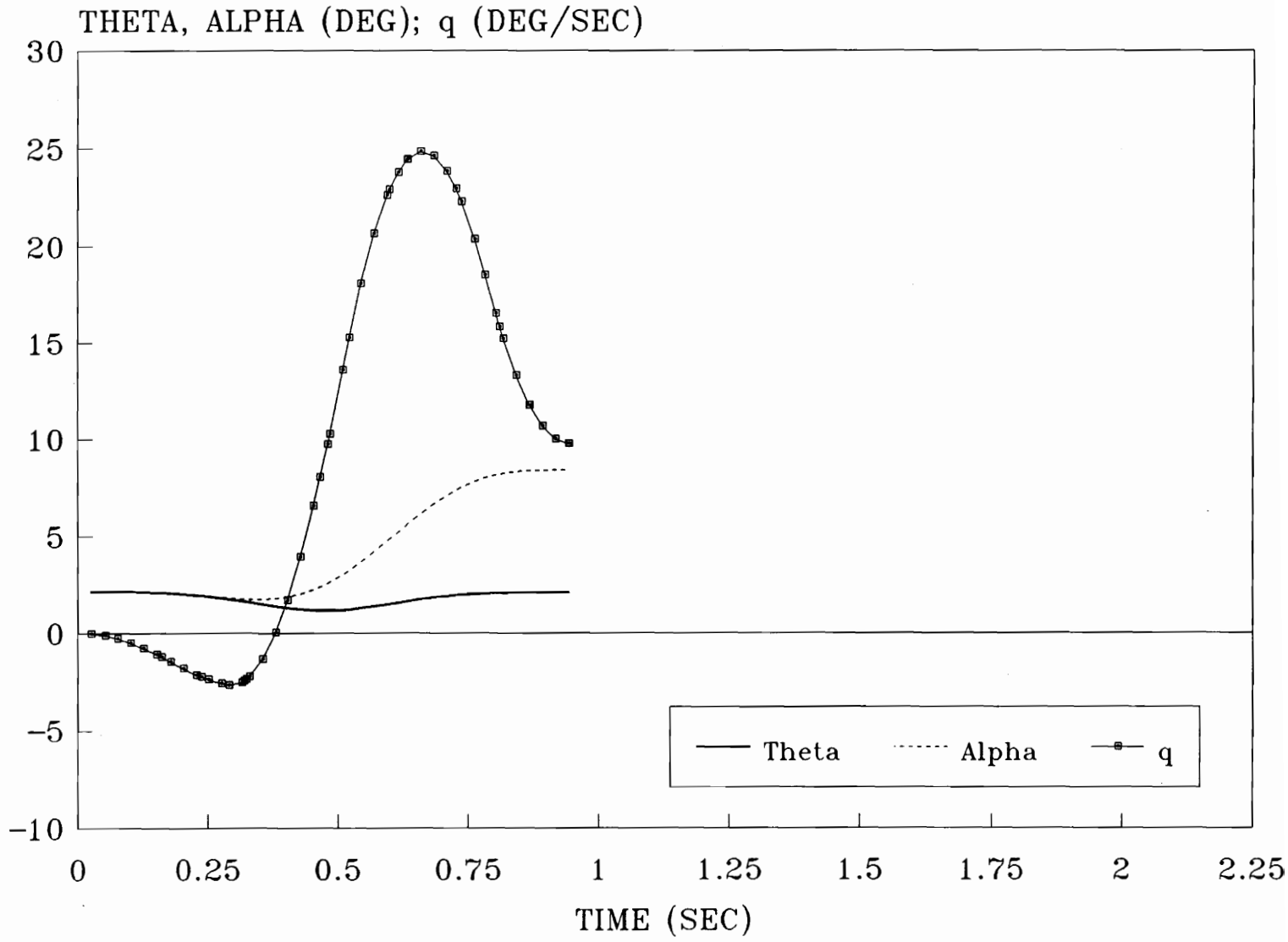

Figure 25. Longitudinal State vs Time; Wind-up at 0.75M; with T/V

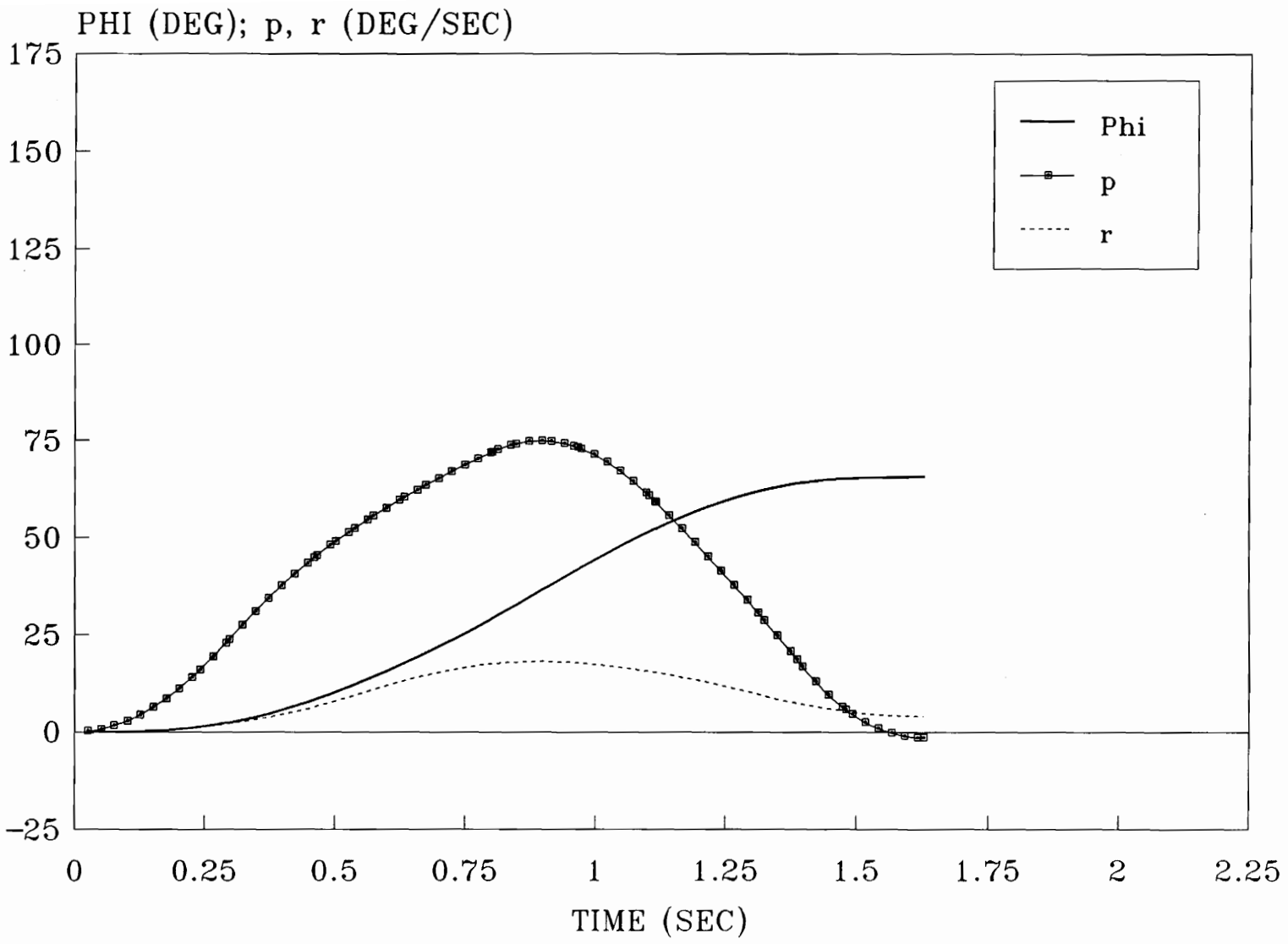

Figure 26. Lat-Dir State vs Time; Wind-up at 0.35M; with T/V

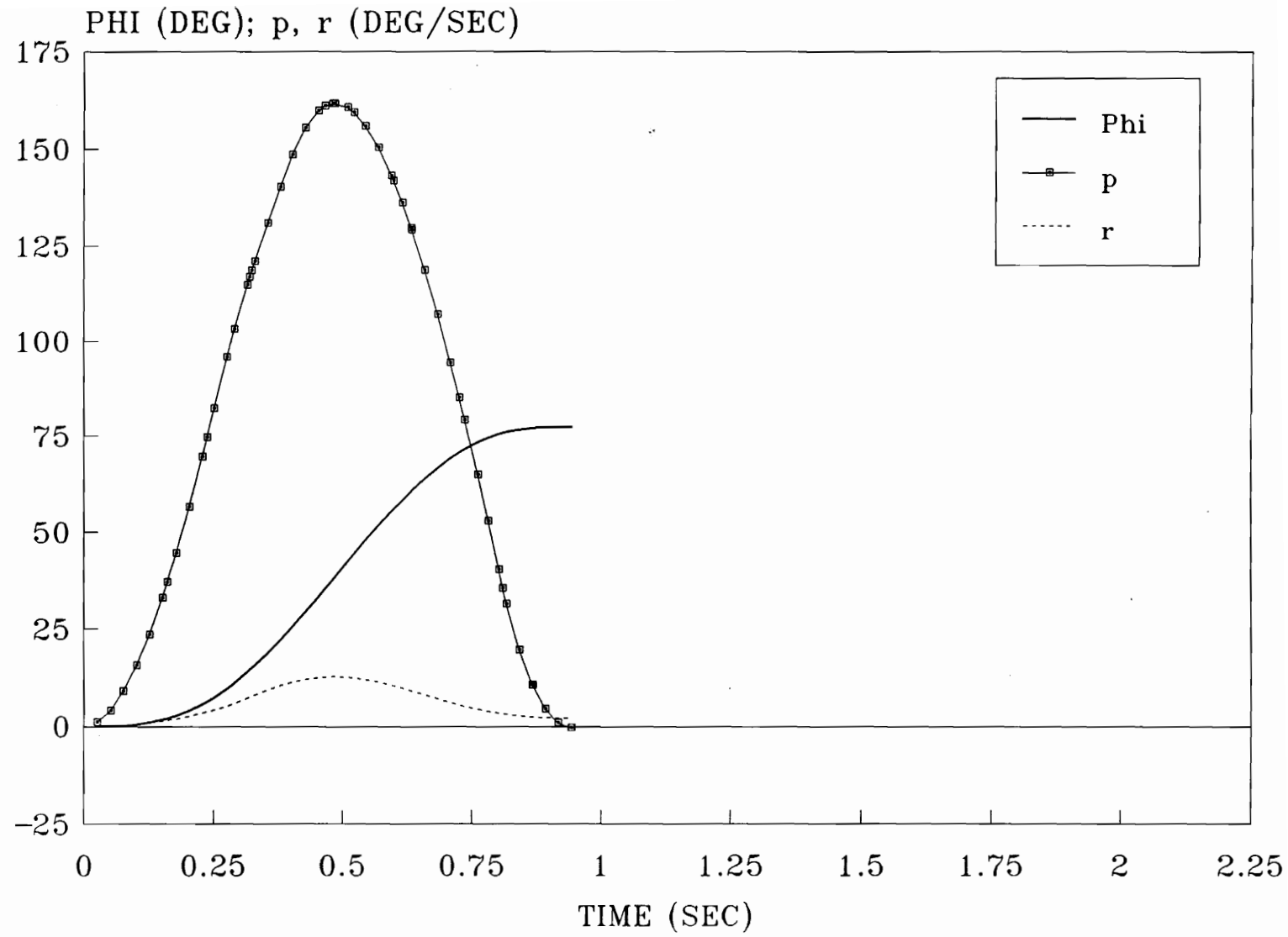

Figure 27. Lat-Dir State vs Time; Wind-up at 0.75M; with T/V

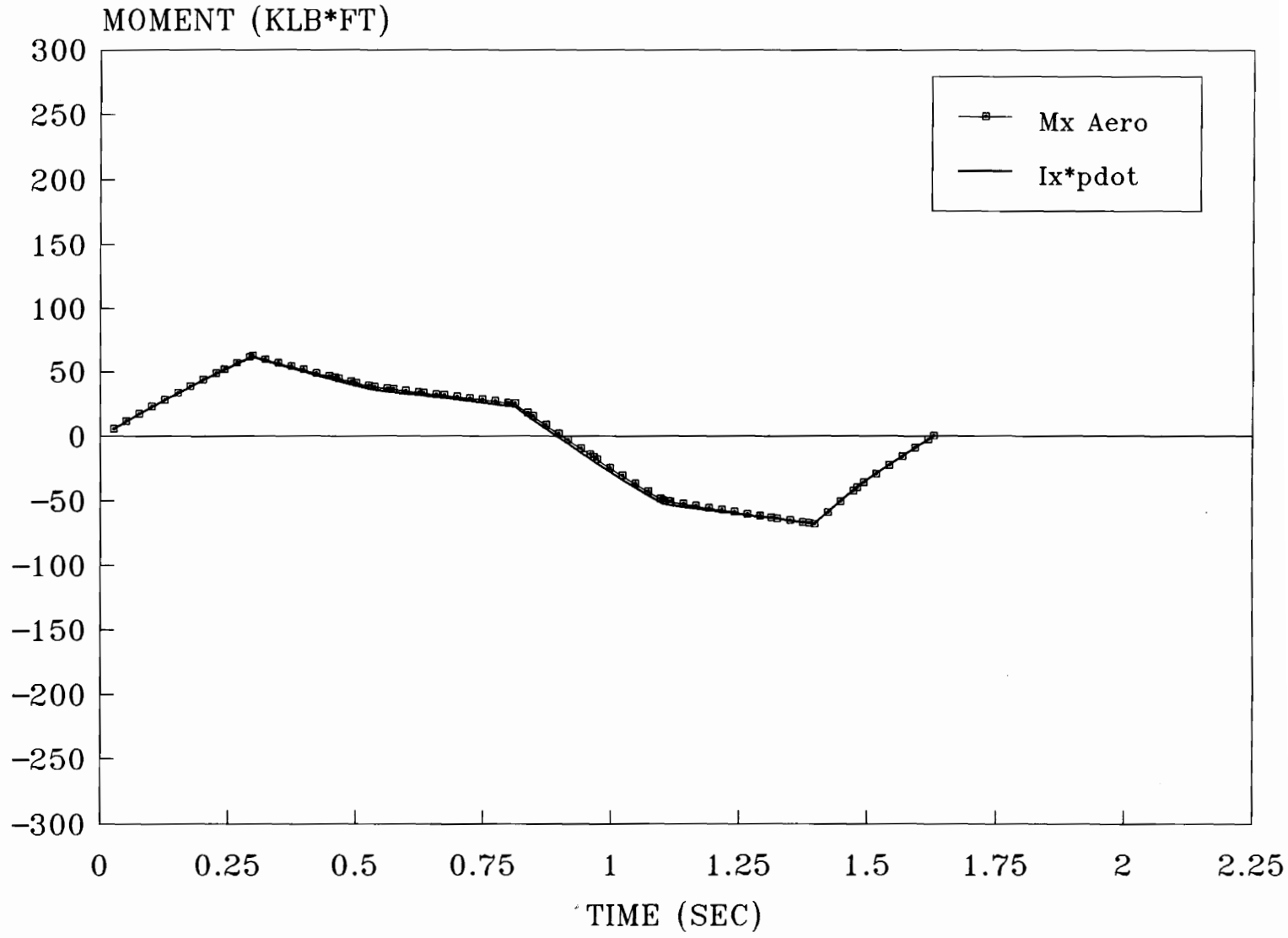

77

NW01E

Figure 28. Roll Moment vs Time; Wind-up at 0.35M; with T/V

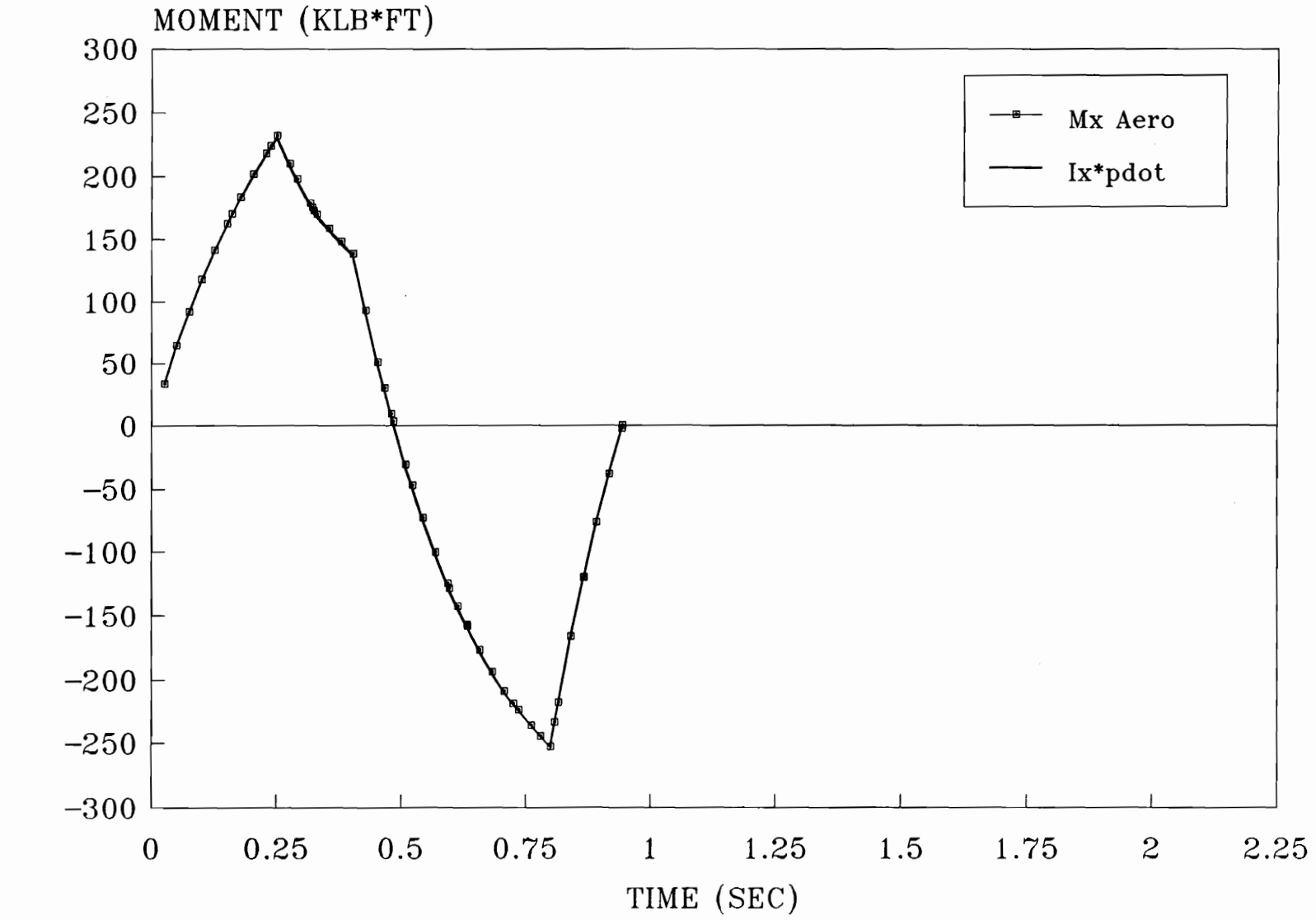

Figure 29. Roll Moment vs Time; Wind-up at 0.75M; with T/V

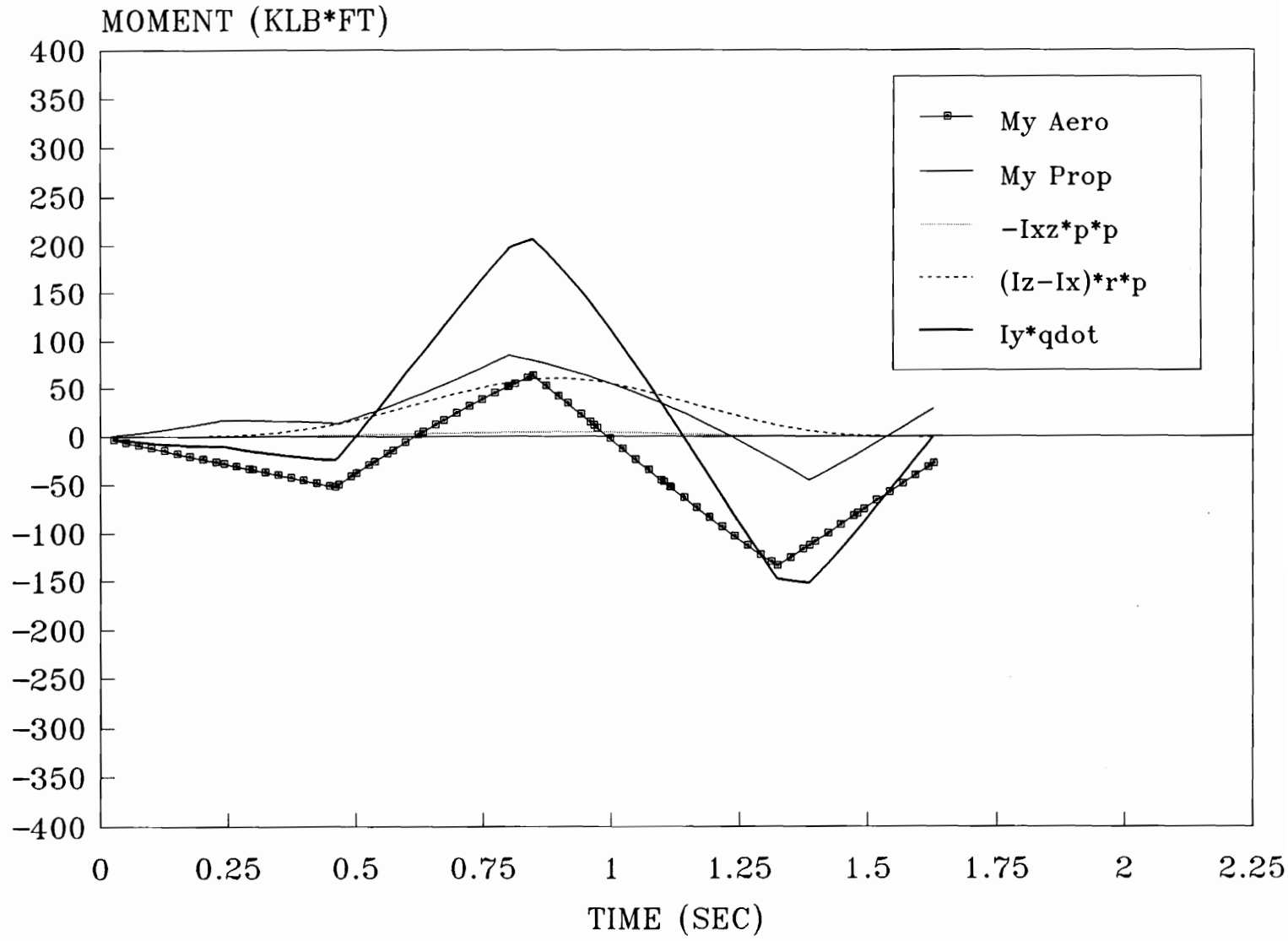

NWOLE

Figure 30. Pitch Moment vs Time; Wind-up at 0.35M; with T/V

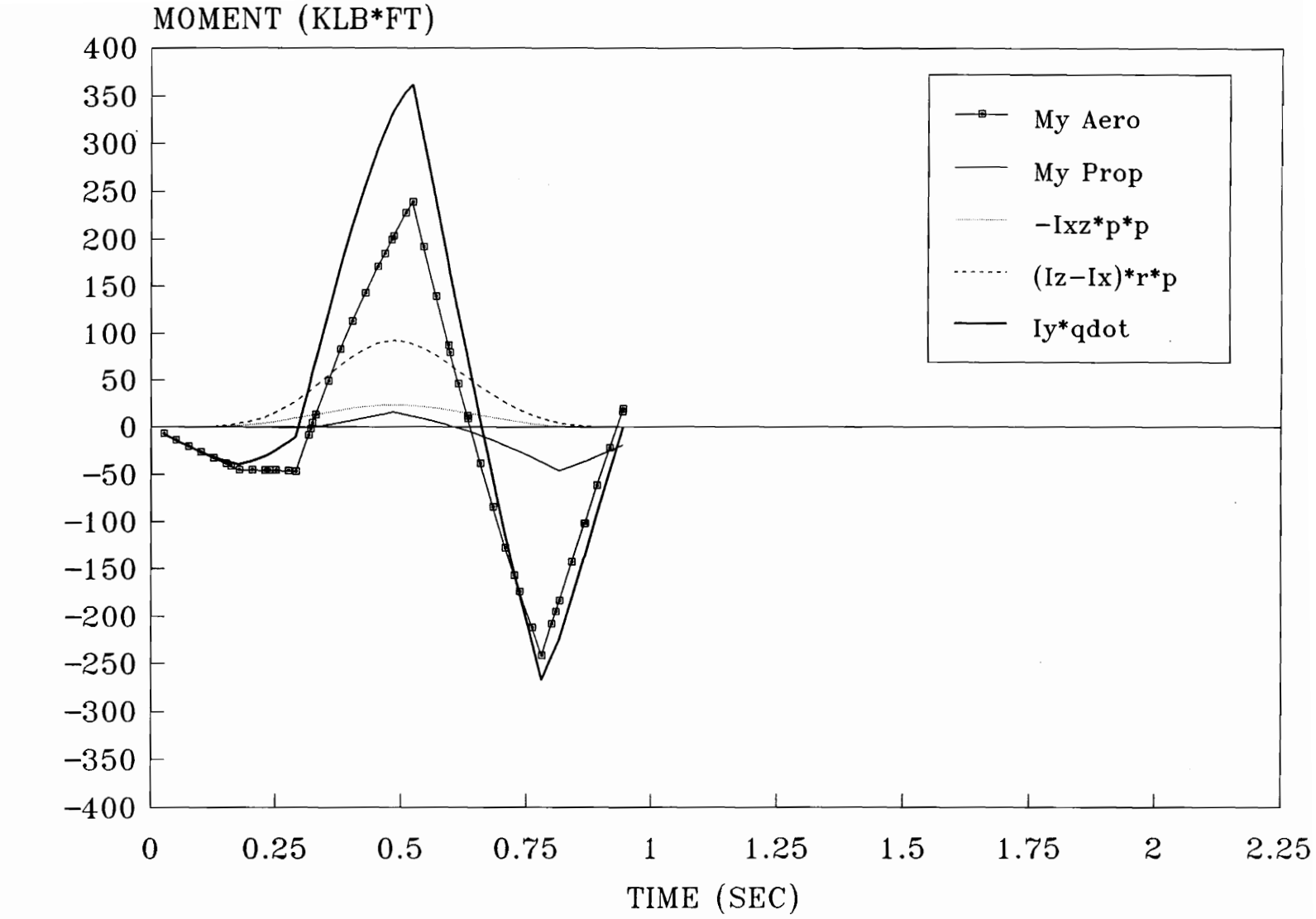

Figure 31. Pitch Moment vs Time; Wind-up at 0.75M; with T/V

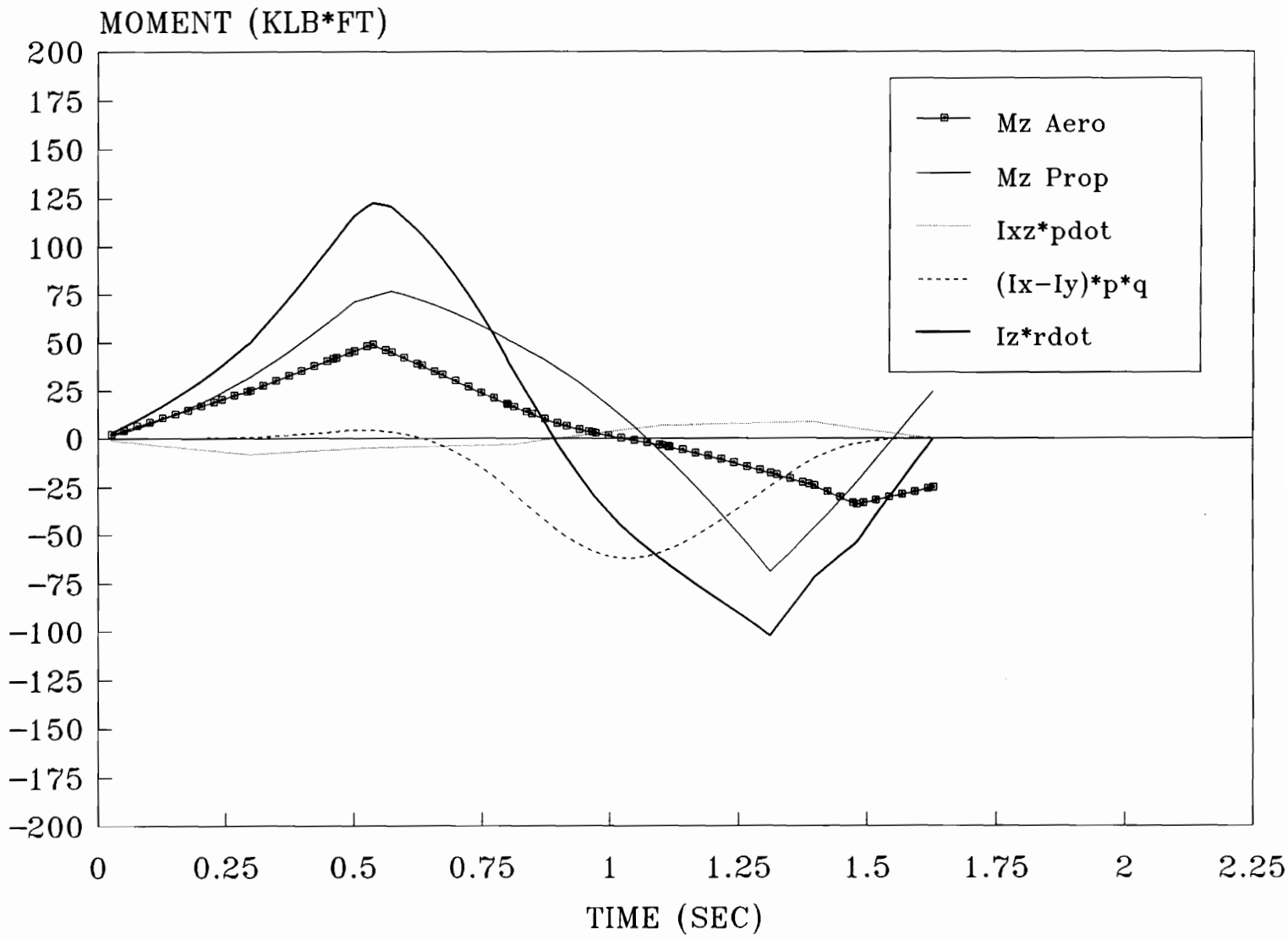

Figure 32. Yaw Moment vs Time; Wind-up at 0.35M; with T/V

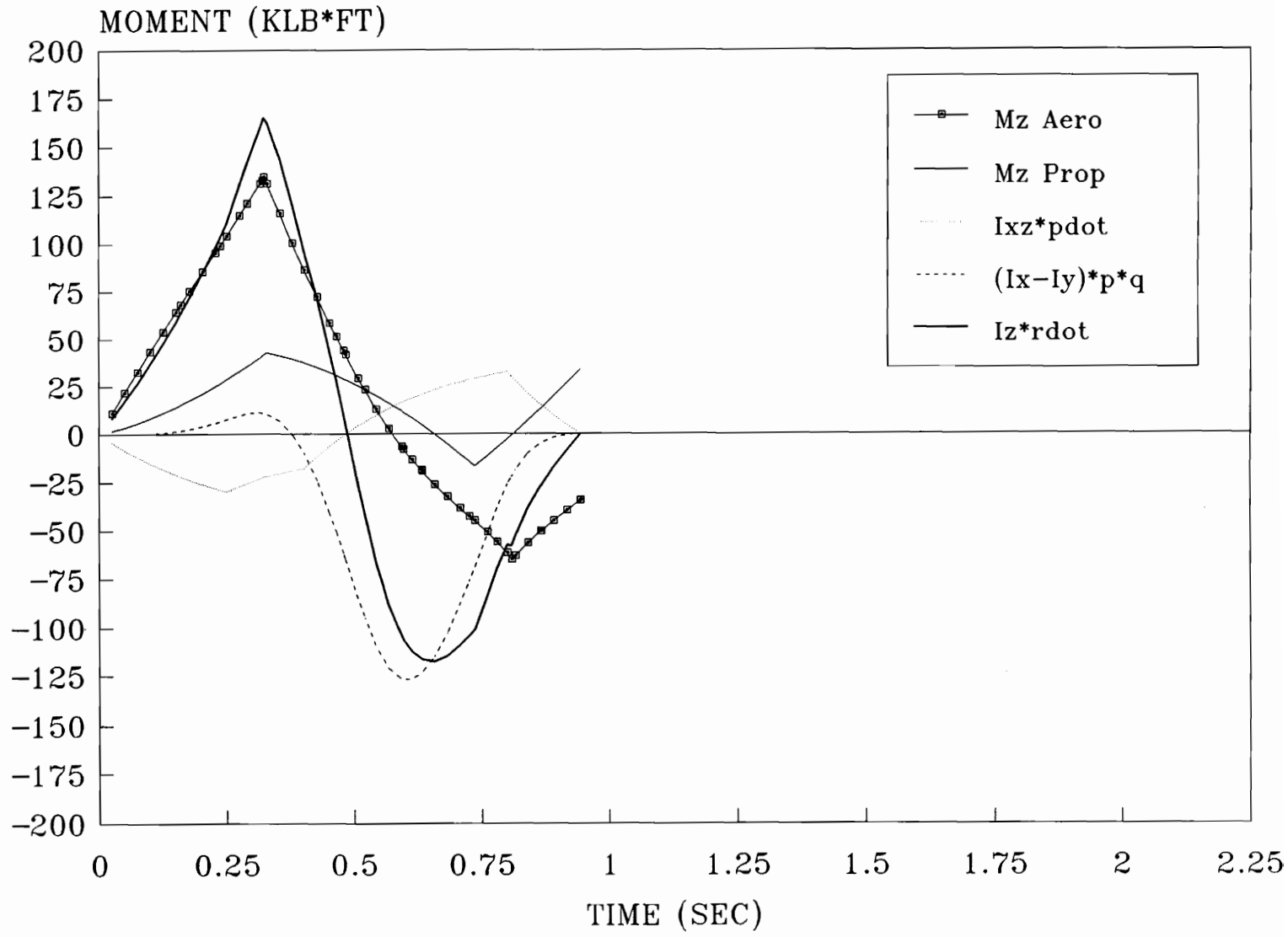

Figure 33. Yaw Moment vs Time; Wind-up at 0.75M; with T/V

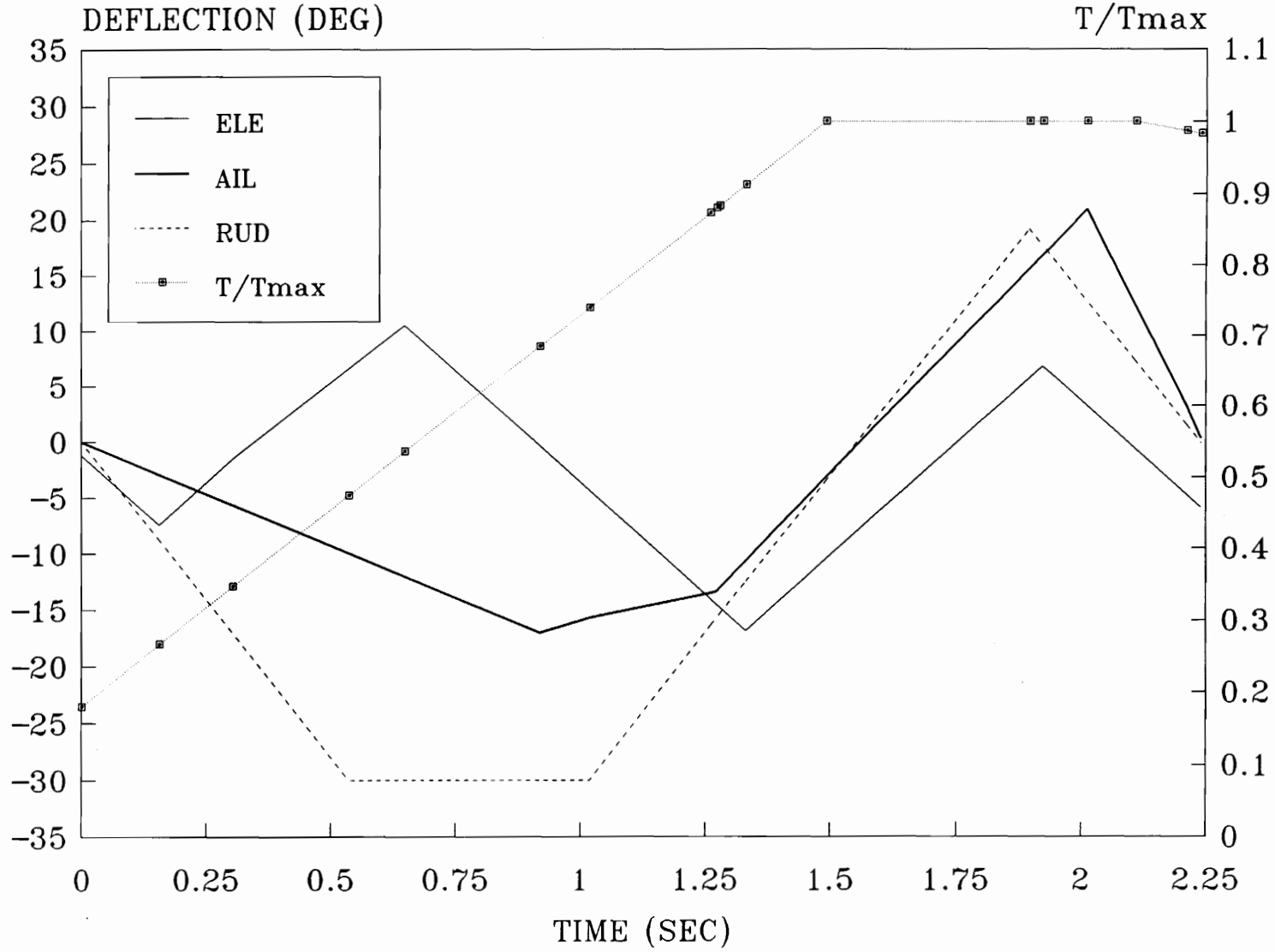

Figure 34. Control vs Time; Wind-up at 0.35M; no T/V

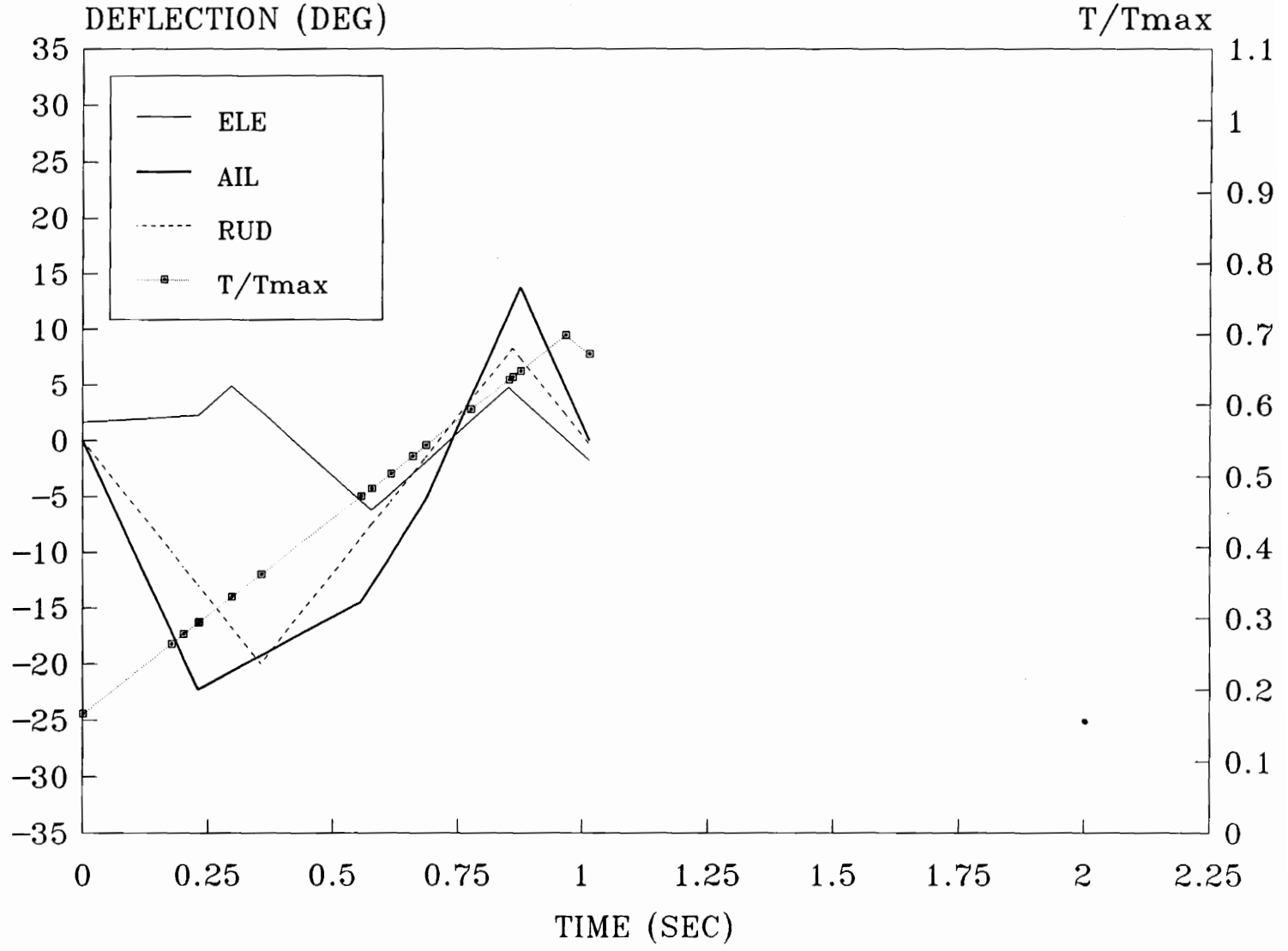

Figure 35. Control vs Time; Wind-up at 0.75M; no T/V

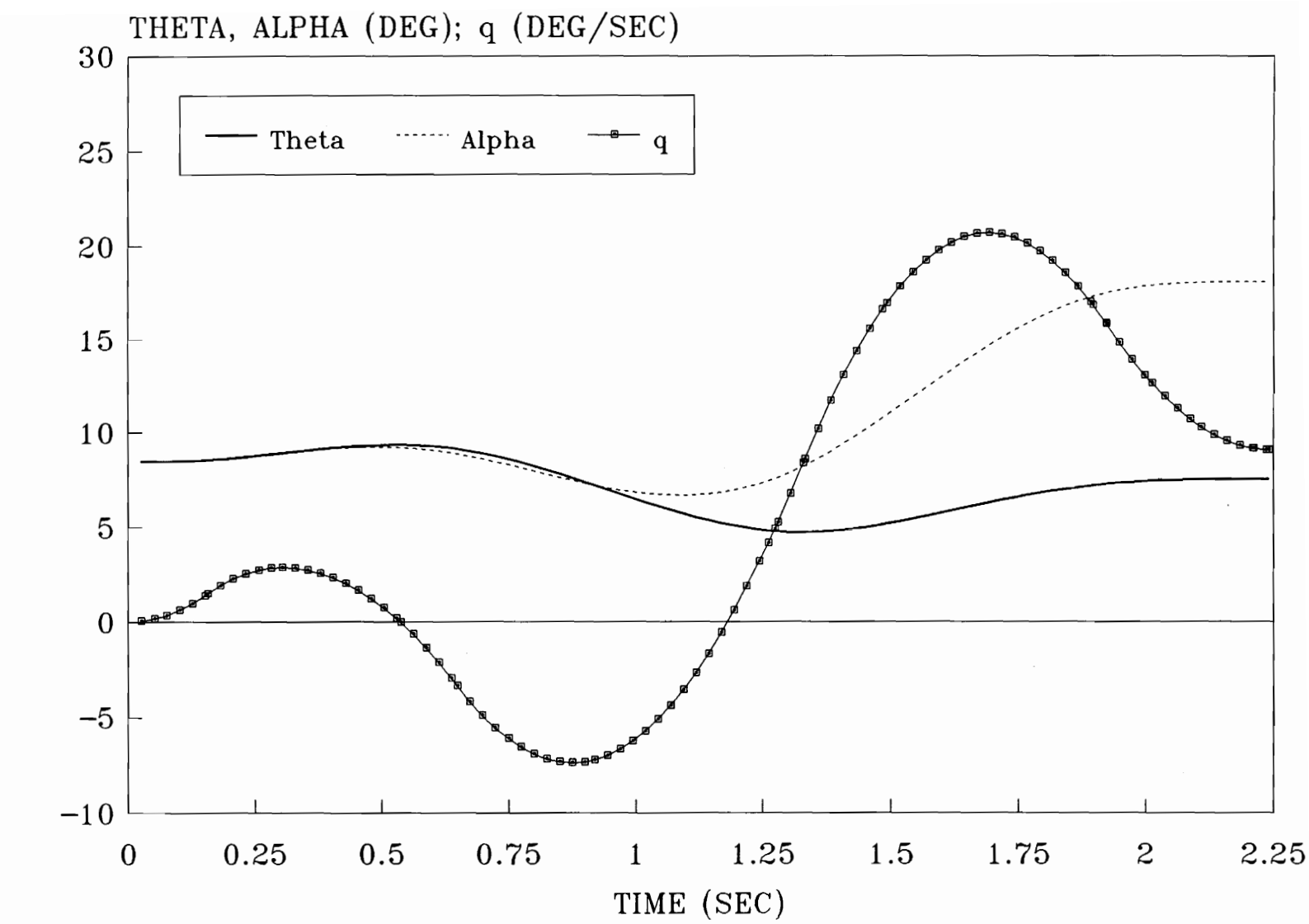

Figure 36. Longitudinal State vs Time; Wind-up at 0.35M; no T/V

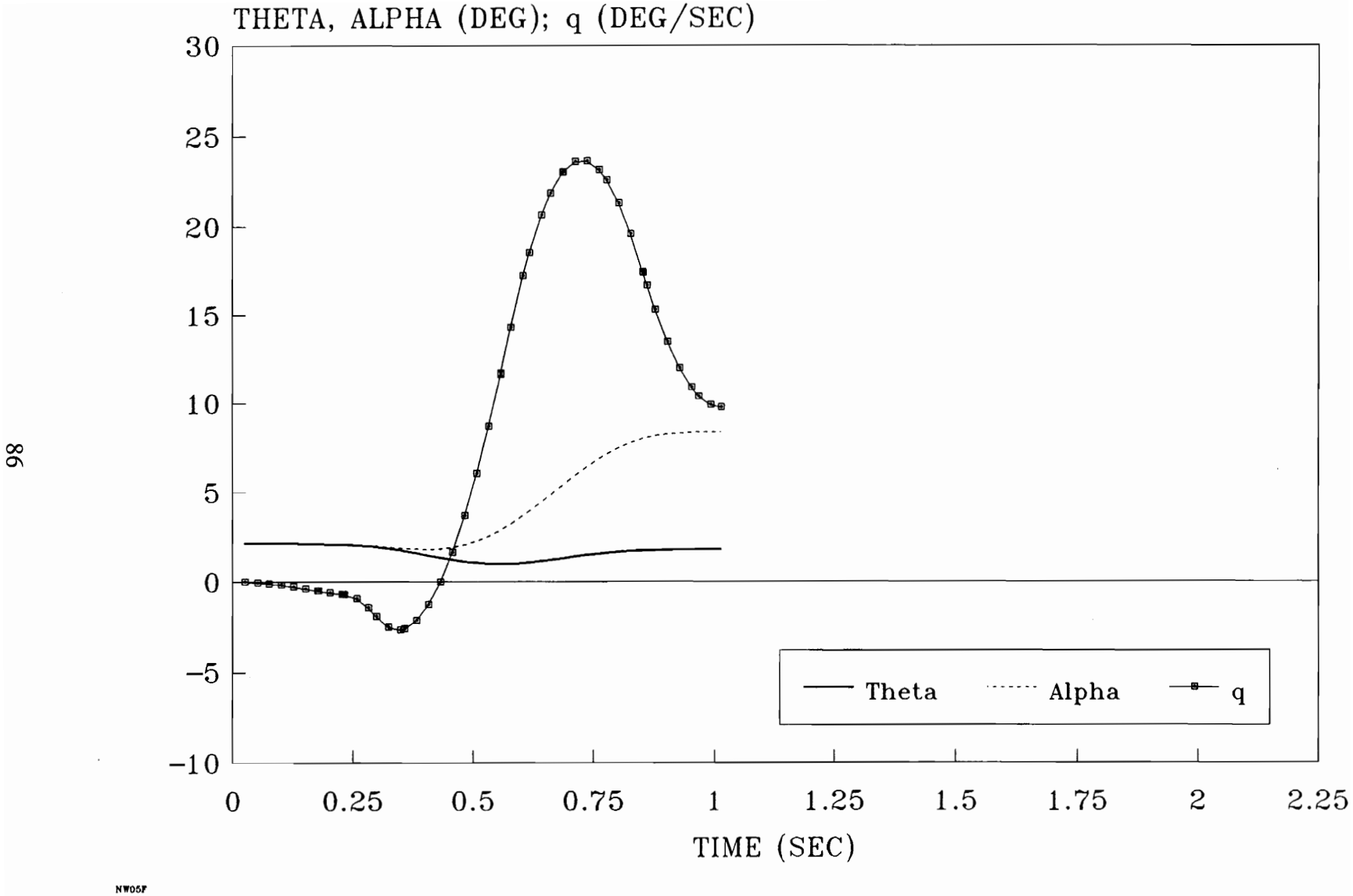

Figure 37. Longitudinal State vs Time; Wind-up at 0.75M; no T/V

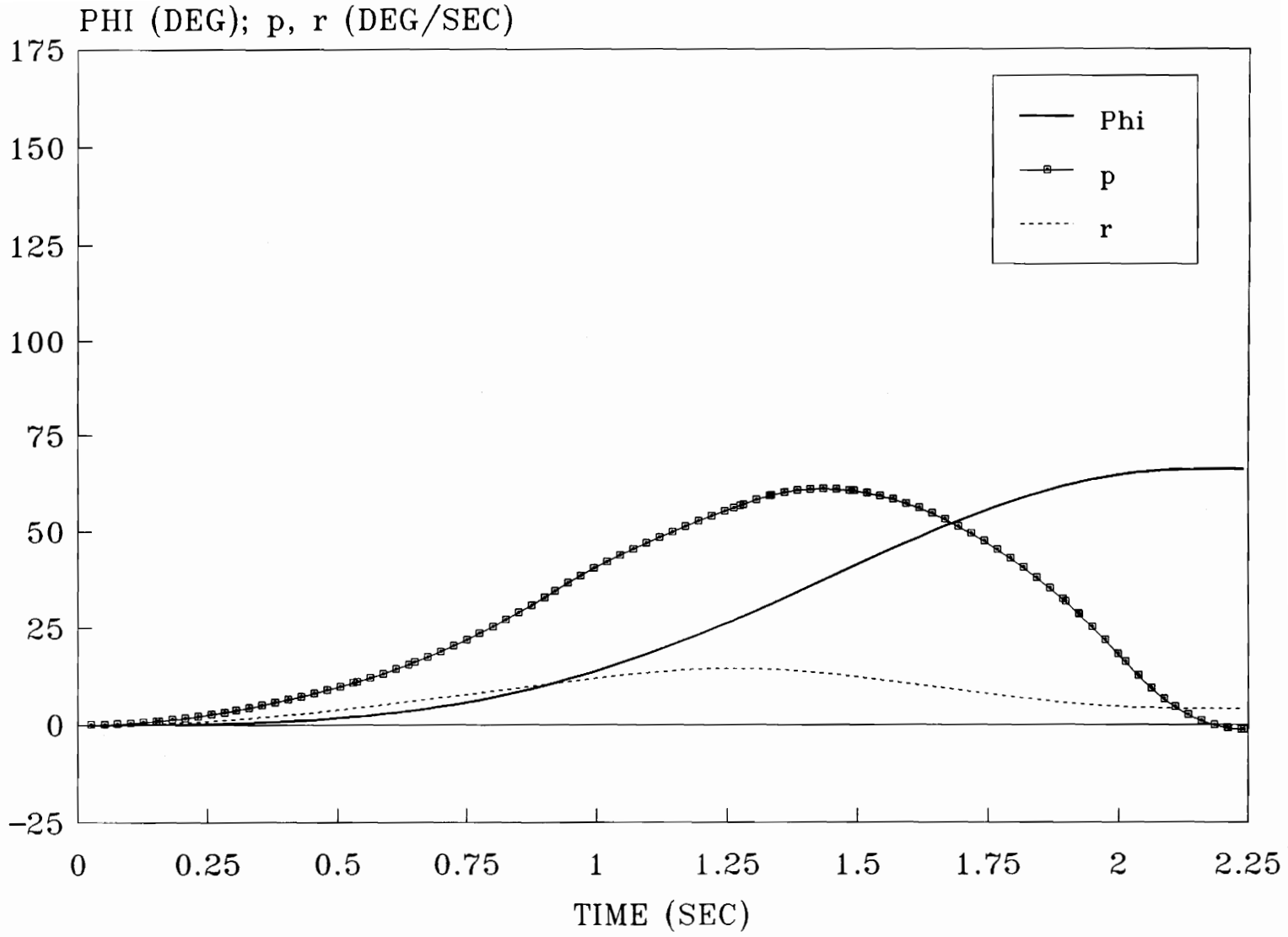

Figure 38. Lat-Dir State vs Time; Wind-up at 0.35M; no T/V

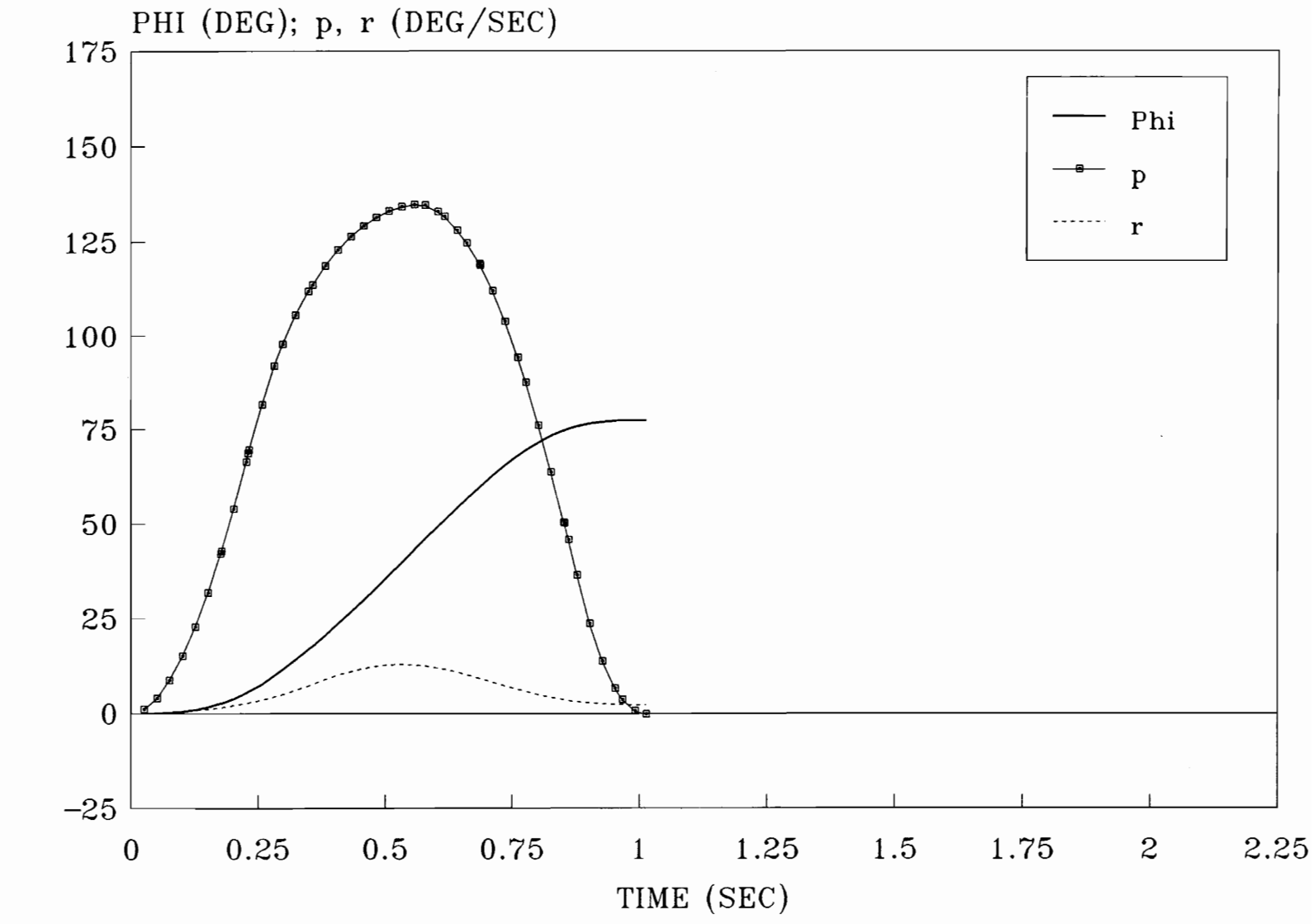

Figure 39. Lat-Dir State vs Time; Wind-up at 0.75M; no T/V

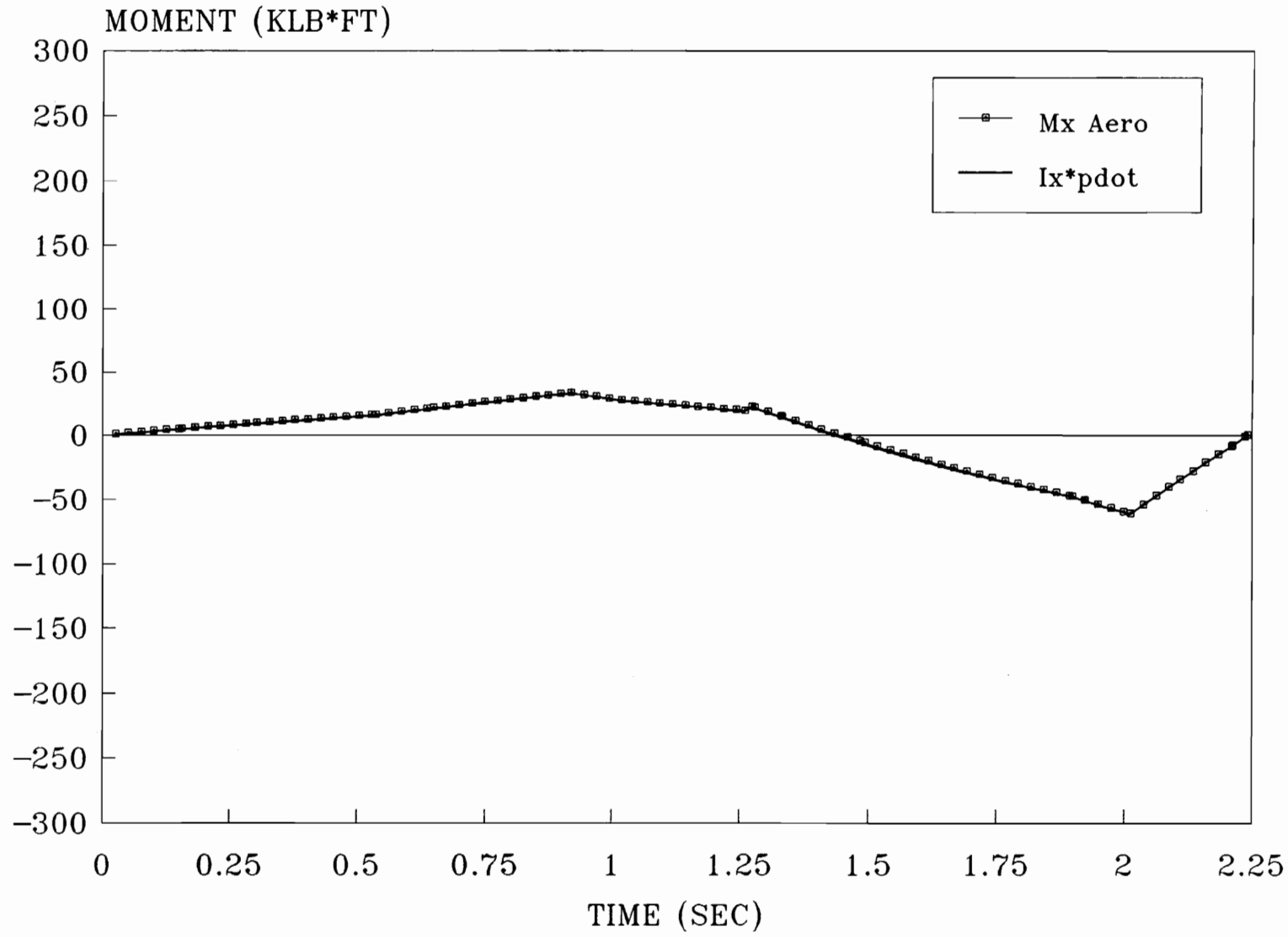

Figure 40. Roll Moment Components vs Time; Wind-up at 0.35M; no T/V

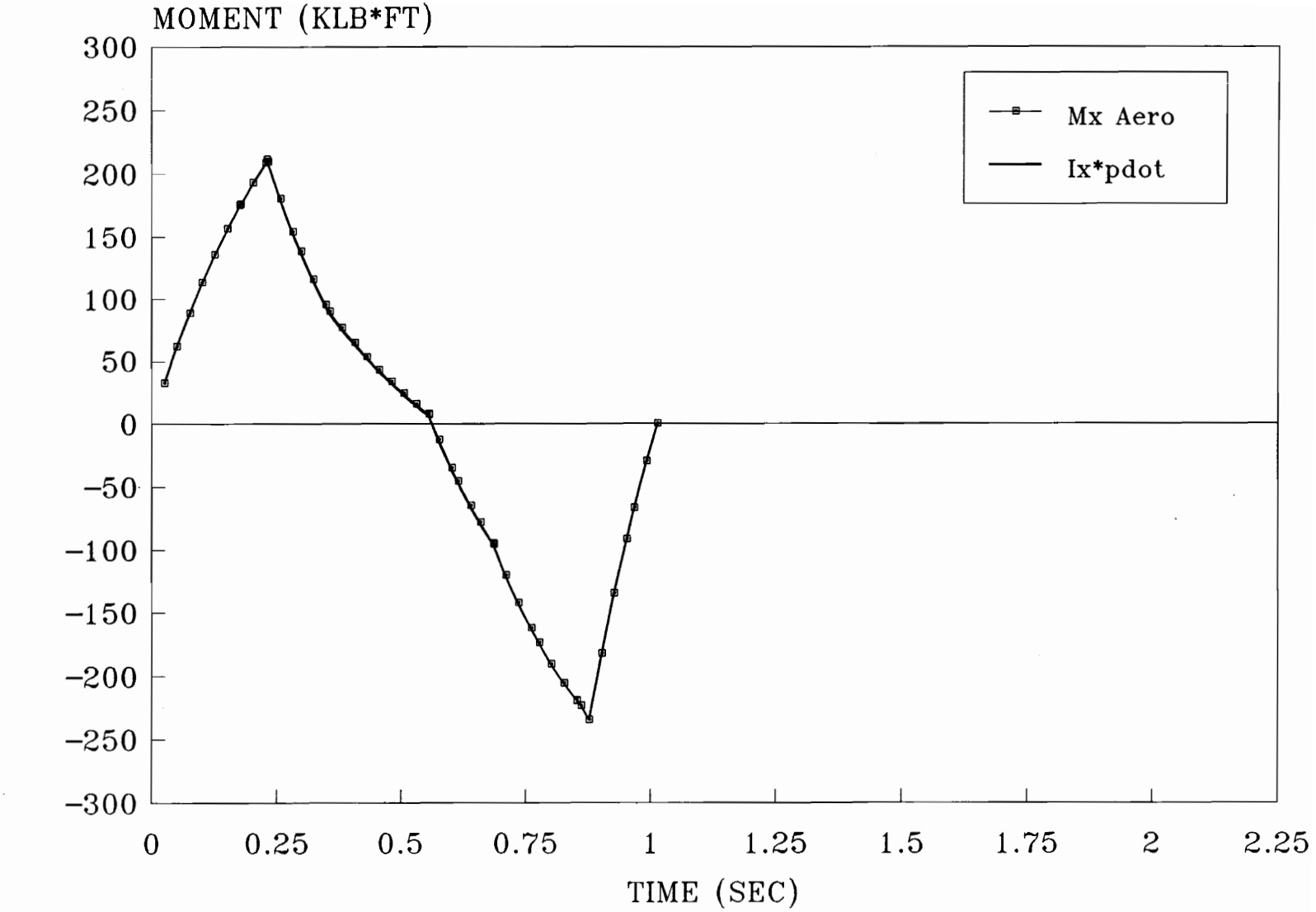

Figure 41. Roll Moment Components vs Time; Wind-up at 0.75M; no T/V

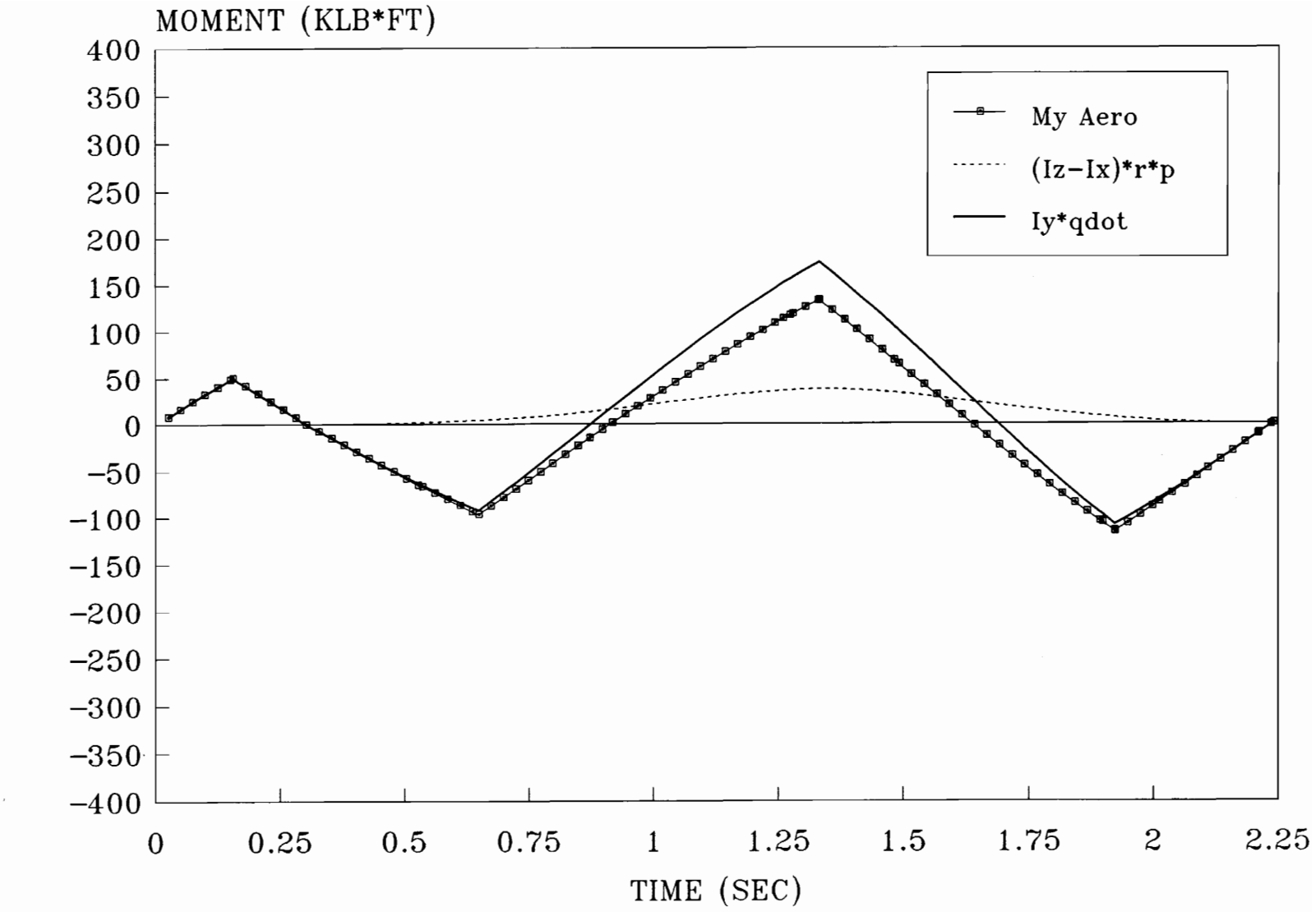

Figure 42. Pitch Moment Components vs Time; Wind-up at 0.35M; no T/V

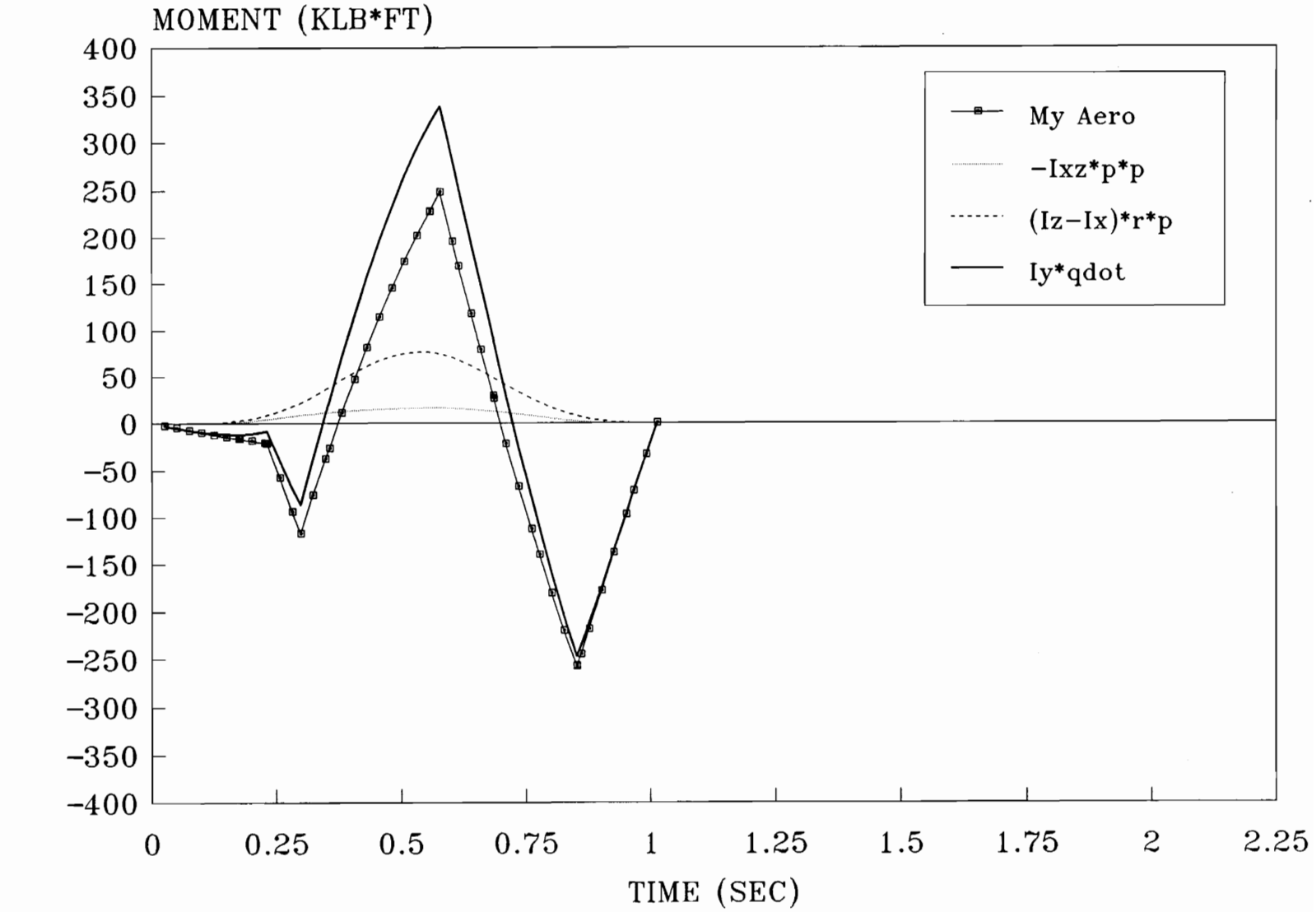

Figure 43. Pitch Moment Components vs Time; Wind-up at 0.75M; no T/V

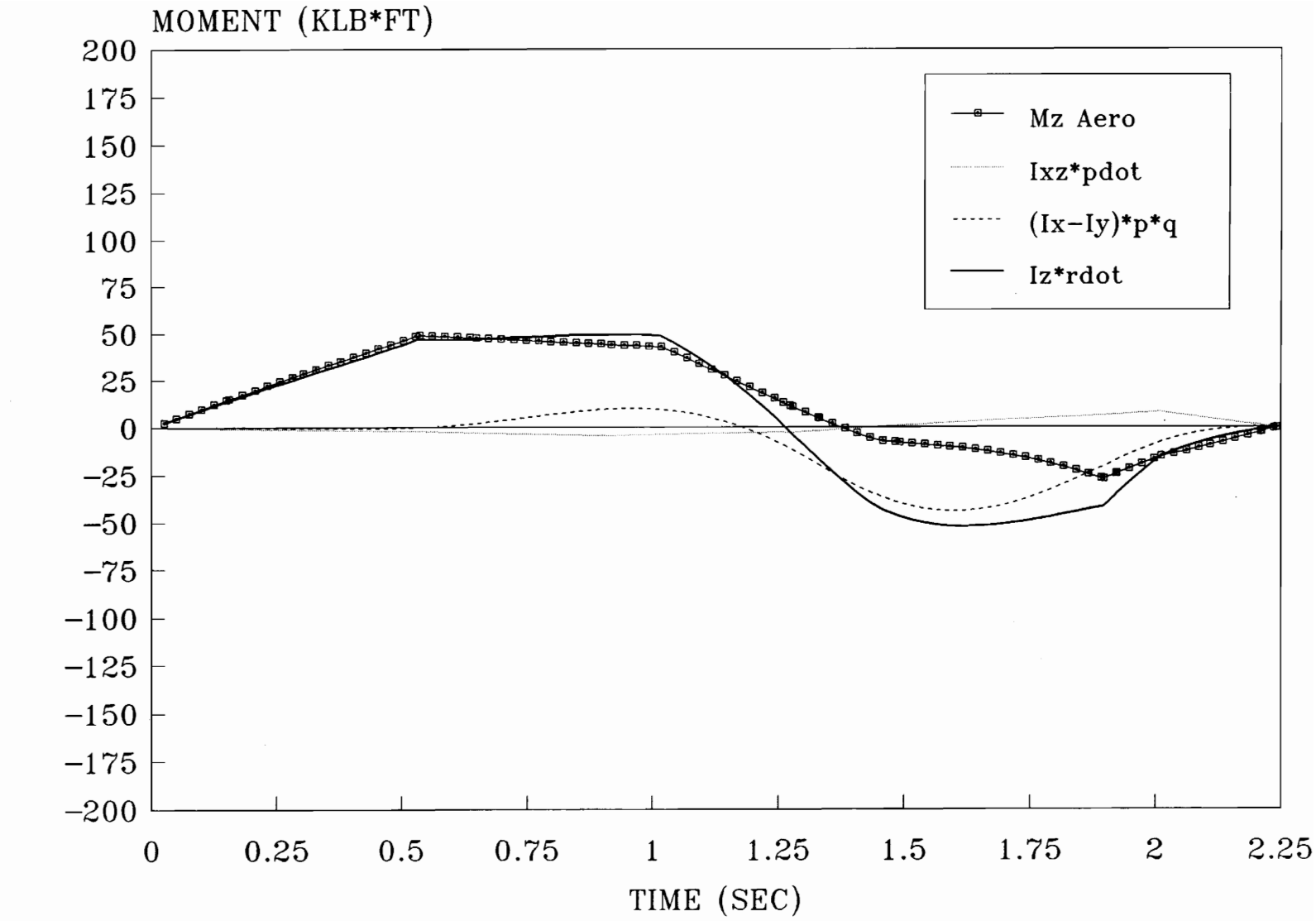

Figure 44. Yaw Moment Components vs Time; Wind-up at 0.35M; no T/V

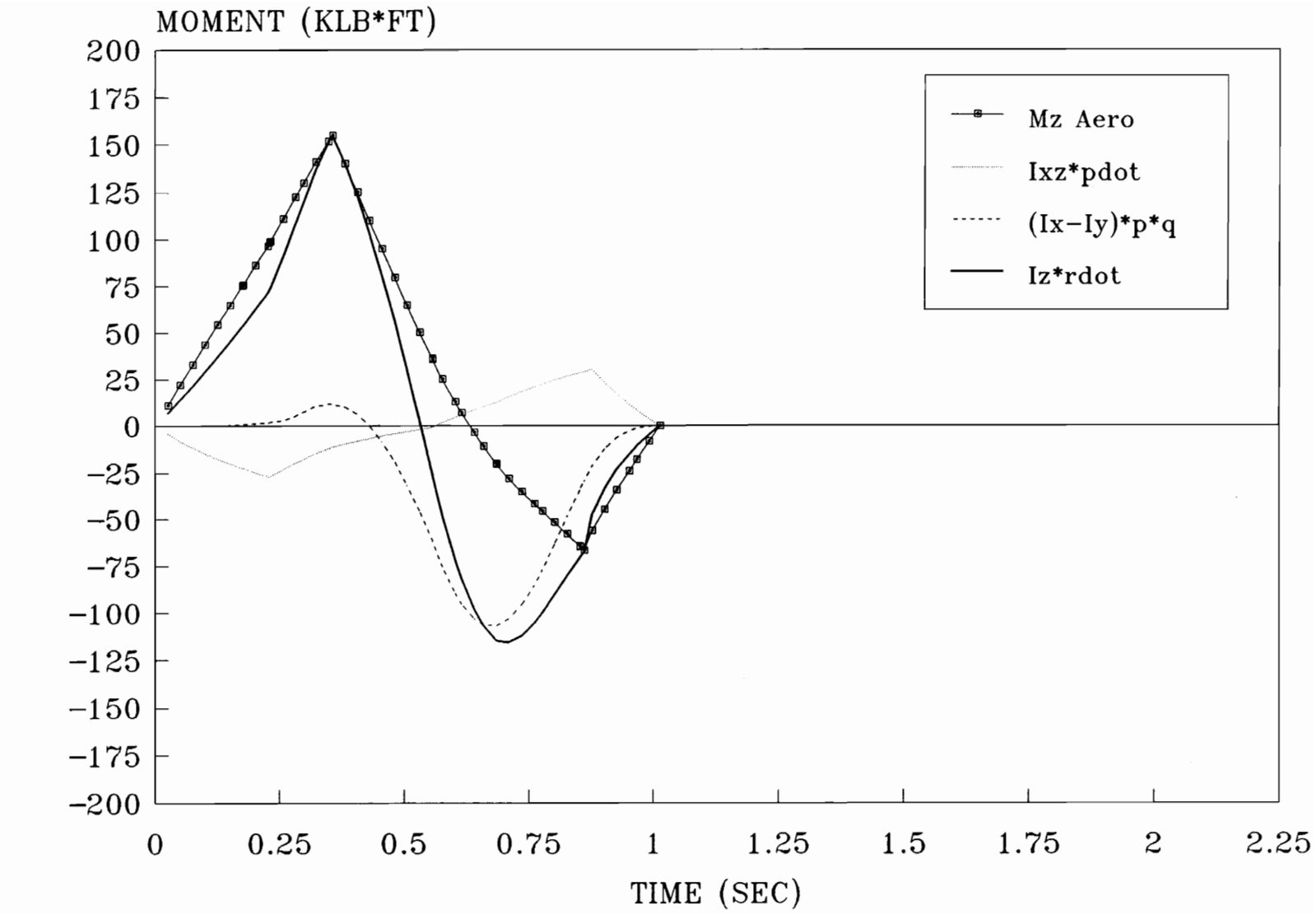

Figure 45. Yaw Moment Components vs Time; Wind-up at 0.75M; no T/V

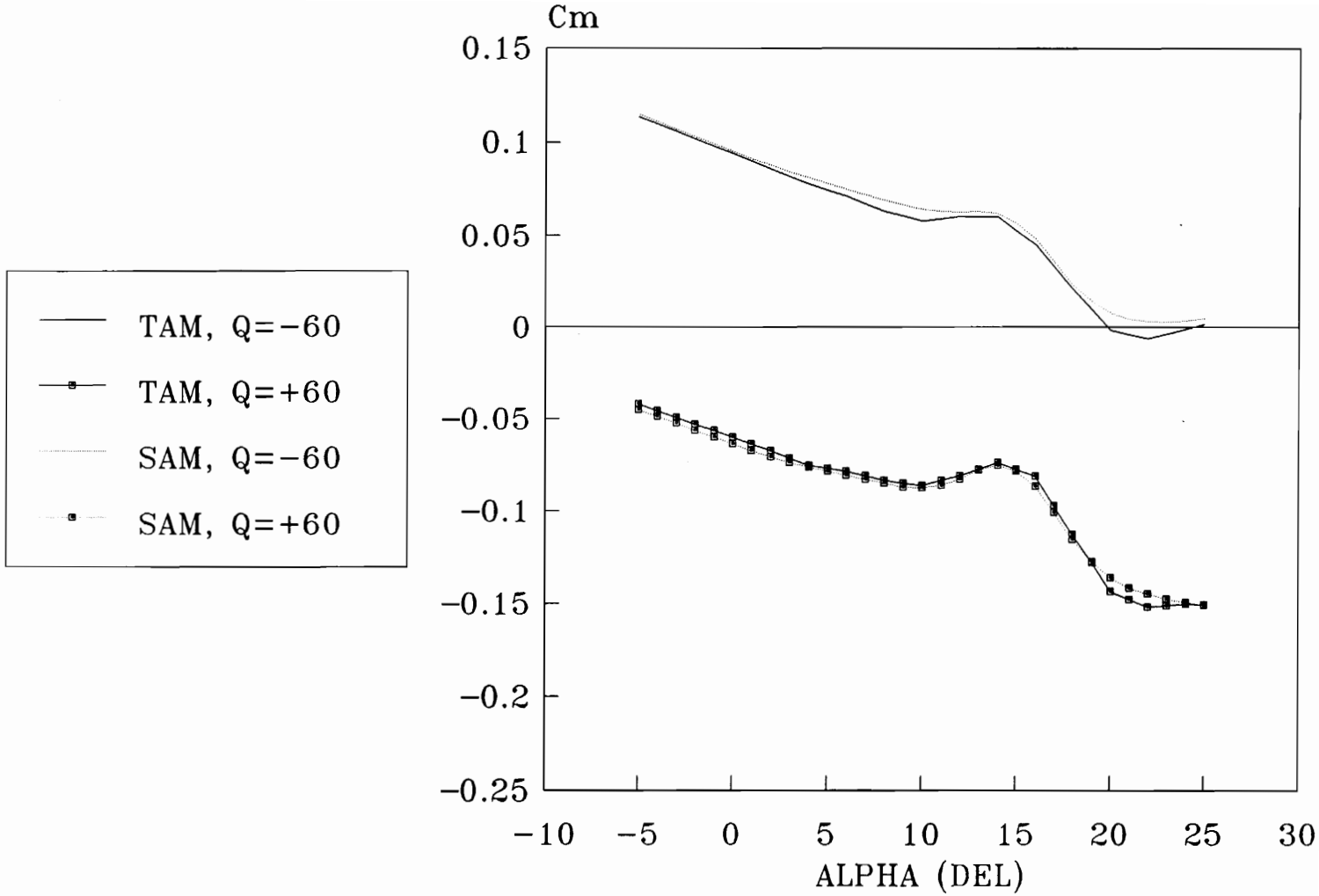

Figure 46. C_m vs α at 0.35M, q = ±60 deg/sec, TAM/SAM data

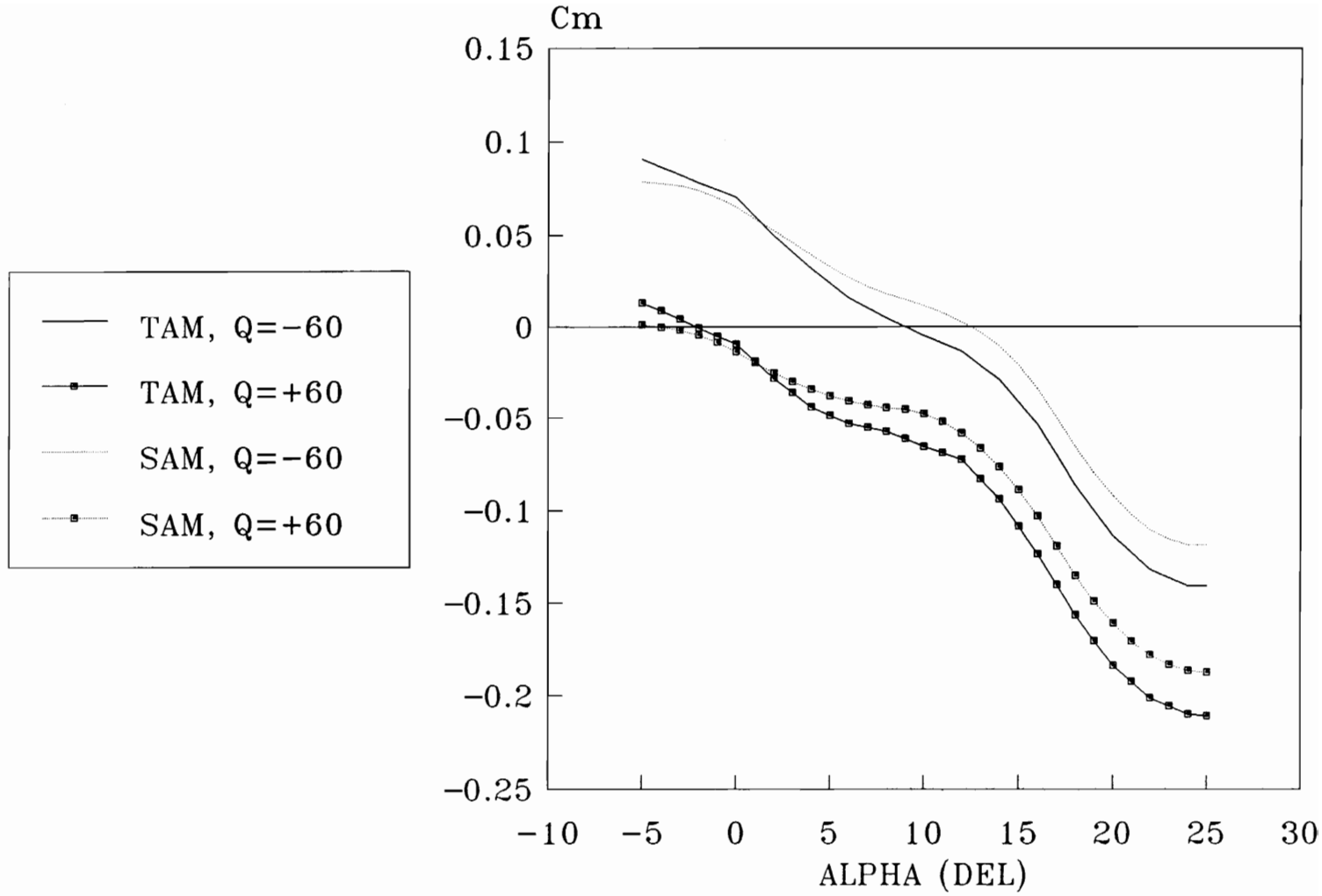

Figure 47. C_m vs α at 0.75M, q = ±60 deg/sec, TAM/SAM data

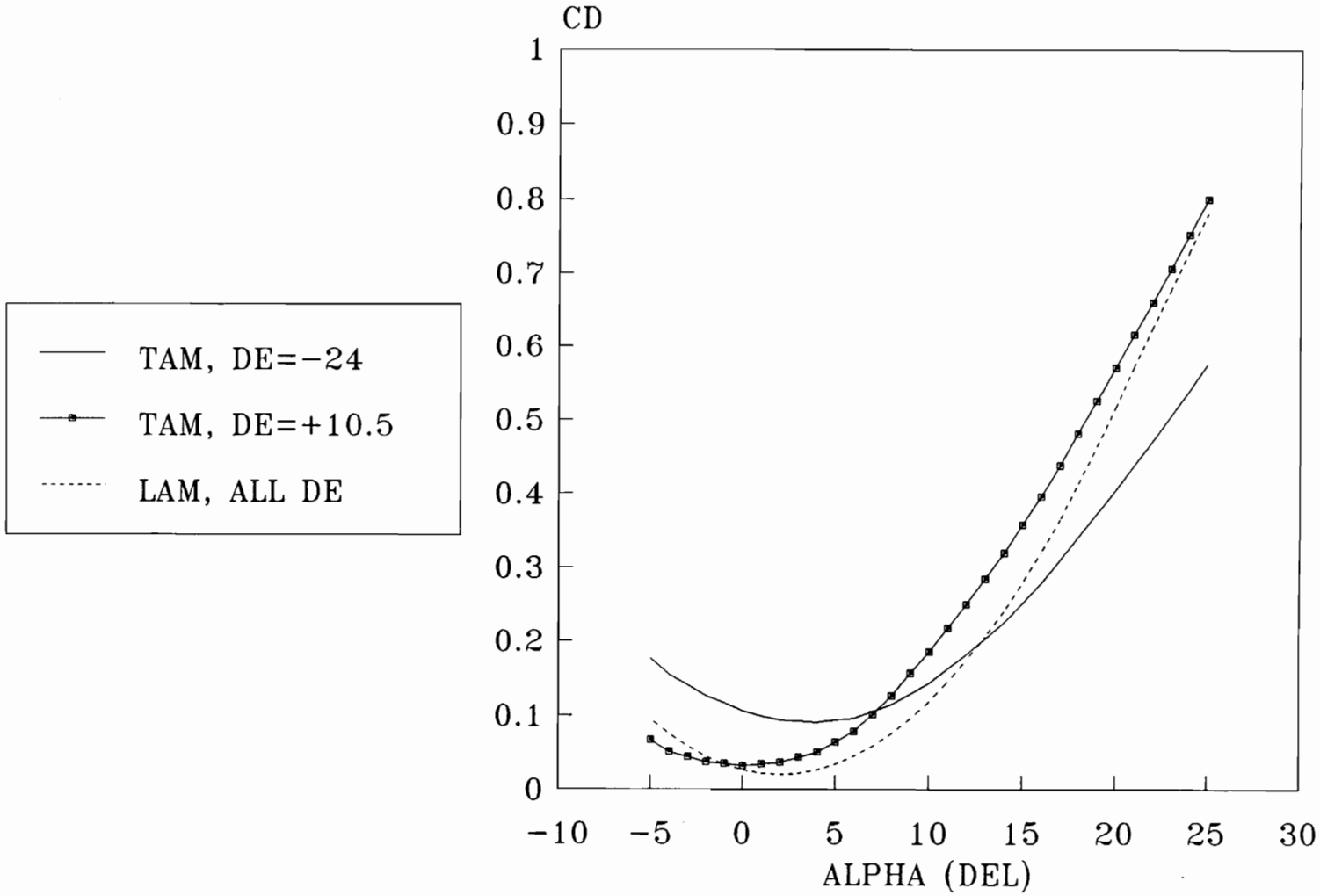

DRAG COEFFICIENT VS ALPHA, M = 0.35

ELEVATOR DEFLECTION = −24 & 10.5 DEG

Figure 48. C_D vs α at 0.35M, δ_e = -24,+10.5 deg, TAM/LAM data

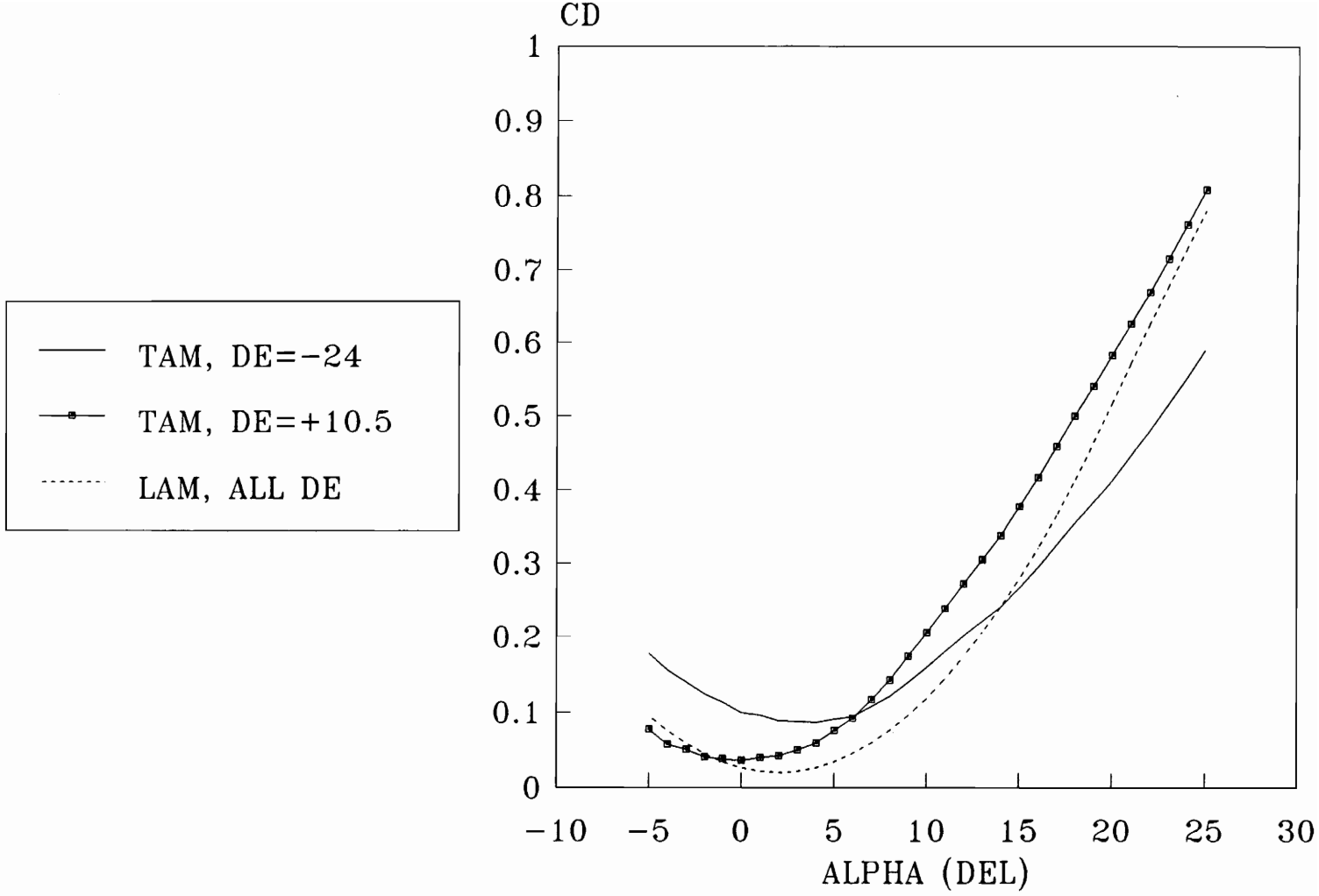

DRAG COEFFICIENT VS ALPHA, M = 0.75

ELEVATOR DEFLECTION = −24 & 10.5 DEG

Figure 49. C_D vs α at 0.75M, δ_e = -24,+10.5 deg, TAM/LAM data

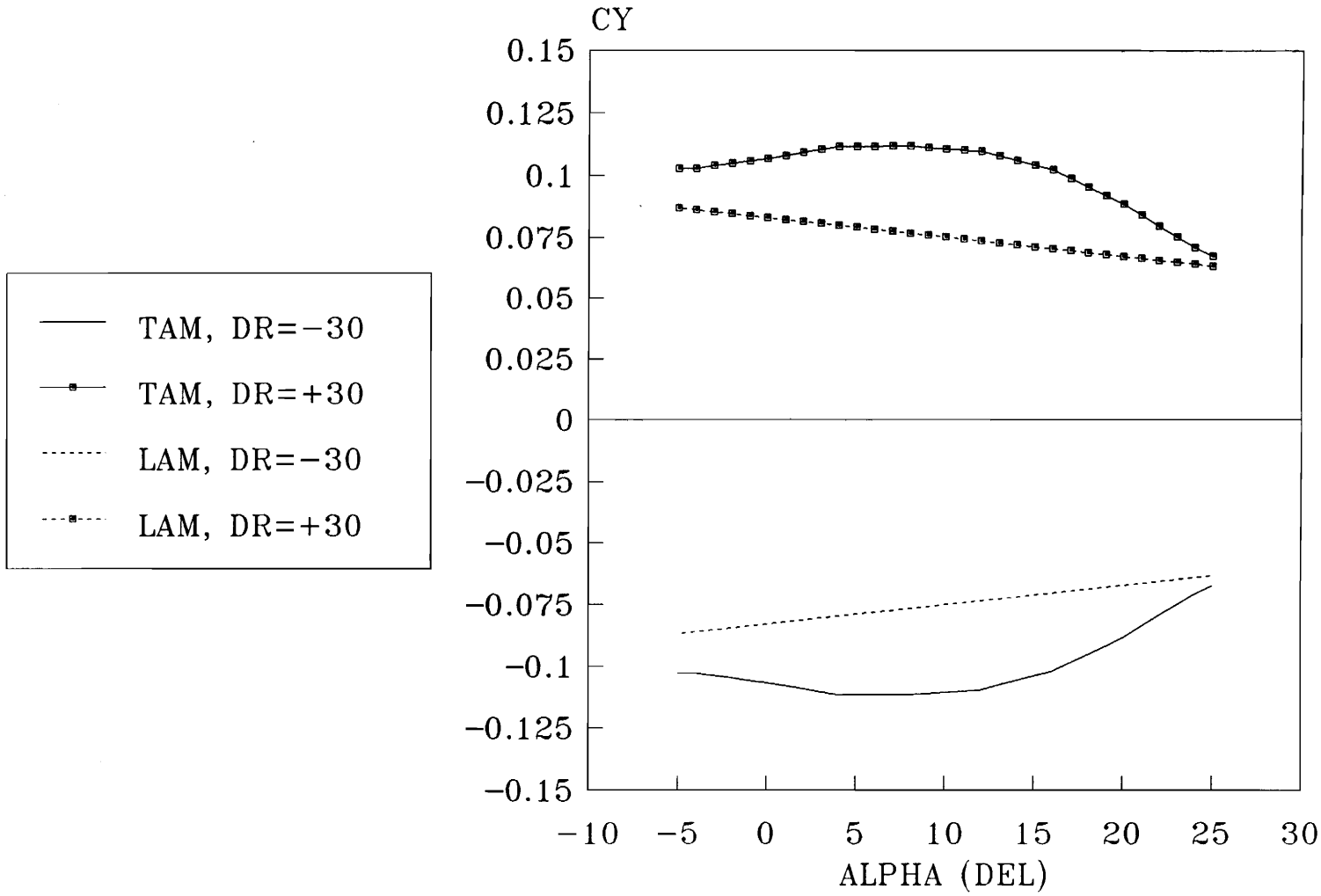

Figure 50. C_Y vs α at 0.35M, $\delta_r = \pm 30$ deg, TAM/LAM data

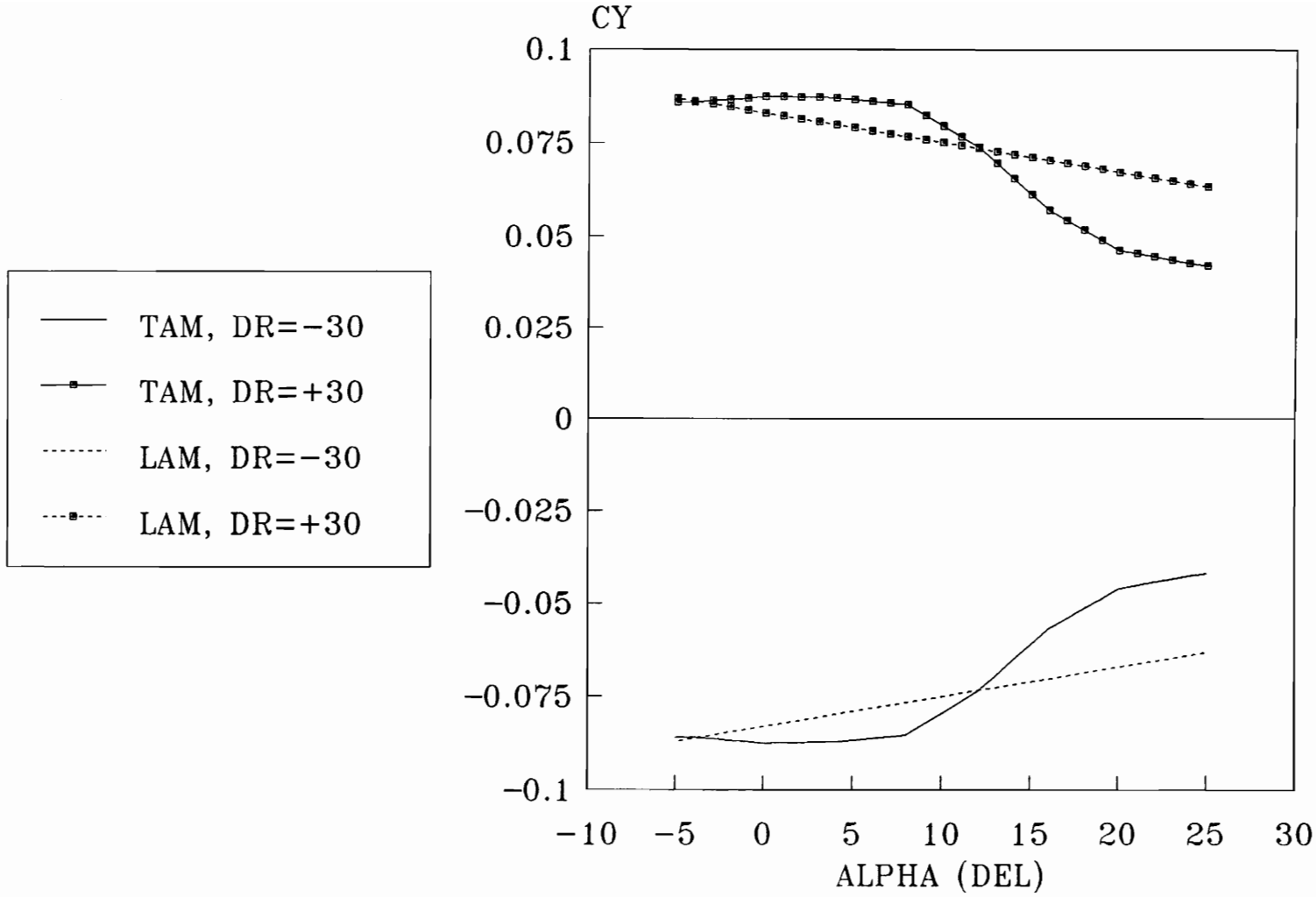

Figure 51. C_Y vs α at 0.75M, δ_r = ±30 deg, TAM/LAM data

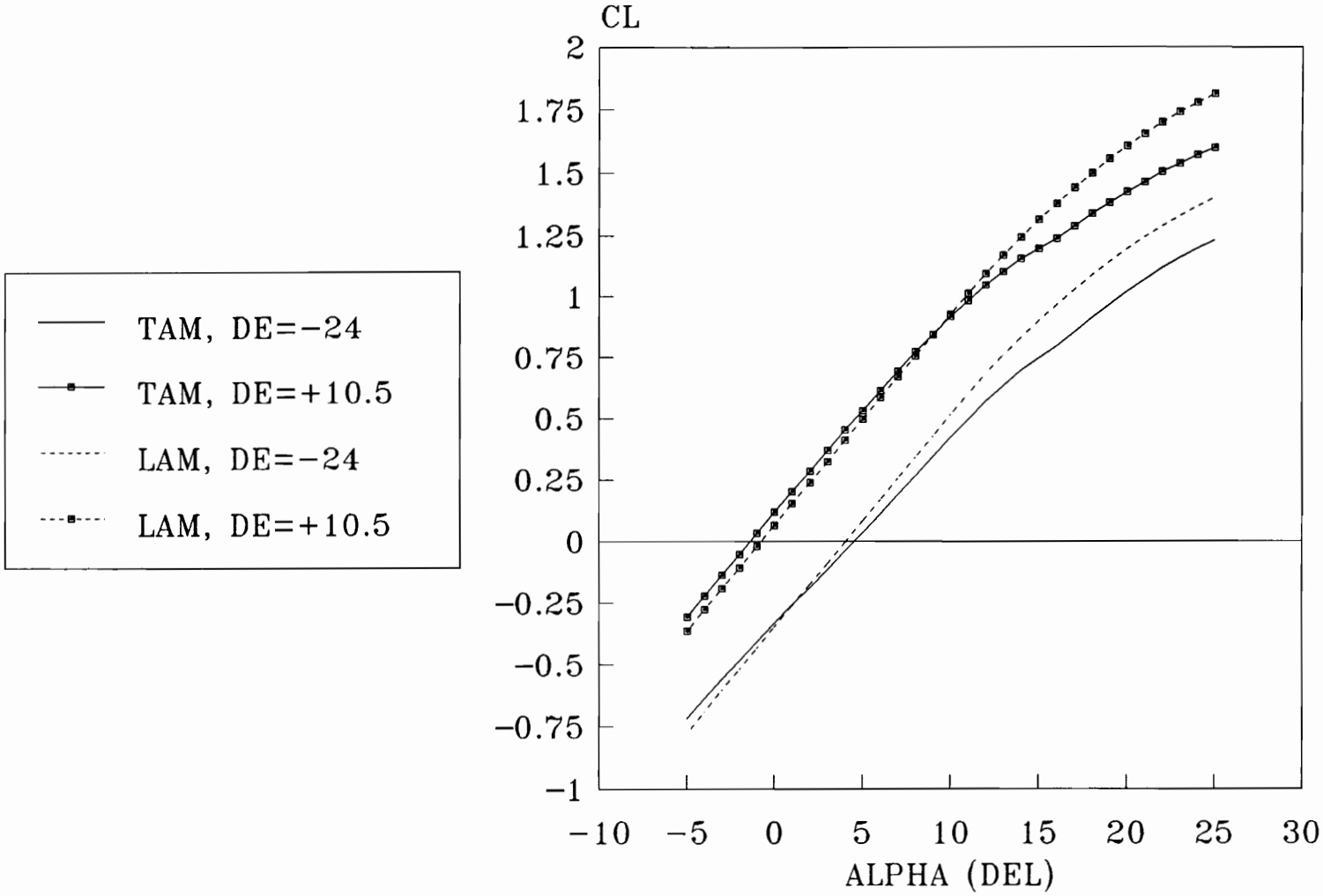

Figure 52. C_L vs α at 0.35M, δ_e = -24,+10.5 deg, TAM/LAM data

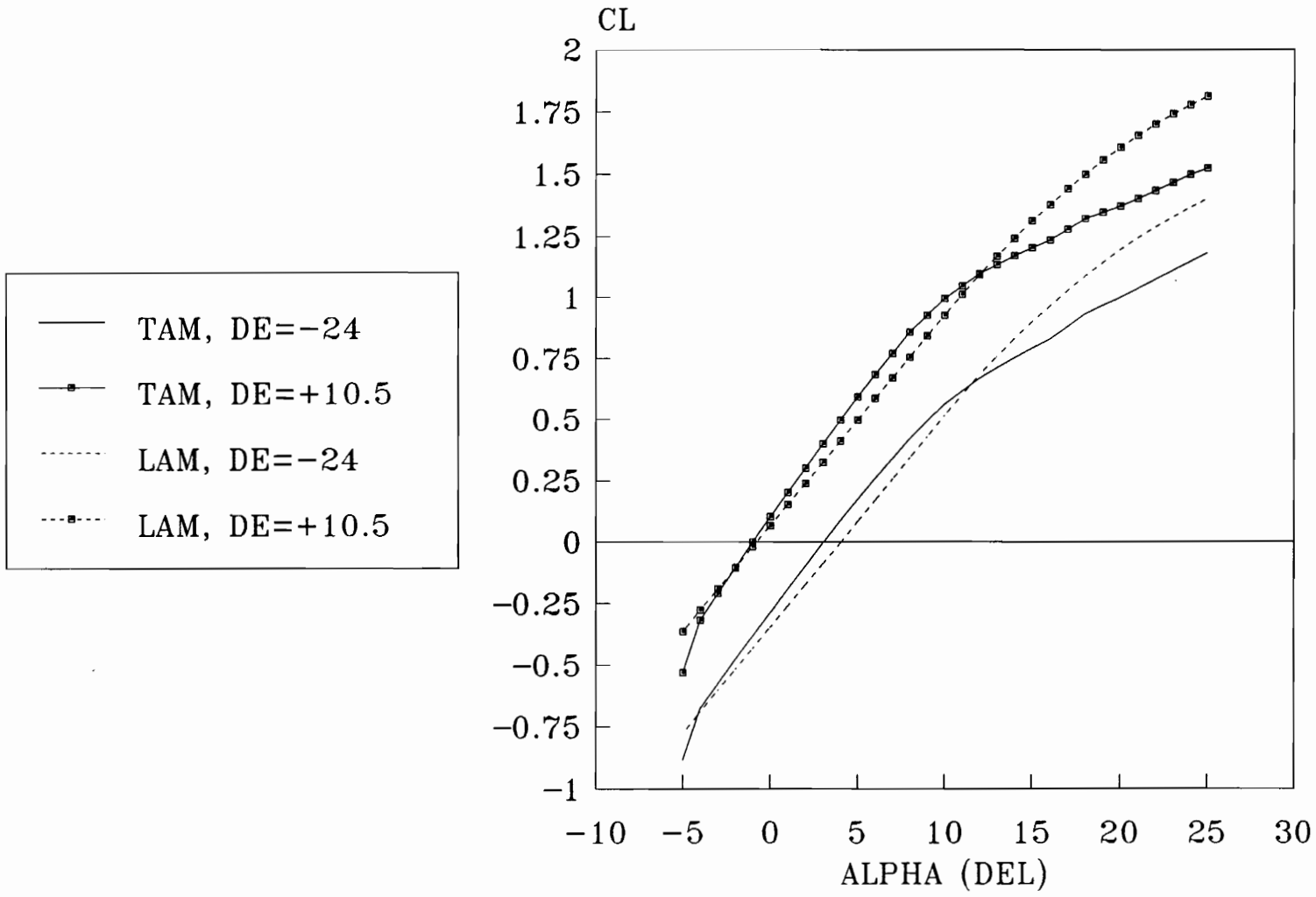

Figure 53. C_L vs α at 0.75M, δ_e = -24,+10.5 deg, TAM/LAM data

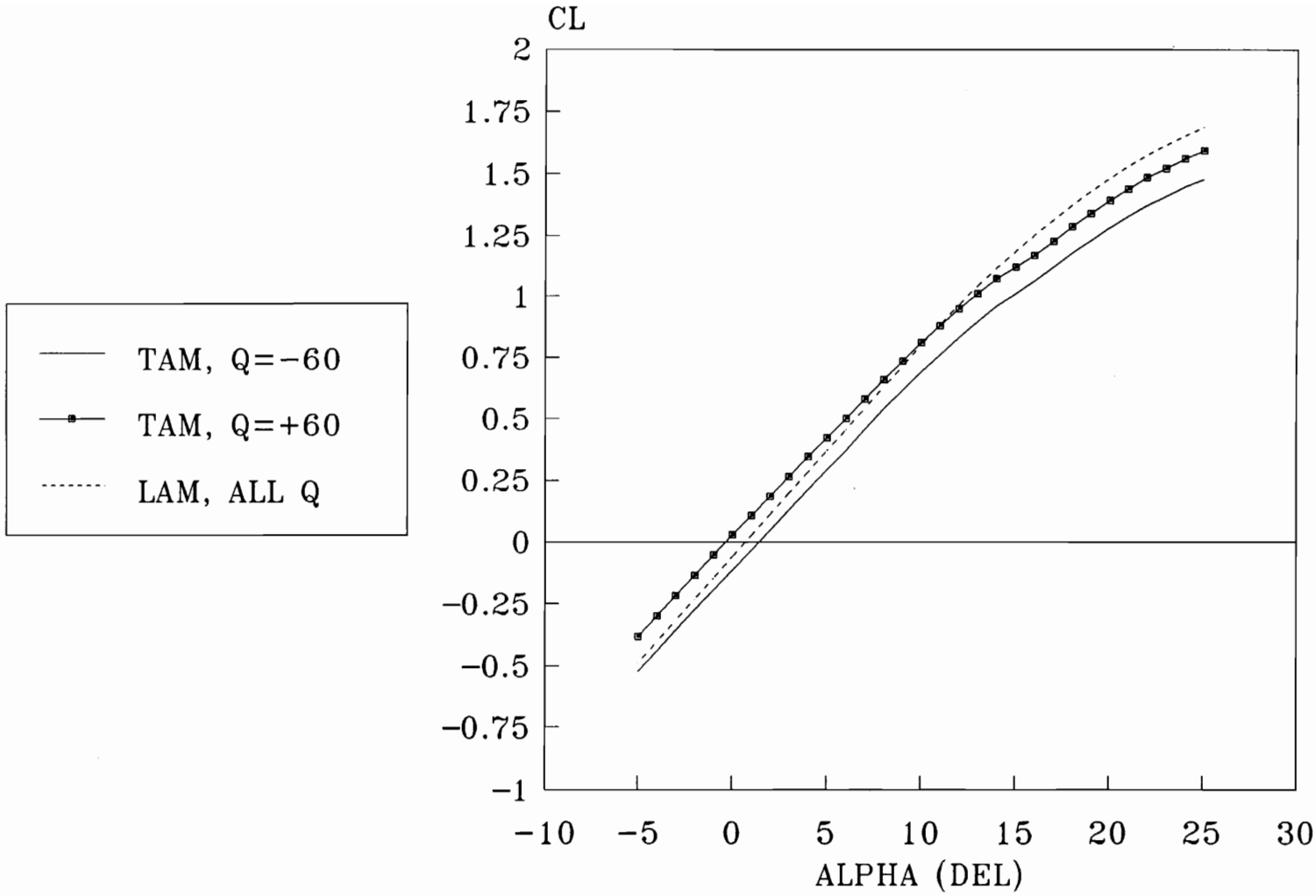

Figure 54. C_L vs α at 0.35M, q = ±60 deg/sec, TAM/LAM data

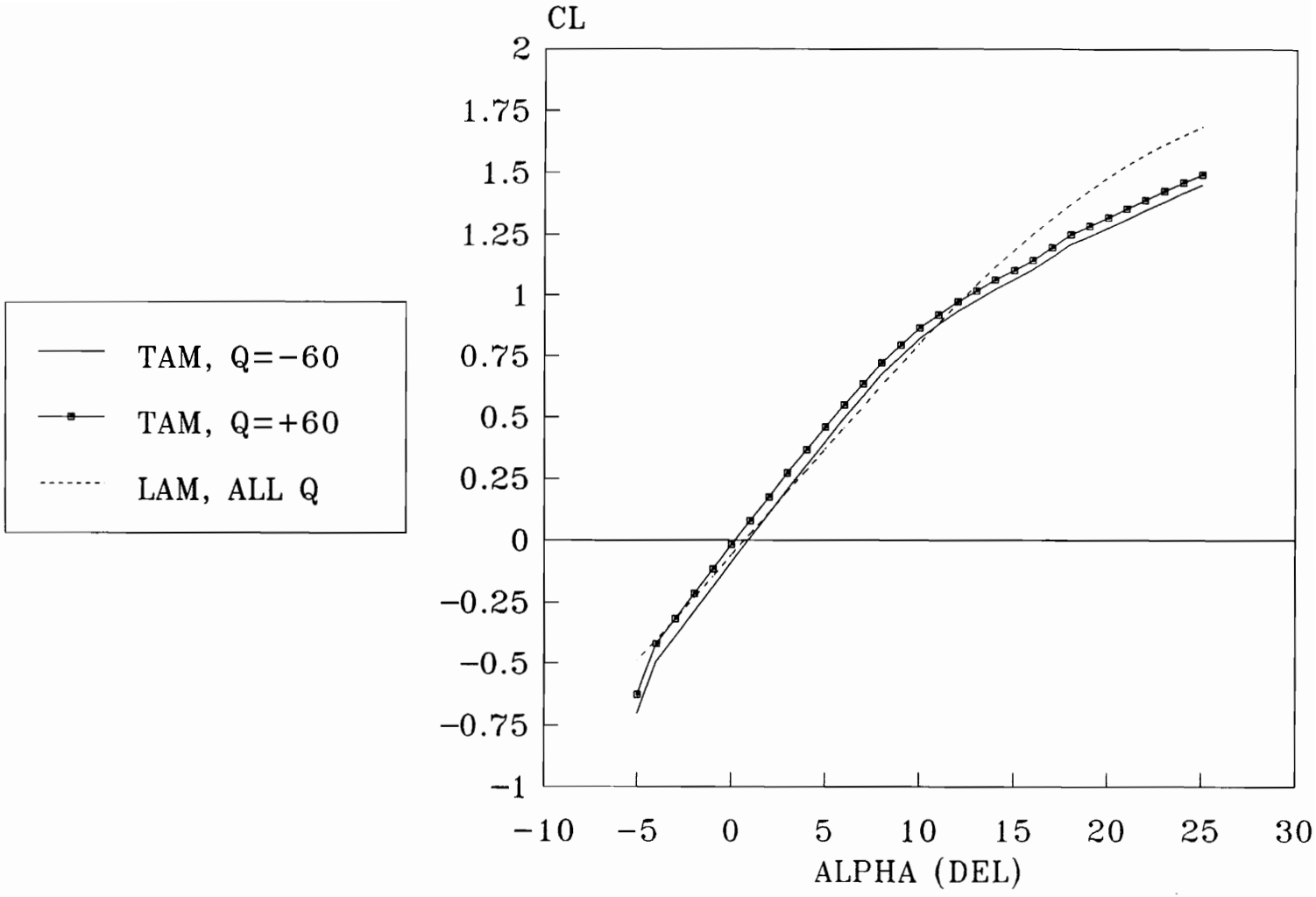

Figure 55. C_L vs α at 0.75M, q = ±60 deg/sec, TAM/LAM data

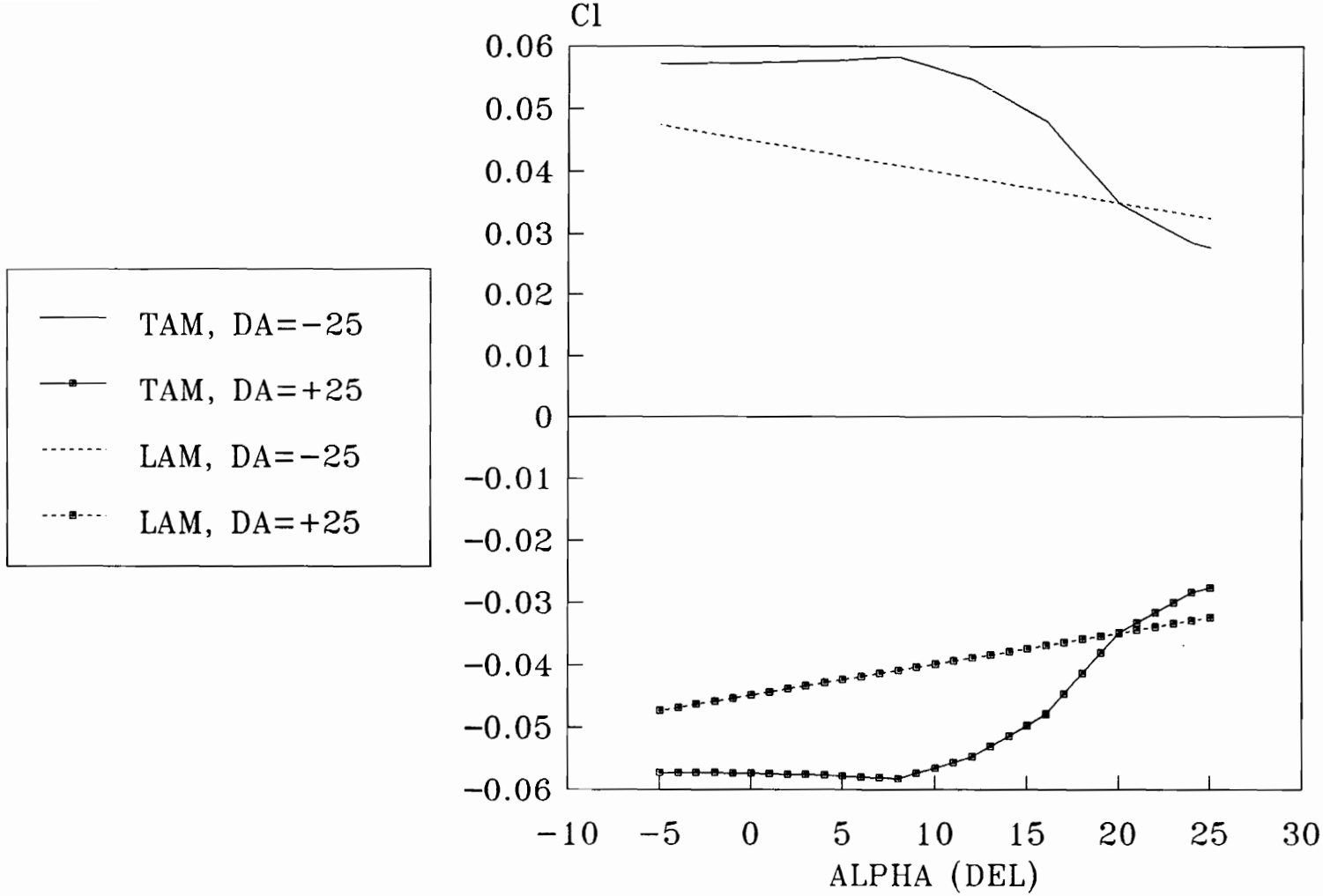

Figure 56. C_l vs α at 0.35M, δ_a = ±25 deg, TAM/LAM data

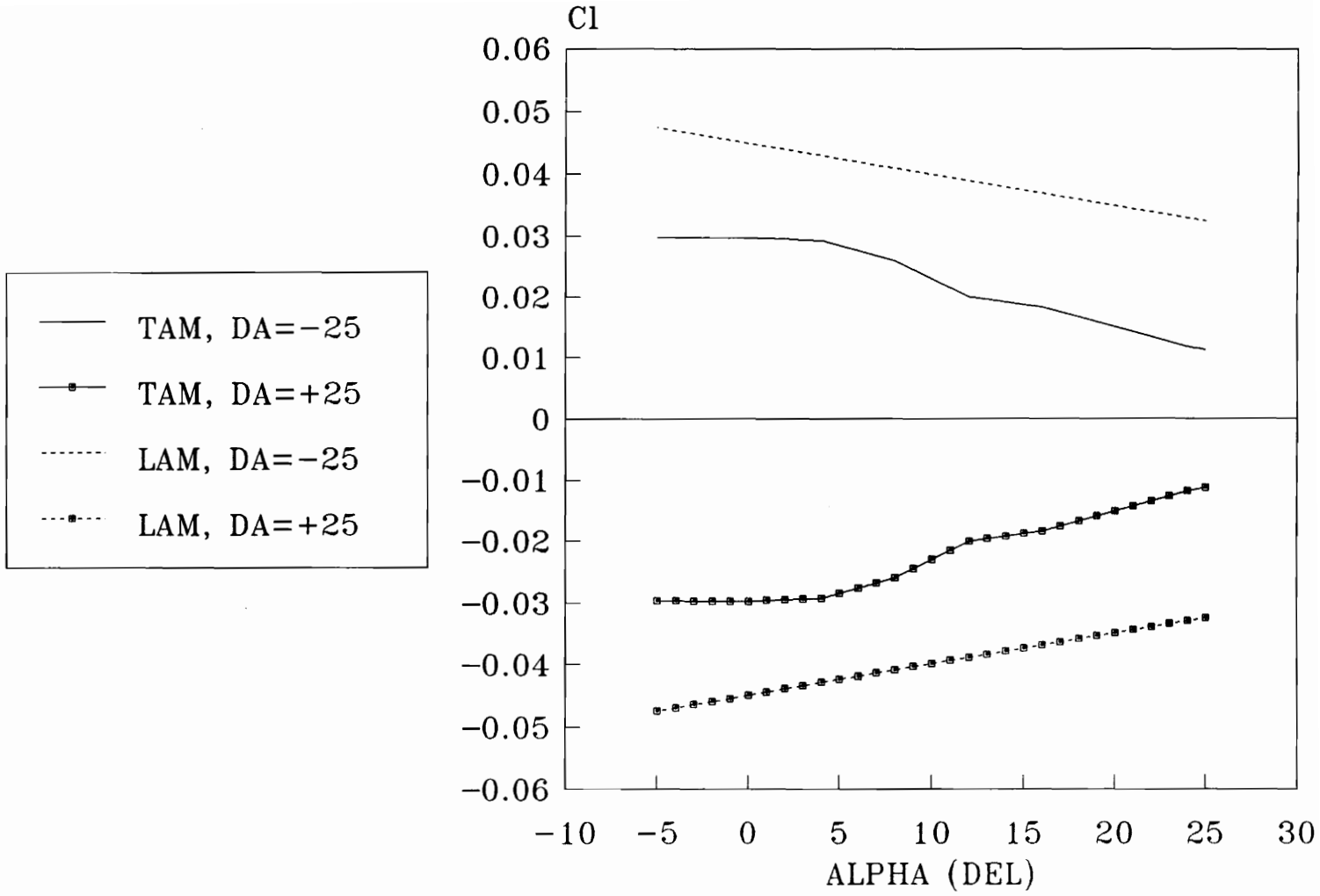

Figure 57. C_l vs α at 0.75M, δ_a = ±25 deg, TAM/LAM data

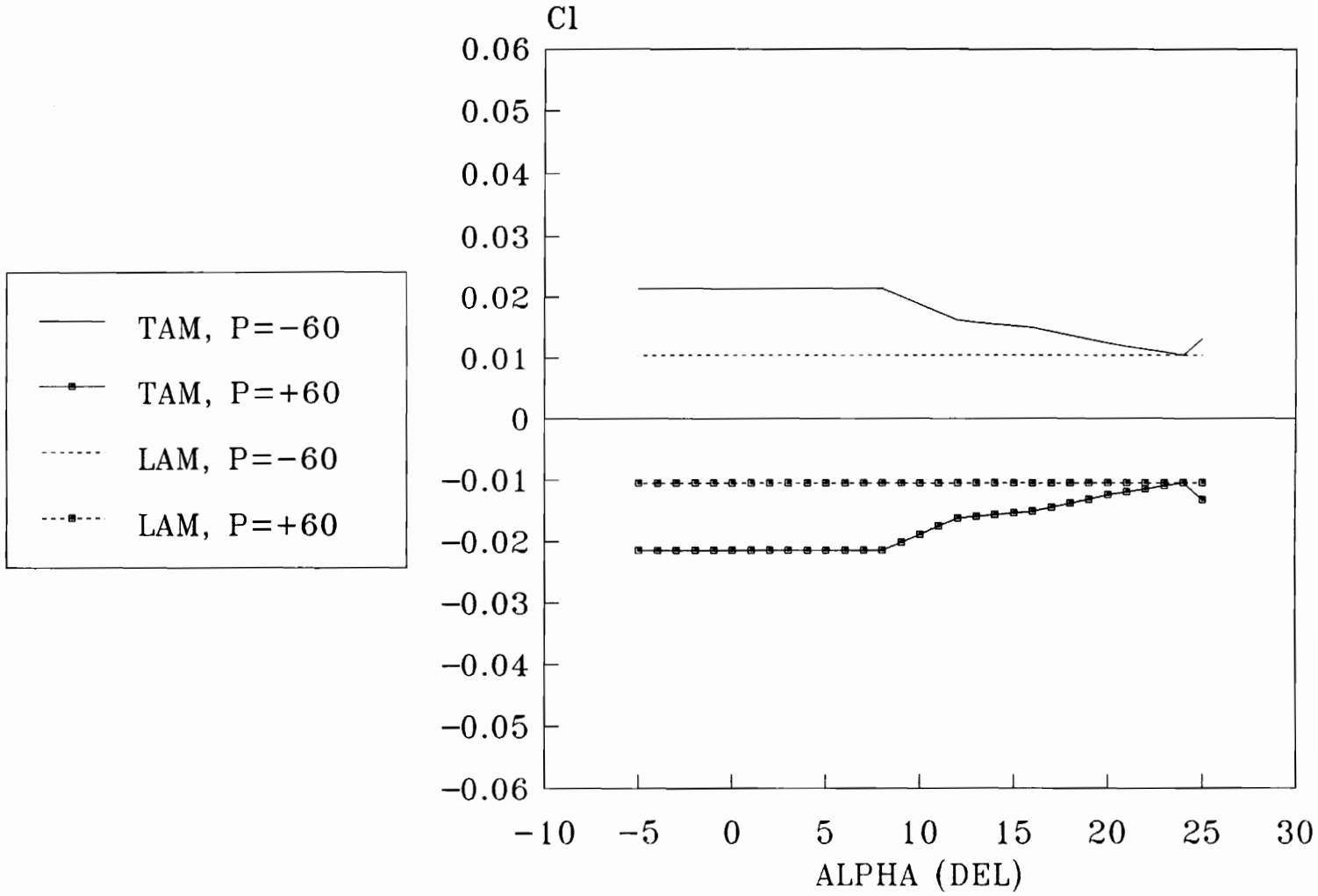

Figure 58. C_l vs α at 0.35M, p = ±60 deg/sec, TAM/LAM data

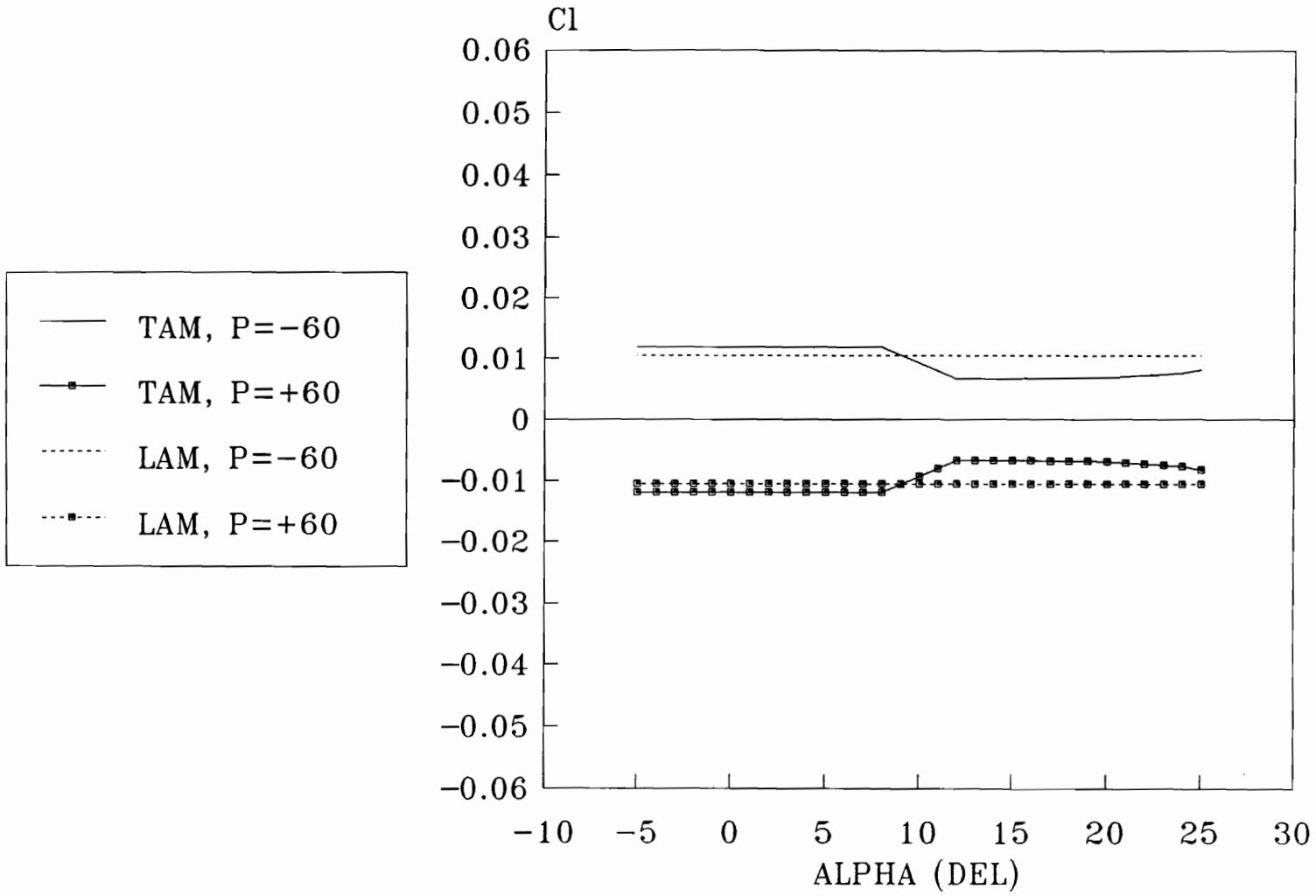

Figure 59. C_l vs α at 0.75M, p = ±60 deg/sec, TAM/LAM data

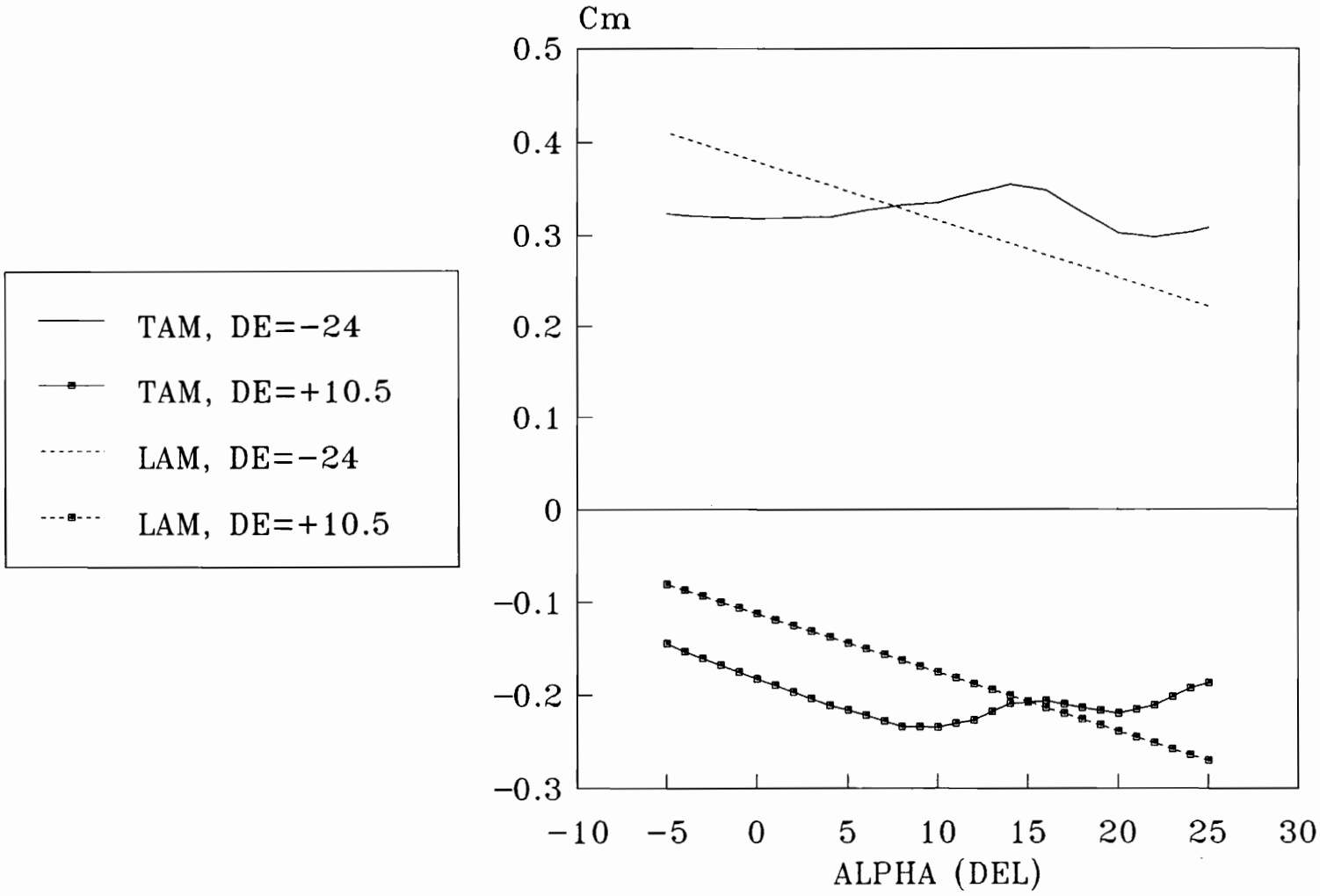

Figure 60. C_m vs α at 0.35M, δ_e = -24,+10.5 deg, TAM/LAM data

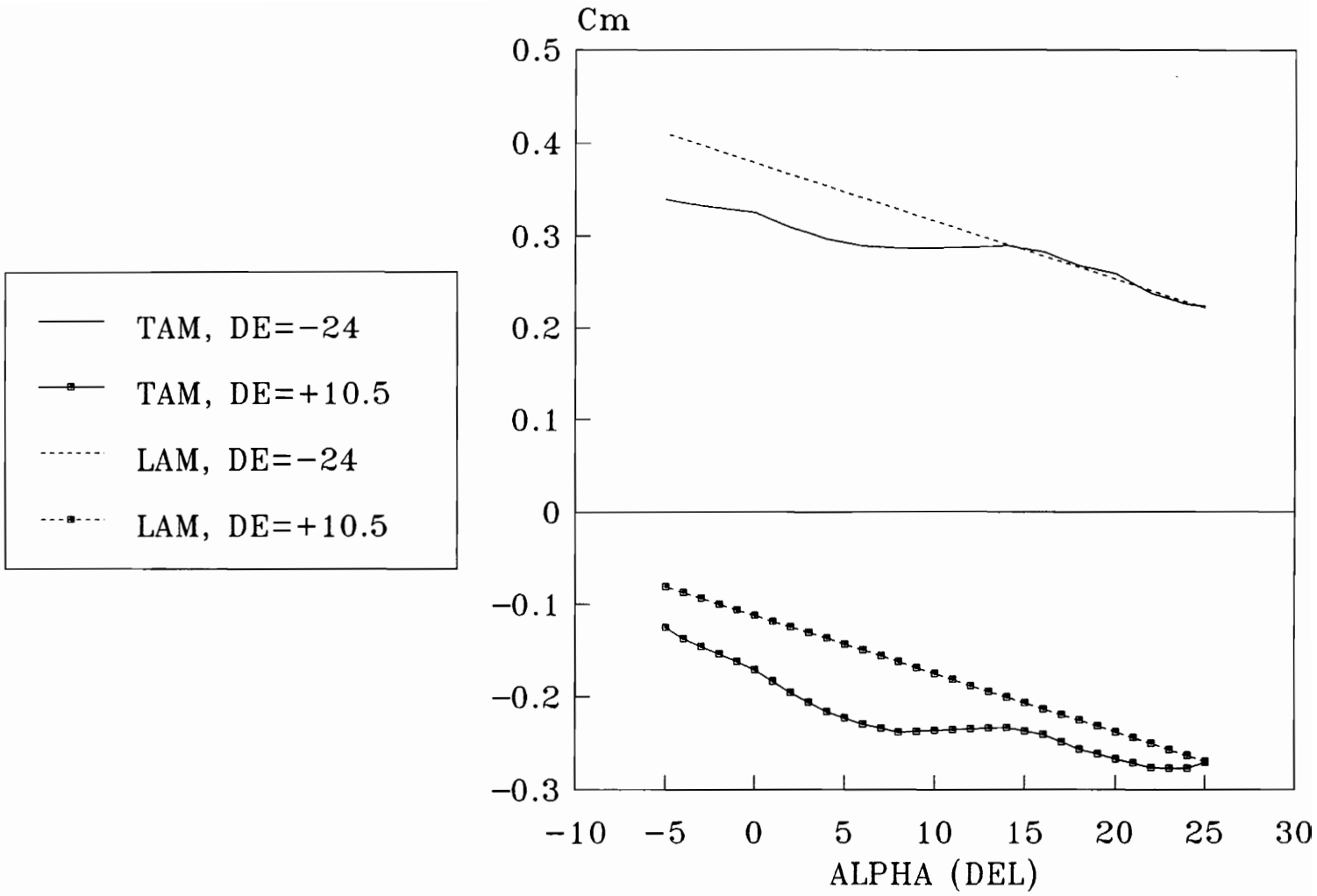

Figure 61. C_m vs α at 0.75M, δ_e = -24,+10.5 deg, TAM/LAM data

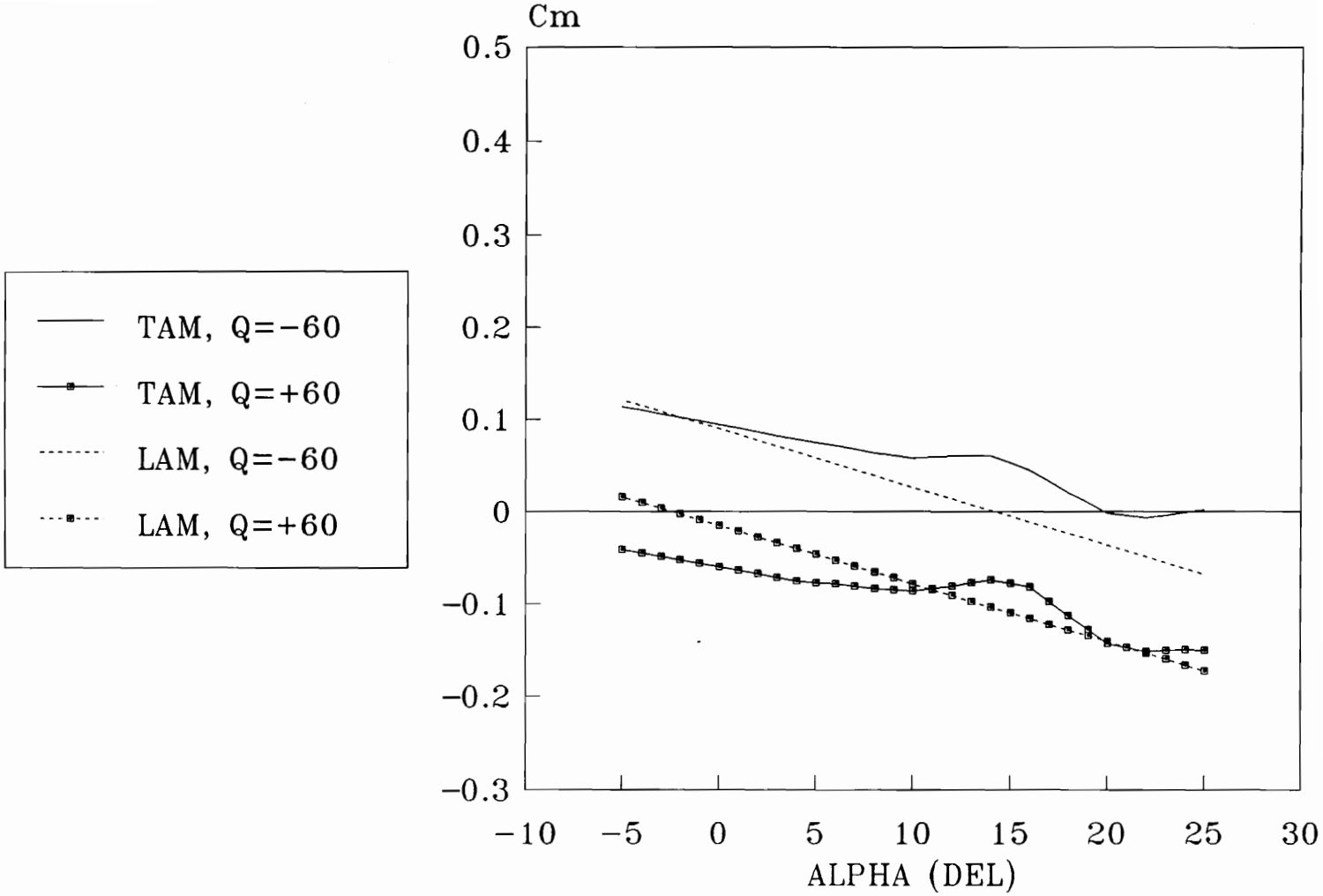

Figure 62. C_m vs α at 0.35M, q = ±60 deg/sec, TAM/LAM data

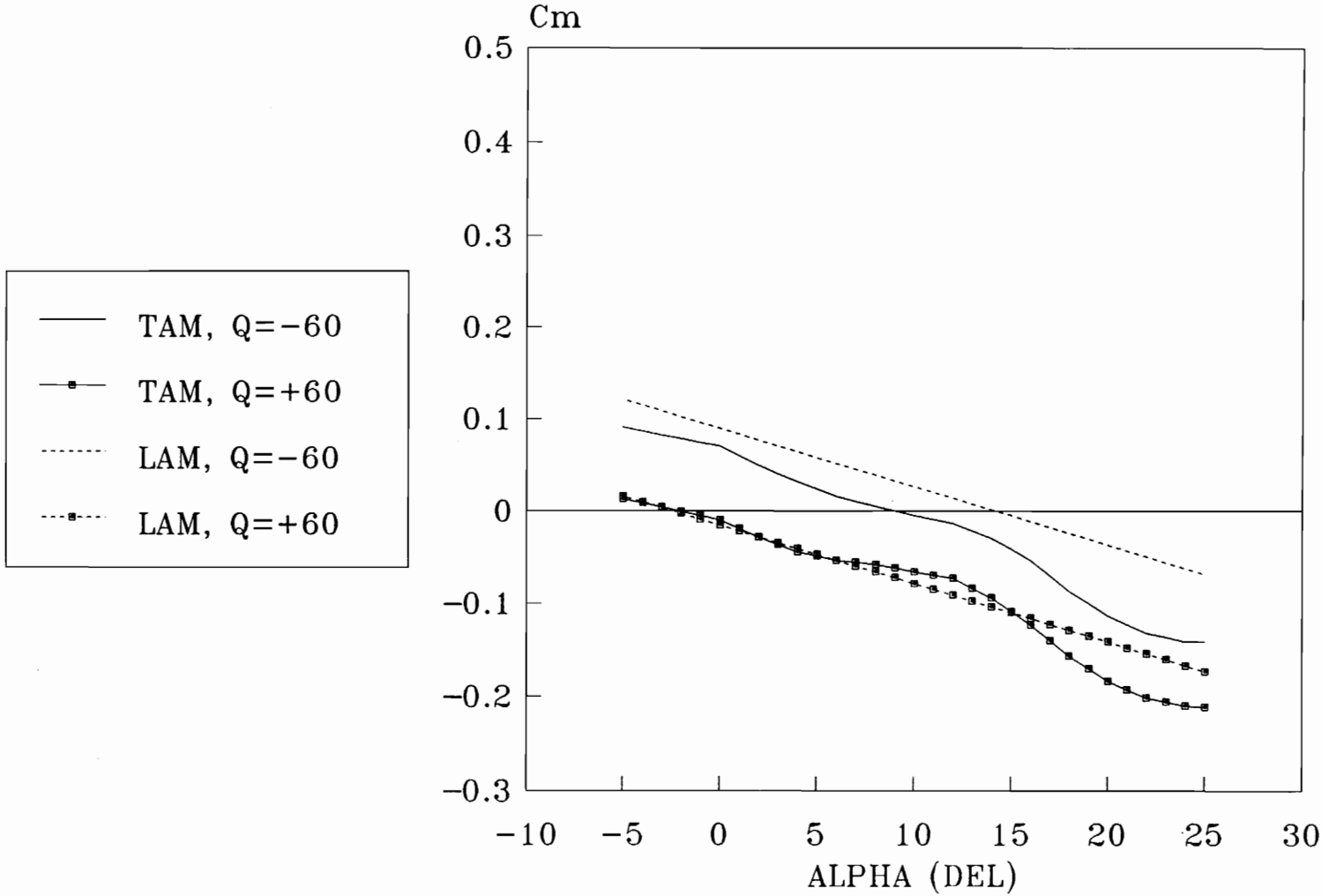

Figure 63. C_m vs α at 0.75M, q = ±60 deg/sec, TAM/LAM data

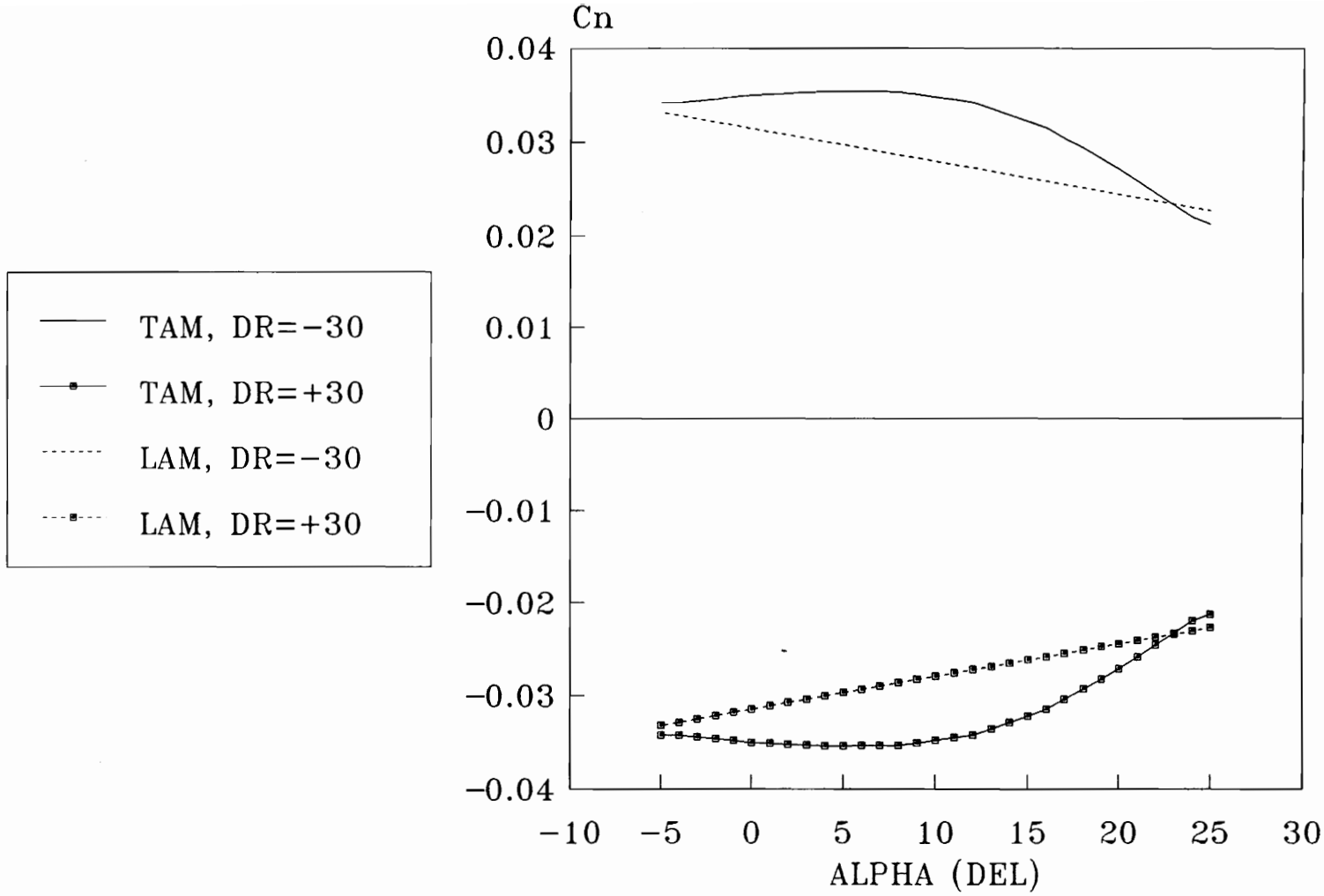

Figure 64. C_n vs α at 0.35M, δ_r = ±30 deg, TAM/LAM data

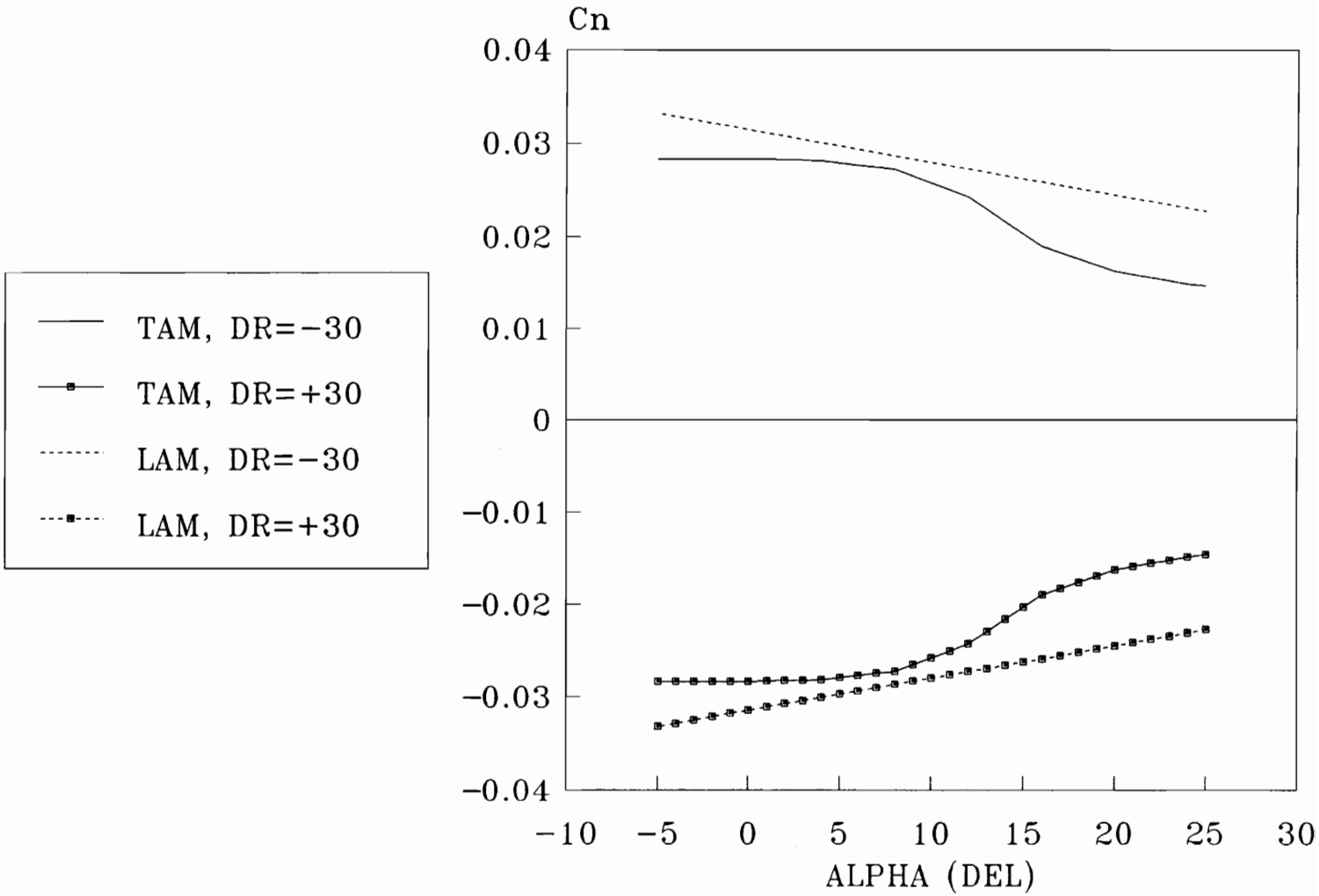

Figure 65. C_n vs α at 0.75M, δ_r = ±30 deg, TAM/LAM data

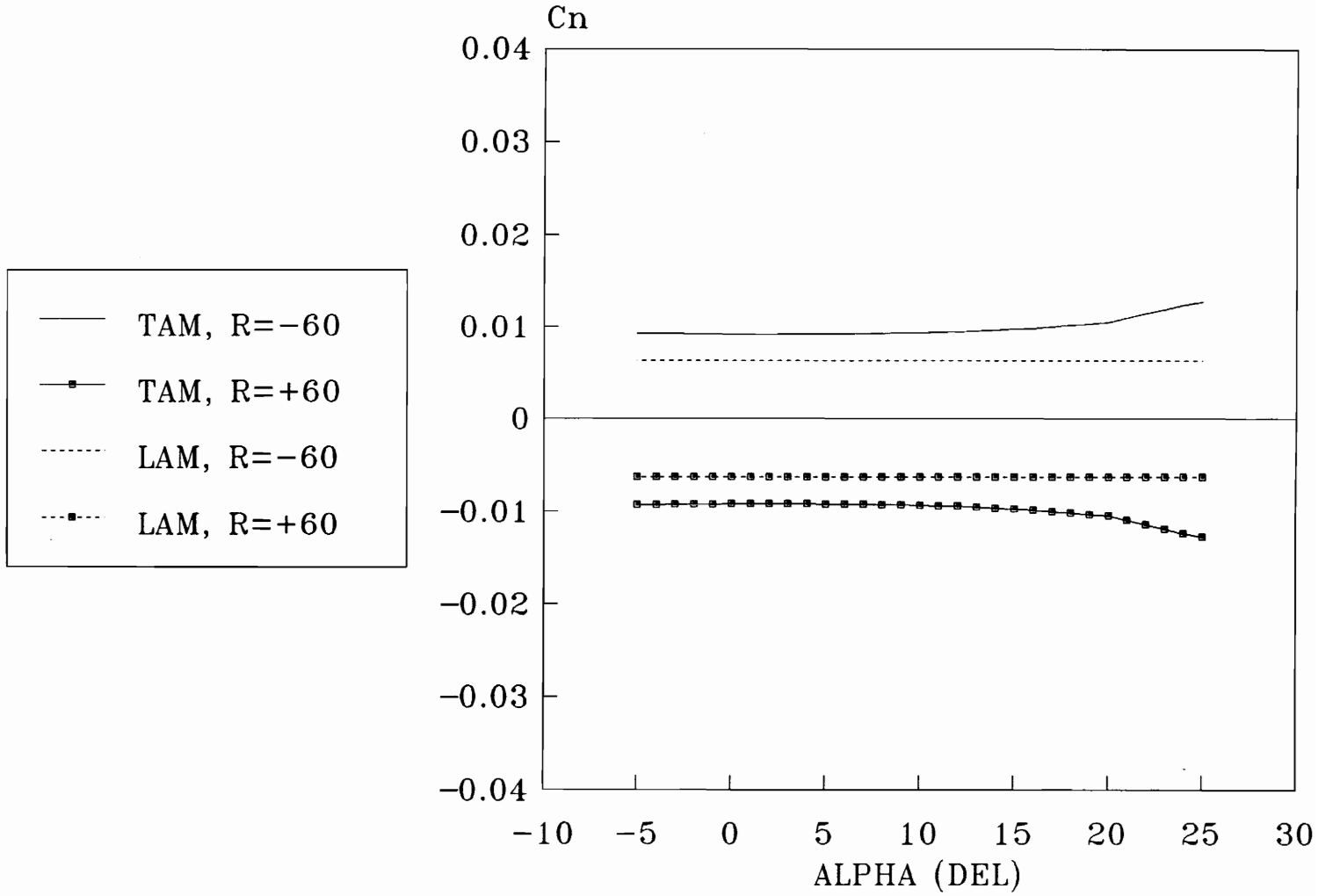

Figure 66. C_n vs α at 0.35M, r = ±60 deg/sec, TAM/LAM data

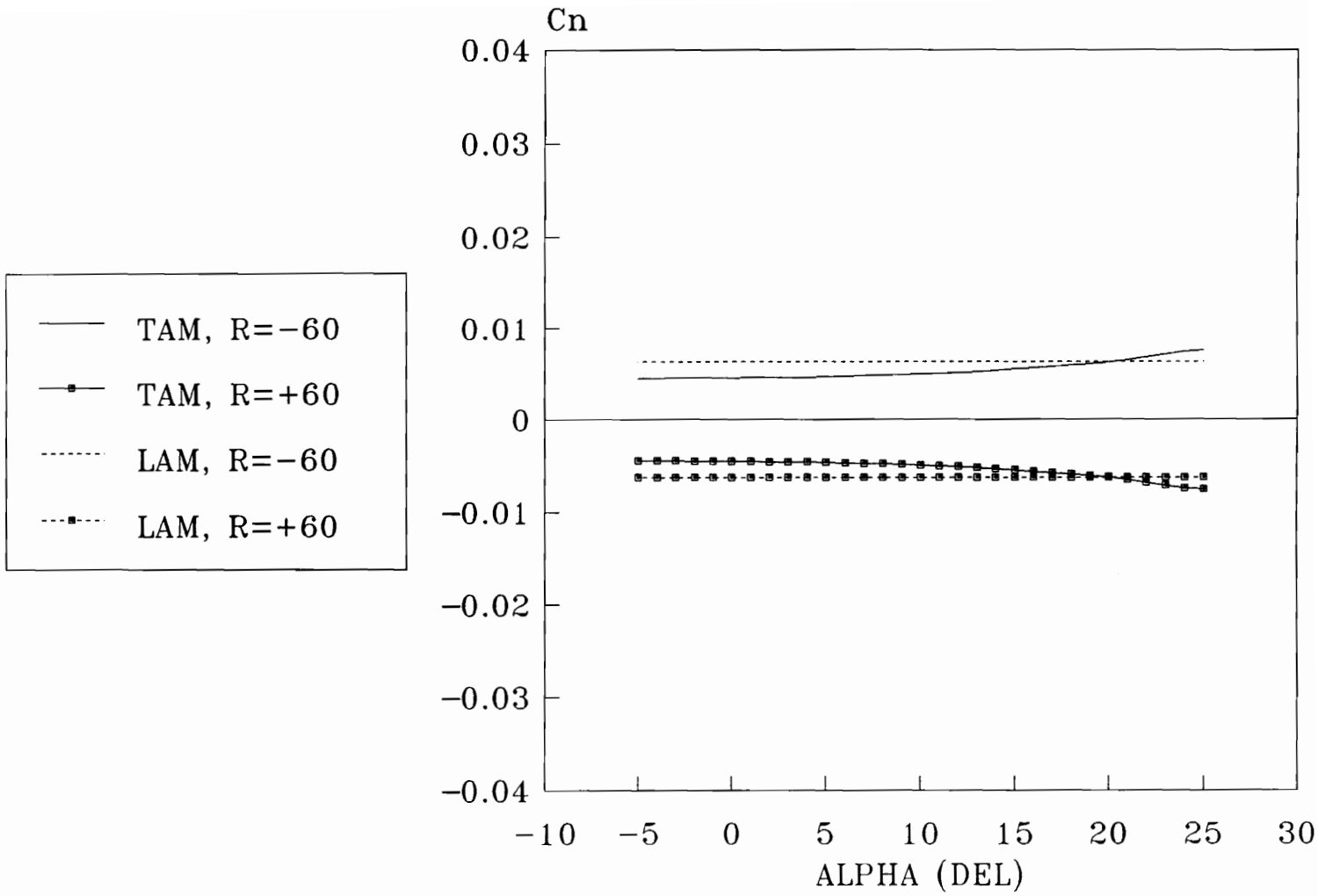

Figure 67. C_n vs α at 0.75M, r = ±60 deg/sec, TAM/LAM data

VITA

Michael E. Dwyer was born on July 21, 1964 in Vienna, Virginia. Mr. Dwyer received his Bachelor of Science Degree in Aerospace and Ocean Engineering at Virginia Tech in 1986. Mr. Dwyer has been employed as an aerospace engineer at Analytic Services (ANSER), Incorporated, in Arlington, Virginia, since 1985.